Spray-dried nanosuspensions for pulmonary drug targeting and *in vitro* testing thereof

Inauguraldissertation

zur

Erlangung der Würde eines Doktors der Philosophie

vorgelegt der

Philosophisch-Naturwissenschaftlichen Fakultät

der Universität Basel

von

Kateřina Šimková

aus der Tschechischen Republik

2021

Genehmigt von der Philosophisch-Naturwissenschaftlichen Fakultät
Auf Auftrag von

Fakultätsverantwortlicher	Herr Prof. Dr. Georgios Imanidis
Korreferent	Herr Prof. Dr. František Štěpánek

Basel, 27. April 2021

Prof. Dr. Marcel Mayor

Dekan

Let your teacher be Love itself.

Rumi

It is difficult to say what is impossible;

for the dream of yesterday,

is the hope of today,

and the reality of tomorrow.

Robert H. Goddard

Abstract

Pharmaceutical formulation development can be a challenging task during which many, sometimes contradicting factors need to be considered such as the formulation composition, suitability of excipients for each manufacturing step, or scalability of the process(es) applied. Development of dry powder formulations for inhalation can be especially challenging as only particles of very narrow aerodynamic particle size can enter the lungs while they are in fact designed by nature to prevent entry of foreign material. Additionally, there are mechanisms in place that quickly remove any particles that do enter them. Formulations with micronised drug substance particles are mostly being used to bypass the anatomical obstacles but the drug's deposition efficiency is commonly rather low. Utilisation of particle engineering, which leverages on favourable particle properties being tailored through a manufacturing process, offers a possibility to address these anatomical and performance challenges; however, their manufacturing is often linked to usage of organic solvents. A formulation scientist also needs to keep in mind that for any kind of formulation, drug dissolution is the key prerequisite for bioavailability and thus also for the drug's action. This can be a challenging step especially for a poorly water–soluble drug depending on its solubilities in the respective biological fluids as these are made up of water most of the time. Due to the obstacles inhaled drug particles encounter on their way to dissolved state, the drug needs to dissolve before it is cleared by the body's defence mechanisms to effectively work. Thus, study of the dissolution kinetics of solid formulations is of considerable interest. Unlike for orally delivered drug substance, no fully established pharmacopoeial dissolution method for inhaled medicines exists, likely due to the complexity to mimic reasonably well the *in vivo* situation.

The objective of this work was to combine industry-viable manufacturing processes to engineer inhalation powders of superior pharmaceutical performance and prolonged lung residence time thanks to favourable physical-chemical properties, and to study dissolution behaviour and biological fate of these powders using a dissolution vessel and *in vitro* cell culture system, respectively. The work intentionally used industrially established processes and only water as a solvent to offer the possibility to ultimately introduce this as platform technology for pulmonary formulation development allowing optimised inhalation drug product performance.

High-energy wet media milling was used for production of nanoparticles of a poorly-water soluble model drug (budesonide). The nanosuspension was stabilised using D-α-tocopherol polyethylene glycol 1000 succinate, which allowed to create nanosuspension of ≈ 260 nm median particle size at specific energy input of ≈ 137 MJ/kg. Subsequently used particle engineering *via* spray drying aimed to create composite particles of maximal fine particle fraction for deep lung deposition, maximal geometric size, minimal density, and fast dissolution. Spray drying at high Peclet numbers was crucial to successfully achieve this goal and it guided the choice of formulation composition and process parameters. Among the tested additives were leucine, trileucine, mannitol, albumin, glycine, and a pore former ammonium carbonate. Different spray drying temperatures and atomising pressures, as well as feedstock concentration, were screened to obtain formulation of the above-mentioned desirable properties. The most favourable

formulation, prepared with the nanoparticulate drug together with leucine and ammonium carbonate, exhibited a high fine particle fraction of 61% as assessed by the next generation impactor deposition and had a median particle size of ≈ 4.4 µm. The deposition efficiency correlated well also with the bulk and effective density measurements for which this formulation had lowest and second lowest values, respectively. The aerodynamic performance was well above the commercial, carrier-based product, which reached only 21% of fine particle fraction. Interestingly, when the micronised drug was not processed by wet media milling, even with the use of same additives and process conditions, only 22% of fine particle fraction could be reached. This suggested that the wet media milling step was indispensable for improved aerodynamic performance and that only the combination of the processes allowed to harness the advantages of both. Moreover, the geometric size of the composite spray-dried particles was larger than that of the micronised drug, offering additionally the potential to evade phagocytosis for a longer time period compared to the micronized drug as this is a size-driven process.

Within the first part of the work, five formulations of comparable geometric particle size, but different densities and particle shapes were studied in depth to assess their dissolution behaviour. For this purpose, a USP2 paddle apparatus was modified with the aim to mimic closely the *in vivo* conditions in terms of liquid hydrodynamics and volumes. For the modification, an insert from impactor stage, on which aerodynamically classified particles were deposited, was placed into the dissolution vessel; the setup thus resembled a USP5 (paddle-over-disk) apparatus. Using such setup, the dissolution behaviour of powders from three different stages was studied as a function of particle properties such as aerodynamic particle size, shape, or specific surface area. A permeable polycarbonate membrane was fixed onto each insert, which enabled the creation of an inner and outer compartment of different volumes. In the inner compartment, between the membrane and the insert surface, a small liquid amount of 200 µL was in direct contact with the powders and allowed dissolution in small, unstirred liquid volume. In the outer compartment was 300 mL of the stirred dissolution media into which the drug permeated upon its dissolution in the inner compartment. Dissolution of all aerodynamically classified fractions showed a very fast onset and was largely completed within 30 minutes irrespective of the formulation and the impactor stage. To further analyse this observation, mathematical kinetic modelling was used to deduce the drug's dissolution rate coefficients in each formulation in all three stages. From this it was found that the dissolution rate was determined by the properties of the drug nanoparticles, mainly particle size, rather than by the variable properties of the composite microparticles., This then explained why no differences among the formulations and stages were observed when same drug nanoparticles were used in the formulations.

Second part of the work aimed to investigate these aerodynamically classified composite powders even further using an *in vitro* cell culture system, which should have provided more representative *in vivo* conditions compared to the dissolution vessel. For this purpose, the next generation impactor was successfully modified for the first time to allow deposition on an A549 cell culture, cultivated on a low-profile, Matrigel®-coated cell culture insert. These alveolar type II cells were grown at an air-liquid interface, which allowed formation of a surfactant layer similar to the one present in the alveolar lung region. It was again of interest to evaluate whether particle properties like shape, density, or size affect the dissolution behaviour in this miniaturised setup. In this setup, it was assumed that the drug dissolution starts immediately upon particle deposition and any dissolved solute is translocated into the intracellular compartment, where it may be metabolised, and is eventually transported into the basal compartment. The drug amount

in the basal solution was determined for four to eight hours upon deposition, while its amount on the cell surface and in the interior of the cell monolayer was evaluated at the end of the experiments. Any induced cell damage was assessed also at the end of the experiment by measurement of the lactate dehydrogenase leakage from the cell membrane. Significant differences in the total deposited drug amount and the amount remaining on the cell surface at the end of the experiment were found between different formulations and impactor stages. The deposited amount negatively affected the dissolution of the drug as it took rather long (≥ 4 hours) for larger powder amounts to dissolve despite the drug's nano-range size. In fact, the dissolution took considerably longer than in the dissolution vessel setup, implying potential negative impact on local bioavailability as alveolar phagocytic clearance has similar half-life. Prolonged time required for complete drug dissolution and cell uptake in case of the large deposited powder amounts also suggested initial drug saturation of the surfactant layer. Interestingly, irrespective of the stage or formulation, roughly half of the deposited drug amount was taken up by the cells and metabolised to a large extent to its metabolic conjugate with oleic acid. Additionally, kinetic modelling was performed to evaluate the kinetics of drug dissolution and its uptake into the cells, metabolism into the oleate metabolite, and release into the basal solution, and supported the conclusions made based on the experimental results. However, it is important to note that partial cell damage was observed, which was possibly caused by the impaction of particles on the cells. This clearly indicated the need to further improve the experimental setup to reduce the cells membrane damage.

This work provided many insights into dry powder for inhalation formulation development and *in vitro* testing of inhalation powders. It focused on formulation composition and process optimisation and use of industrially established, solely water-based processes. This potentially allows establishment of the presented approach as a platform technology. It clearly showed that when formulating inhalation powders using this platform, equal importance needs to be given to drug pre-processing by particle size reduction as to spray drying if advantageous aerodynamic performance over carrier-based formulations should be achieved. It also showed that large particles of low density and enhanced aerodynamic performance, which could be used for targeted drug delivery, can be engineered using only water-based processes. Thorough *in vitro* testing using two different drug dissolution configurations showed the clear need to consider the test's purpose to select a relevant setup. For predicting local bioavailability, the newly developed cell culture *in vitro* system was able to provide useful insights into the process and kinetics of drug dissolution and cell uptake following powder deposition on an alveolar cell surface and it further highlighted the importance of fluid volume for formulation properties' study. As stage-specific drug distribution in different cell compartments and drug's amount in each compartment are relevant for local bioavailability and therapeutic effect, this setup offers more possibilities for biopharmaceutical performance prediction of dry powder for inhalation formulations while using state-of-the-art equipment.

Acknowledgements

First and foremost, I would like to express my deepest gratitude to Prof. Georgios Imanidis for his dedicated supervision and guidance, and for his support and belief in me throughout the studies. I very much appreciate the fruitful discussions we had and the hours we spent on discussing the scientific aspects of this work to the smallest details, which led to two great publications.

Further, I wish to thank Prof. František Štěpánek from the University of Chemistry and Technology Prague for being the co-referee of this work and for dedicating his time to this role.

This work was financially supported in part by the Rectors' Conference of the Swiss Universities (CRUS) within the Scientific Exchange Programme NMS-CH and in part by the University of Applied Sciences and Arts Northwestern Switzerland (FHNW), School of Life Sciences, where I have conducted my work. Both funding bodies are greatly acknowledged.

I am very grateful to all the people who have accompanied me and influenced me along this long and complex, yet rewarding journey:

My thanks go to the colleagues and lab mates from the Institute of Pharma Technology at FHNW who made the good times there even better: Camille Adler, Barbora Donner, Nicholas Gautschi, David Hilber, Fatos Hoxha, Tarik Cheema, Alexandra Machado, Zdravka Mišič, Martin Novak, Wiebke Saal, and Benjamin Zaugg. A special thank you goes to Ursula Thormann for her great support with the cell work and her contributions to the second article. I am as well grateful to Prof. Berndt Joost for welcoming me in his work group at the IPT.

I also wish to thank from the bottom of my heart my long-term friends, Jitka Georgievová and Lucie Horáková, for their love and support in tough times even if many kilometres separate us. A special, huge thanks go to my first lab mate and later on a dear friend, Miriam Schirmbeck, who introduced me to wet media milling and who was always there for me when I needed it. I also shall not forget the extensive support, encouragement, challenging discussions, and sometimes a needed push I have received throughout my studies from Jan Kendall de Kruif, to whom I am very grateful.

Last but not least, I would like to thank my family, especially my mother Marina, for encouraging me to explore the world and for always supporting me wherever my journey brings me. Mám tě ráda Emko!

Table of Contents

Chapter 1

1 Introduction

1.1 Background

It is not an overstatement to claim that pulmonary drug delivery is one of its kind. First appearing in ≈ 1500 BC, inhalation of vaporized remedies such as from henbane leaves was mostly applied to treat breathlessness and noisy breathing. Asthma and consumption (nowadays called tuberculosis) had been the most common diseases afflicting the mankind since centuries though they have been treated in earnest only for less than a hundred years. It was the usage of inhaled anaesthetics during the 19th century that considerably popularised this delivery route. [1] It is unique in the sense that lungs are by their nature designed to not allow any foreign particles to enter or in the case that happens, to remove the xenobiotics quickly by various removal mechanisms. By intentionally bringing drugs to the lungs, we are therefore trying to circumvent the natural processes. Yet, lungs present a very attractive delivery route: it is a logical choice for local treatment of the pulmonary tree diseases, while for the systemic treatment lungs offer several advantages such as a very large absorption area, thin air-blood barrier, high blood perfusion, or avoidance of first-pass effect. [2]

First inhalation therapies using a kind of a device were based on inhalation of volatile substances in form of vapours, while solid substances were indirectly inhaled using pipes or by smoking cigarettes. Later on, also pressurized systems and devices for direct dry powder inhalation started to be used, though they have seen an advent only during the 20th century. [2] However, already in the 19th century it has been noticed that large droplets do not help the deep lungs, setting the first basis for particle-size dependant treatment [1]. This has been made more accurate in the 1970s by visualising regional deposition of radiolabelled materials, which showed that particles of aerodynamic particle size of 5 μm and smaller, ideally in the 1 – 5 μm range, can effectively reach the pulmonary structures [3].

In fact, it is the aerodynamic behaviour of a particle in an air stream that is one of the main aspects guiding the particle's deposition. In line with this, the diameters for consideration and any comparison are the aerodynamic ones. As explained in detail in chapter 2.1.2.1, this diameter is proportional to particle's geometric particle size and square root of particle density, and inversely proportional to square root of particle shape factor. All these properties, together with inhalation flow rate, device specifics, and lung anatomy, determine how long upon inhalation will a particle follow the air streamlines, passing through bifurcating airways, before it comes into contact with the lung surface and deposits on it. When it comes to pharmaceutical powders, which are of

interest within this work, the density of most drug substances is close to 1 g/cm^3 and they do not possess unusual, for example needle shape unless intentionally done so. Therefore the geometric particle size of such dry powder for inhalation (DPI) formulations needs to be approximately in the above-mentioned 1 – 5 μm range. [4] Such small geometric sizes are usually achieved by jet milling or other micronisation processes. However, very small particles exhibit also poor flowability due to strong cohesion, which can lead to handling challenges during manufacturing, and thus they are commonly mixed with notably larger (≈ 100 μm) particles that serve as carriers for the drug substance particles. Frequently, the amount of drug that can reach the lungs using such formulations is rather low (usually 10 – 30% of the total dose). Low delivery efficiency means that a lot of the drug deposits in the mouth and throat, where it can cause for example hoarseness or irritation. The drug that does not reach the site of action in the lungs is eventually swallowed, causing possibly systemic side effects when the drug is orally bioavailable [5]. Another aspect for consideration might be the economic side as low delivery means that the expensive drug substance is mostly wasted and not used to its full potential.

Particle engineering of pharmaceutical processes, such as of spray drying, offers a good way to address these disadvantages of the traditional DPI formulations. Spray drying is a rather simple, one-step process that allows control over particles properties like the geometric particle size and density. Particles can even be engineered in such a way that they have large geometric particle size and low density, while maintaining the aerodynamic particle size in the desired range [6]. Particles with these properties, often called large porous particles (LPP), can advantageously evade phagocytic alveolar clearance, which prolongs particles' retention in the lungs. Also their handling might be improved thanks to reduced cohesion forces [7]. For successful production of low-density, porous or hollow particles, the particle engineering concept that is based on the Péclet number should be followed with the aim to create particles with high Péclet number [8]. Aside from spray drying process parameters, it is the excipients present in the feedstock that impact the particle size and its distribution, the density, cohesion, and aerosolization properties [9]. As the engineered particles do not use any carrier, their delivery efficiency into the lungs is often notably higher (commonly 60 – 80%). Despite the many advantages these engineered products bring, the amount of commercially available formulations leveraging on these processes is still very limited [10]. This is likely due to increased complexity as well as manufacturing costs such formulations have, which in cases where a suitable, notably cheaper alternatives exist might not justify their choice. Nonetheless they are used for formulations intended for systemic delivery as they can largely deposit in the lower respiratory tract where systemic absorption occurs. They also offer the possibility for pulmonary delivery of macromolecules such as proteins or peptides as they provide the stabilisation possibility for such rather fragile molecules.

One of the biggest challenges contemporary pharmaceutical industry faces is poor water solubility of many new drug candidates that emerge from combinatorial screenings. Their share is said to be more than 50% and can be expected to rise [11]. Therefore, the techniques for formulating these "brick-like" drugs are in the spotlight of many companies as water is a common processing solvent. Water is of course also the basis for all dissolution media in the body and thus poor water solubility can negatively affect the drug's bioavailability. Increasing the specific surface area of the drug by formulating it as nanoparticles, especially the closer the size comes to the 100 nm range, is one of the ways to address this issue. Many approaches exist for nanoparticle formation but in general they are of two-pronged character: either bottom-up, where the nanoparticles are built from the molecular structures (*e.g.* antisolvent precipitation), or top down,

where the nanoparticles are formed by particle size reduction. Industrially viable are mainly the top down techniques such as high pressure homogenisation or wet media milling due to more feasible scale up process. [12]

Many of the drugs currently used for inhalation therapies do have poor water solubility (*e.g.* budesonide, fluticasone propionate, beclomethasone dipropionate). Though in most instances poor aqueous solubility of the inhalation drugs does not seem to pose such a critical property, as in case of orally delivered drugs, it can still be the main cause of slow dissolution kinetics and thus also poor absorption and low local bioavailability [13]. As means to improving the dissolution rate, such drugs could be processed to nanoparticles; though it ought to be noted that in the pharmaceutical field such term is often used for all submicron (< 1 μm) particles. However as implied earlier, nanoparticles are too small to be effectively delivered to the lung surface and are mostly exhaled [14]. Forming a composite microparticle composed of nanoparticles and matrix former(s) might be a solution to this obstacle. Forming a composite microparticle can be done for example by spray drying of a nanosuspension. Aside from dissolution rate and bioavailability enhancement, such composite dry powder for inhalation presents a formulation that also positively addresses concerns with drug distribution homogeneity, aerosolisation, drug loading, and particle size distribution. [9] Nanoparticles also support spray drying at high Péclet number due to their low diffusion coefficient, making them a suitable starting material for this engineering technique [8]. Though in few instances nanoparticles of poorly water soluble drugs have been already spray dried, this was not done with the aim to create a DPI formulation of optimised drug product performance by for example leveraging on the particle engineering principles such as the Péclet number consideration.

Dissolution testing is a key assessment done for nearly any solid or semi-solid drug formulation as together with biological membrane permeability it guides the bioavailability of a drug for its action in the body. It can be also used as a quality control test to assess differences among the formulations of the same drug. Similarity of dissolution kinetics is one of the important requirements that in some instances oral generic formulations need to fulfil if sufficient equivalence between the original and the generic products wants to be claimed without a clinical bioequivalence trial. This is thanks to a well-established *in vitro-in vivo* correlation there exists for certain categories of oral products. However, this kind of correlation has still not been fully established for inhalation drugs. This is likely due to the complexity of the respiratory system and due to lack of any pharmacopoeial method that would allow relevant assessment of the dissolution kinetics despite the many years of research invested in this topic. [15,16] The problem of method development lies in finding a representative setup that would mimic well enough the dissolution conditions in the respiratory system. Depending on where in the lungs the particle lands, both the thickness and composition of the liquid as well as of the membrane are different. The lung liquid volume is generally very scarce as only a total of 10 – 70 mL is present in the lungs, spread over the vast lung area. [17] Additionally, particles do not deposit only in one particular place, rather they distribute along the pulmonary tree with a prevalence in either the central or peripheral area. The disease state usually also greatly changes the deposition pattern or lining liquid thickness and composition. And as mentioned above, removal of the particles from the lung surface by different mechanisms acting at the same time takes place. All these aspects make the development and validation of a dissolution test for inhalation products with claim of bioequivalence rather challenging. Several methods for dissolution testing of inhalation formulations have been utilised so far, leveraging mainly on modifying the USP2 method or using the Transwell cell culture supports, flow through cells, or Franz cells [18]. However, great

variability exists among the different methods in terms of dissolution medium volume and its composition. Some promising setups, such as with the Transwell inserts that mimic better the small lung liquid volume, do not mimic well the gradient caused *in vivo* by the absorption and transport into the epithelial cells, mucosa, or circulation. Also only rarely have powders of different aerodynamic particle sizes been compared and this was never done in a setup that would aim to closely mimic the *in vivo* conditions especially in terms of the dissolution volumes.

Bioavailability-relevant is also the study of the drug fate upon its dissolution [15,19,20]. The site of action is rarely on the epithelial side of the lungs. Often, the drug needs to cross the epithelial membrane and bind to the receptors on the smooth muscles or to the nuclei in the epithelial and endothelial cells [21]. Variation in the disease-related changes such as in the airway morphology, pH, and viscosity of the epithelial lining fluid, and the near impossibility to take any samples at the site of action, make the study of the drug's fate in a representative manner difficult. Animal and *ex vivo* models have to be still quite often used for study of *in vivo* fate as no *in vitro* models have so far been able to reliably substitute these ethically questionable approaches. Yet, many efforts are being put into *in vitro* models' development with the aim to mimic closely the *in vivo* conditions. For example cell culture models grown at the air-liquid interface (ALI) [22] or co-culture systems that contain also the phagocytic and/or dendritic cells have been developed [23]. A still rather new, yet very promising step further is the complex microfluidic-based lung-on-a-chip device, which offers within an *in vitro* setup a more accurate representation of the *in vivo* physiology [24]. Unfortunately, due to its complexity it is less convenient to use in common research laboratory. Therefore, most often testing of particles' fate is done using cell culture permeable supports. It is desirable to study aerodynamically classified powders to assess whether different particle size behaves differently. It is also beneficial to use cell models representative of where the particles would be expected to land, whether in the upper or lower respiratory tract. Aerodynamic assessment of inhaled formulations is described in pharmacopoeias and is commonly done using an impactor or impinger. Obtaining sample for cell culture testing from such device is however challenging as this requires modification of the device. Most research studies have so far utilised the old impinger system that however does not offer good classification possibilities. The most commonly used classification device, the next generation impactor (NGI), has never been modified to accommodate cell culture supports.

1.2 Objectives

The overall objective of this work was to engineer a poorly water-soluble drug substance, processed by wet media milling, into a composite dry powder inhaler formulation using the spray drying process and to create a formulation of enhanced drug product performance. The aim was to lay basis for this process combination so that it may become an industrially viable technology platform for processing of poorly water-soluble drugs. Further, the objective was to establish *in vitro* systems that closely mimic the *in vivo* physiology and that allow deeper study of the aerodynamically classified powder properties that are crucial for understanding particle dissolution and further fate upon particle's deposition on a cell surface. For this, *in vitro* methodology based on combination of the next generation impactor with cell line was established. Figure 1.1 graphically summarises the contents of this work.

As this work was multidisciplinary, bringing together pharmaceutical process development, dry powder formulation engineering, and *in vitro* cell culture testing in light of pulmonary drug delivery, the theoretical background laid down in chapter 2 covers the various fields necessary for better understanding of the work done and gives an overview of the state of the art including the persisting gaps there still are in terms of manufacturing process and formulation assessment. Attention is first paid to the pulmonary drug delivery, lung anatomy, and behaviour of particle upon inhalation as the key topics for understanding the requirements governing the formulation development and the restrictions related to this niche delivery system. Then, drug dissolution and its governing processes are described, and background is given on the particle size reduction as one of the ways of addressing poor dissolution kinetics. Dry powders for inhalation, their preparation and characterisation including the use of cell culture systems then complement the theoretical chapter, providing additional indispensable information relevant for this work.

The aim of the pharmaceutical engineering part of the work was to utilise wet media milling and spray drying processes to prepare composite powders where nanoparticulate, poorly water-soluble model drug substance would be embedded within a matrix, forming a microparticle of large geometric particle size and low density for enhanced aerodynamic performance and phagocytosis avoidance. The aim was to optimise each process to yield the best possible product. For wet media milling, the objective was to evaluate the role of the stabiliser (the type and concentration) and process parameters for creation of a stable nanosuspension, which was a prerequisite for the subsequent spray drying process. For spray drying, the goal was to develop a process that leverages the particle engineering principles and that supports spray drying at high Péclet numbers as means for creation of low-density particles. Therefore, the aim was to study the effect of matrix-forming additives of different diffusivity and solubility and to find their optimal concentration, hand in hand with studying the process parameters that support high Péclet number process. Further the aim was to explore usage of a pore former as an additional mean to lowering the particle density without the necessity to use an organic solvent since the overall goal was to utilise solely water throughout the whole manufacturing platform. Dissolution being a crucial prerequisite for drug's successful biological action, a USP2 system was modified in order to assess the dissolution kinetics of five engineered, aerodynamically classified powders. Firstly, the optimal construction of the modified USP2 setup had to be identified in terms of polymer membrane material and dissolution medium volume. Once this was set, the objective was to understand how dissolution kinetics of the powder is affected on one hand by the different particle characteristics and on the other hand by the different deposition location. For the latter, three different impactor stages were always assessed within the dissolution setup. For thorough

evaluation of the dissolution behaviour, the goal was to also employ a kinetic model. All the above-mentioned aspects are described in chapter 3.

Immediately upon drug dissolution in the mucous lung liquid or surfactant layer, the processes of absorption, distribution, metabolism, and elimination start taking place. To study these in as much as possible representative manner, various *in vivo* or *in vitro* systems might be used. The aerodynamic particle size directly affects the place of particle deposition within the lungs and thus also the type of *in vivo* structures the particle interacts with. It is thus worth to aerodynamically classify the formulation for study of inhalation powder fate. The further aim of this work was therefore to modify the next generation impactor and to enable powder deposition on the air-liquid interface of surfactant layer of an A549 cell culture. This modification was done for the first time ever and allowed combining the state-of-the-art impactor with a cell culture deposition to study the particle-cell interaction. The goal was to study any effect of formulation composition and particle's physical-chemical properties on the kinetics of the processes of particle dissolution in the surfactant layer, its uptake into the intracellular compartment and metabolism, and further transport into the apical layer. The aim was to as well apply the multicompartment kinetic modelling based on the cell physiology to delineate the processes. This biopharmaceutical characterization with impactor-cell culture combination is depicted in chapter 4.

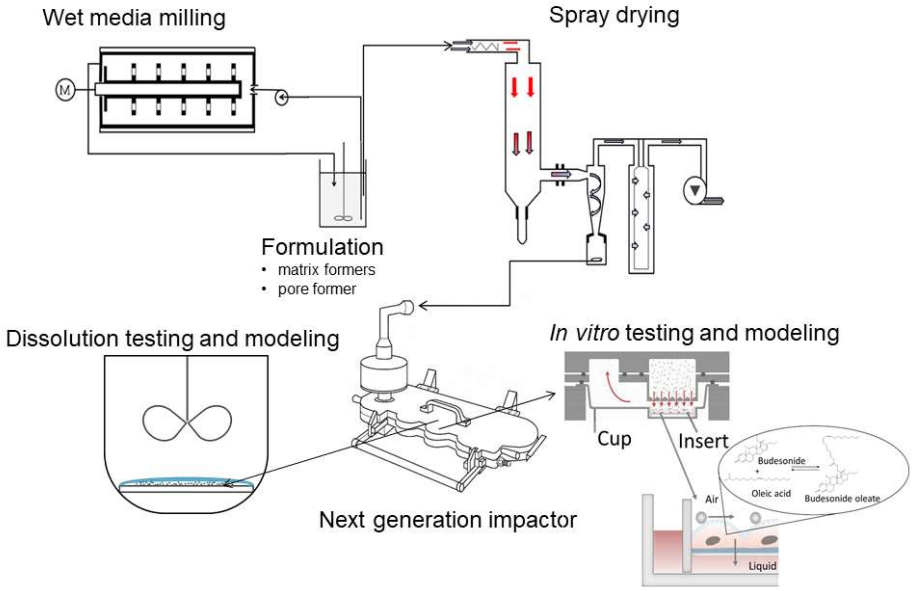

Figure 1.1 Graphical summary of the work

Chapter 2

2 Theoretical background

2.1 Pulmonary drug delivery

Pulmonary drug delivery is a niche, lesser known delivery system that compared to oral drug delivery is being leveraged by rather limited number of pharmaceutical companies. Traditionally, it has been used for local delivery of small molecules (*e.g.* glucocorticosteroids) and only recently have there been advances in delivery of molecules for systemic delivery or in delivery of macromolecules to the lungs for local or systemic effect (*e.g.* insulin/Exubera®).

Drugs are delivered to the lungs to achieve:

- local treatment of lung diseases, such as of asthma or chronic obstructive pulmonary disease (COPD), which still represents the vast majority of inhalation applications,
- systemic treatment thanks to drug absorption into the blood stream, which offers several advantages such as rapid onset of action, non-invasiveness, avoidance of first-pass metabolism convenience for drugs with low oral bioavailability, or needle-free delivery of biologicals that need to be applied parenterally [25],
- targeting of specific lung cells (*e.g.* of alveolar macrophages for treatment of tuberculosis)

Lungs however present a rather complex biological system, which as mentioned earlier is well equipped to prevent entry of any foreign material in order to ensure their correct primary function, the oxygen/carbon dioxide exchange. Of course, this exchange is vital for life and thus lung health should be of paramount importance for any human being.

As with every drug delivery system, the physiology of the involved structures has to be properly understood in order to increase the chances of a successful disease treatment. Therefore, the next chapters are dedicated to understanding the basic lung anatomy, the aerosol deposition, and the aerosol interaction with the anatomic structures.

2.1.1 Structure and composition of the pulmonary tree

The pulmonary tree starts at the trachea and terminates at the alveolar sacs and along this way it bifurcates 23 times, creating a very large surface area of around 140 m^2 [26]. It can be divided into the conducting and respiratory airways. The conducting airways (also referred to as tracheobronchial region) comprise the trachea, main bronchi, bronchioles, and terminal bronchioles, and act as a conduit for the inhaled air, which is filtered, warmed, and humidified in this region. The conducting airways bifurcate 17 times before reaching the respiratory airways. Respiratory airways (also referred to as alveolar region) are made by respiratory bronchioles,

alveolar ducts, and alveolar sacs (generations 17-23 in the bifurcating airway model), and they secure the exchange of oxygen/carbon dioxide between the alveolar space and the blood in alveolar capillaries [27] (Figure 2.1).

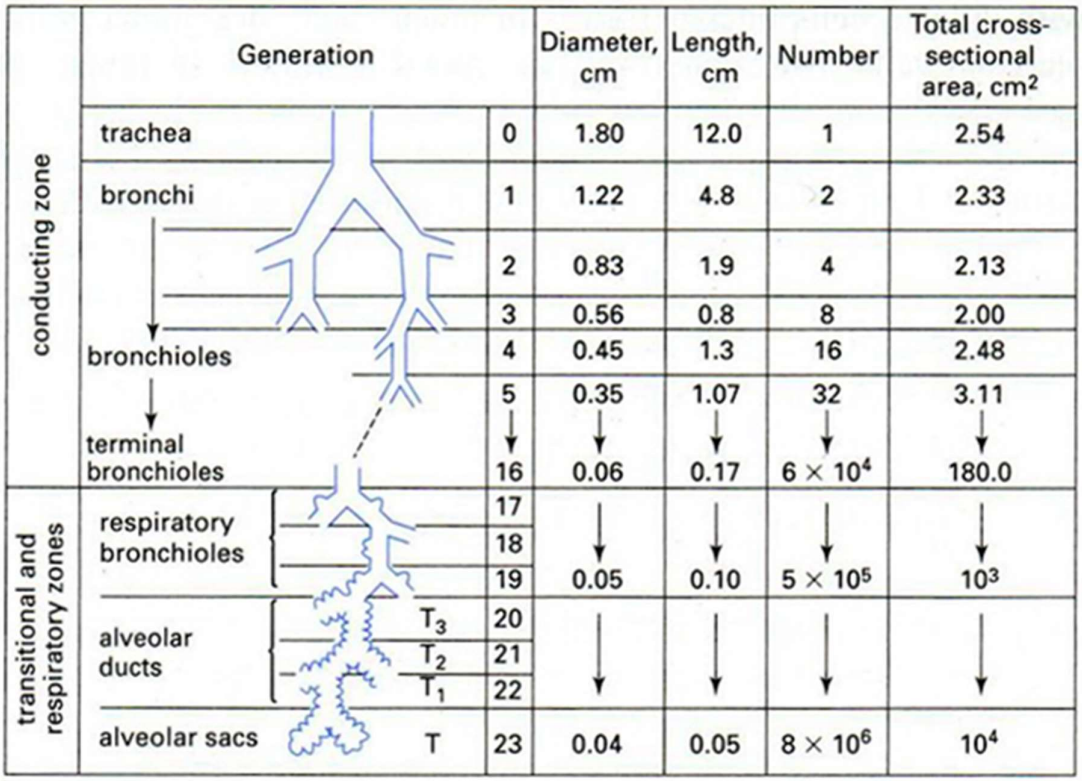

Figure 2.1 Overview of pulmonary tree structure [17].

The composition of the pulmonary tree greatly varies along its whole length (Figure 2.2). The upper part of the tracheobronchial region is composed of several types of cells such as the basal, goblet, ciliated, brush, serous, Clara, and neuroendocrine cells [28]. Also migratory cells such as lymphocytes, leukocytes and mast cells are present in this region. The terminal bronchioles, on the other hand, are only composed of ciliated cells and Clara cells. Alongside the cell composition change occurs also gradual epithelium thinning: epithelial cells in the trachea and bronchi are rather thick (50-60 μm in diameter) [25] while the terminal bronchioles measure only around 10 μm. The surface of bronchial epithelium is covered by mucus, a viscous watery fluid with pH around 6.6 (in healthy individuals) that contains glycoproteins and proteoglycans. This fluid keeps the epithelium hydrated, humidifies the inhaled air to a relative humidity of 99.5% or more, contains antibacterial proteins and peptides, and protects the airways from inhaled chemicals and other xenobiotics [27]. Also, the conducting airways' diameter changes dramatically with increasing generation number from 1.8 cm (tracheal diameter) to 0.06 cm (terminal brochioles' diameter) [29].The cross-sectional area, on the other hand, does not increase tremendously in this region and reaches around 180 cm^2 [4]. Clearance of foreign particles thanks to a mucociliarly escalator is the predominant removal mechanism in this region (chapter 2.1.3.3.12.1.3.3).

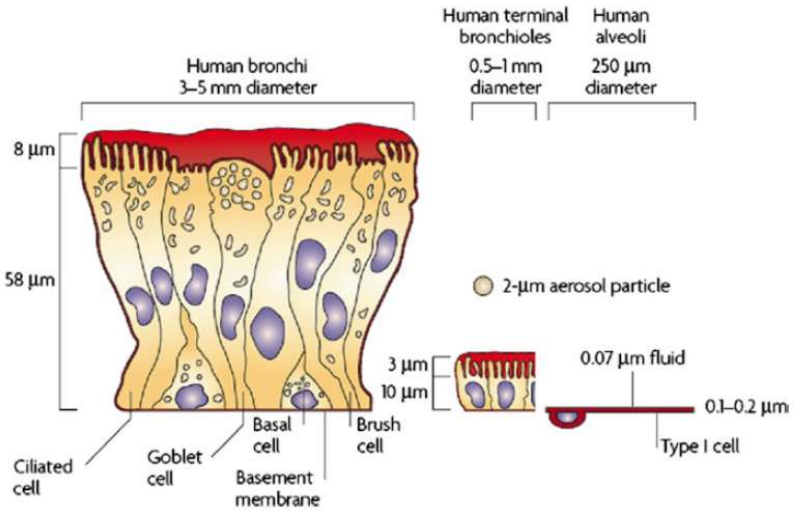

Figure 2.2 Comparison of the lung epithelium at different sites within the lungs [2].

The surface epithelium in the alveolar region, on the other hand, is made of type I and type II epithelial cells (pneumocytes). The squamous type I cells are about 0.1-0.2 µm thin and cover around 93% of the alveolar surface. It is through these thin cells that the oxygen/carbon dioxide exchange occurs. The very small thickness of the alveolar epithelium is also favourable for the systemic absorption of drugs. Type II epithelial cells are cuboidal in nature, cover around 7% of the surface, and are thought to be precursors of type I cells during lung growth and repair [30,31]. They do however possess an important function as they are responsible for the production of the lung surfactant. The surfactant contains approximately 90-95% lipids, with dipalmitoylphopshatidylcholine (DPPC) as the main component, and 5-10% surfactant proteins[32]; however the composition may deviate in pathologic states. The lipids and proteins in the lining fluid reduce alveolar surface tension, increase the wetting, the solubility, and hence also the dissolution rate of poorly water-soluble drugs [33]. Furthermore, in this region are present alveolar macrophages, which phagocytise foreign particles or organisms (chapter 2.1.3.3.2). Diameters of the alveolar airways do not change very much from generation 17 to generation 23 (Figure 2.1). However, it is in this region where the cross-sectional area increases enormously up to 10 000 cm^2, especially thanks to the surface area of the alveolar sacs.

2.1.2 Aerosol deposition

Formulations used in pulmonary drug delivery are aerosols, *i.e.* small solid particles or liquid droplets, which are carried with inhaled air to the lungs. To understand the deposition in the lungs, it is beneficial to be first familiar with the general motion of particles in the air.

2.1.2.1 Theoretical background

Motion of any aerosol particle mostly occurs, due to its small particle size and low velocity, at low Reynolds numbers (Re < 1) where Stokes's law applies. During settling, the gravitational force (F_G) is equal and opposite to the drag force of the air on the particle, F_D (2.1):

$$F_D = F_G \tag{2.1}$$

$$3\pi\eta V d = \frac{(\rho_P - \rho_G) d^3 g}{6} \tag{2.2}$$

where η is dynamic viscosity, V is particle velocity, d is particle diameter, and ρ_P is particle density [4]. Stokes's law allows determination of the settling velocity of a particle, which is settling by gravitation in still air. Solving eq. (2.2 gives the terminal settling velocity V_{TS} (eq. (2.3):

$$V_{TS} = \frac{\rho_P d^2 g}{18\eta} \tag{2.3}$$

which applies for spherical particles with sizes $d > 1$ µm and $Re < 1$. The settling velocity for particles with sizes $d < 1$ µm is higher than predicted by Stokes's law because the relative velocity of air right at the particle surface is not zero and a "slip" occurs on the surface of the particles. To account for this effect, a Cunningham correction factor C_C (sometimes called slip correction factor) is applied and is always greater than one (eq. (2.5). The terminal settling velocity for particles with $Re < 1$ should therefore be written as:

$$V_{TS} = \frac{\rho_P d^2 g C_C}{18\eta} \tag{2.4}$$

$$C_C = 1 + \frac{\lambda}{d}\left[2.34 + 1.05e^{\left(-0.39\frac{d}{\lambda}\right)}\right] \tag{2.5}$$

where λ is the mean free path of a gas, which is defined as "the average distance travelled by a molecule between successive collisions". For instance, the mean free path of air at 20°C/1013 hPa is 0.066 µm.

As aerosol particles are rarely perfect spheres, a shape correction factor ought to be applied to account for this. A dynamic shape factor χ, given by equation 6, is the ratio of the actual resistance force of the irregular particle to the resistance force of a sphere having the same volume and velocity as the irregular particle.

$$\chi = \frac{F_D}{3\pi\eta V d_E} \tag{2.6}$$

where d_E is equivalent volume diameter, *i.e.* diameter of a sphere having the same volume as the irregular particle.

As χ is mostly > 1 (for example 1.08 for a cube), irregular particles settle more slowly than their equivalent volume spheres as follows from eq. 7:

$$V_{TS} = \frac{\rho_P {d_E}^2 g}{18\eta\chi} \tag{2.7}$$

Since particles of different sizes, shapes, and/or densities can settle with the same velocity, an equivalent diameter that describes the aerodynamic behaviour of a particle, rather than its geometric properties, is commonly used in aerosol technology. Aerodynamic diameter, d_A, is defined as the "diameter of a spherical particle with a density of 1 g/cm^3 (density of a water droplet) that has the same settling velocity as the particle". Using the aerodynamic diameter, the settling velocity of a particle is as follows (eq. 8):

$$V_{TS} = \frac{\rho_0 {d_A}^2 g}{18\eta} \tag{2.8}$$

where ρ_0 is the unit density. After rearranging, the aerodynamic diameter of an irregular particle can be expressed by equation 9:

$$d_A = d_E \sqrt{\frac{\rho_P}{\rho_0 \chi}} \tag{2.9}$$

Figure 2.3 demonstrates graphically the concept of aerodynamic diameter. The particles shown in this figure behave aerodynamically the same due to equivalent settling velocities, which are the result of the particles' size, density, and shape.

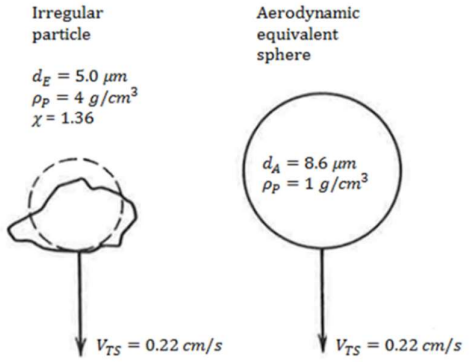

Figure 2.3 An irregular particle and its equivalent aerodynamic sphere of the same settling velocity (adapted based on [4]).

2.1.2.2 *Aerosol lung distribution*

As it was mentioned earlier, only particles of a very narrow aerodynamic particle size range between 1 µm and 5 µm can actually enter the lungs. Deposition of the particles that do enter is essentially influenced by two groups of factors: those determined by properties of the aerosol (such as particle size, shape, density), and those determined by the patient (*e.g.* inspiration airflow velocity and volume, airway geometry, pause time between inspiration and expiration). The mechanism of deposition differs with the regions of airways. Most important ones are inertial impaction, sedimentation, and diffusion [1]. Only in certain situations (for example when needle-shaped particles such as asbestos fibres are inhaled) are important also the less common mechanisms: interception and electrostatic precipitation [4].

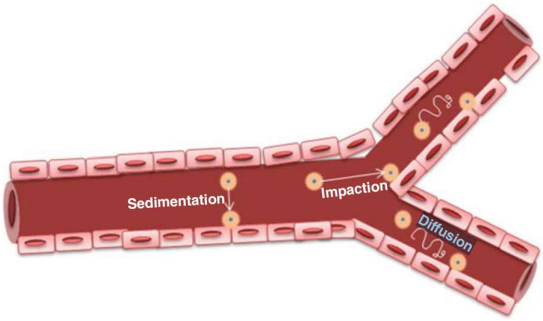

Figure 2.4 Main deposition principle of particles upon entry of the lungs [34].

Inertial impaction of particles is influenced by the geometric diameter and airflow velocity, and applies mainly to particles with d_A > 3 μm (Figure 2.5) [35]. This mechanism is likely to occur in the upper conducting airways, where the velocity of inhaled air is high. Due to their inertia, large particles often fail to follow the air streamlines and impact on the epithelial wall, very commonly where the airway bifurcation occurs. The carrier particles, as well as very large drug particles (≈ 10 μm), usually impact in the throat and trachea, and are swallowed.

Deposition efficiency is governed by Stokes number (eq. 10).

$$Stk = \frac{\rho_p d_E^2 V C_c}{9\eta D} \tag{2.10}$$

where D is characteristic dimension of an obstacle and V is particle velocity[4]. Majority of the aerosol performance testing is based on impaction, and is described in more detail in chapter 2.4.1.

Sedimentation or settling via gravitational forces mostly influences particles between 1 and 3 μm and depends on particle mass and residence time. Particle around this size rage deposit both in the conducting and respiratory airways. Sedimentation is governed by the Stokes's law and therefore a spherical particle will settle with settling velocity as per equation 8.

Particles smaller than ≈ 1 μm are mainly subject to deposition via Brownian motion (diffusion). Diffusion coefficient (D_f), which can be calculated from the Stokes-Einstein equation (eq. (2.11), is proportional to temperature and inversely proportional to particle size and air viscosity [36]. This mechanism dominates in the alveolar region, and breath holding may increase this type of deposition [37]. Yet, it has to be also noted that submicron particles are very often exhaled rather than effectively deposited in the lungs as the time requires for their diffusion and subsequent deposition is usually too short.

$$D_f = \frac{k_B T}{3\pi\eta d_p} \tag{2.11}$$

However, the given particle sizes are rather of an indicative character than strict cut-off diameters since the inhaled particles are distributed along the pulmonary tree (Figure 2.5). Additionally, even if primary particles are small, they might agglomerate into larger secondary particles and deposition in earlier generations if they do not disperse during the inhalation manoeuvre.

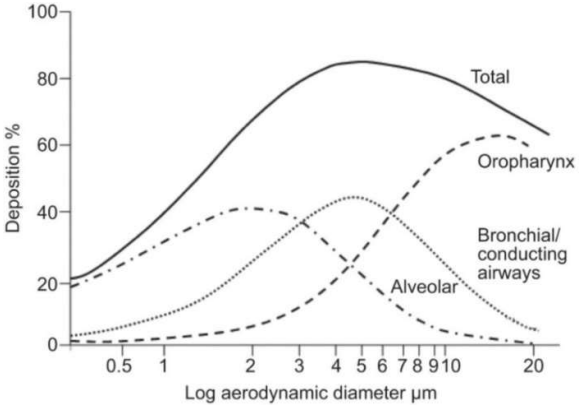

Figure 2.5 Relationship between aerodynamic diameter and lung deposition [38].

2.1.3 Fate of inhaled drugs upon deposition

Once particles successfully deposit on the lung surface, several different actions might take place (Figure 2.6). After the deposition, particles start to dissolve in the lining fluid (chapter 2.1.3.1), which is the prerequisite for a deposited drug to be absorbed (chapter 2.1.3.2), to be bound on a receptor and/or be metabolised. At the same time, the particles can be cleared (chapter 2.1.3.3) by mucociliary clearance or phagocytised if deposited in the tracheobronchial or alveolar region, respectively.

For inhaled, topically-active drugs, the ability to reach the site of action is dictated by the ability of the drug to dissolve in the lung fluid layer and by the transport mechanisms. Factors affecting these processes include the amount of drug deposited, as well as the location, solubility and mobility of the drug in the lining fluid, the particles' deposition pattern, drug binding, permeability of the drug, and the residence time in the lung.

In the oral delivery, a biopharmaceutical classification system exists [39] that helps to divide the expectations regarding drug's *in vitro-in vivo* correlation based on its solubility and permeability as the key properties. Though some attempts have been made to establish similar system for pulmonary delivery (*e.g.* by Eixarch [40]), no reliable system has been developed up until today. Details of the challenges are discussed further in this chapter.

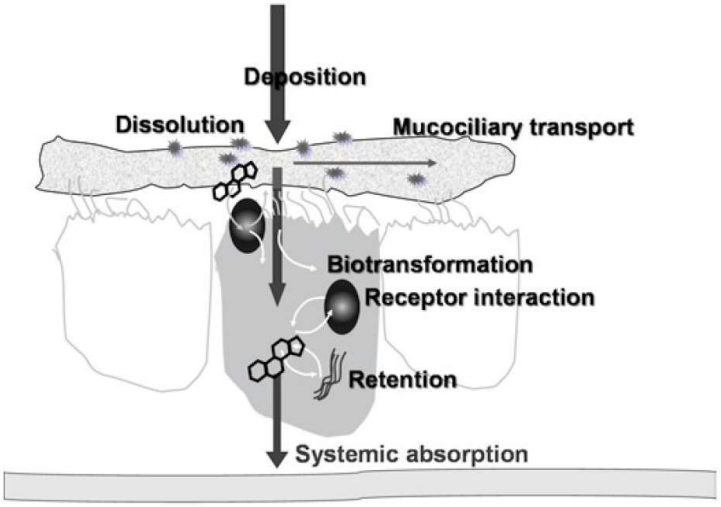

Figure 2.6 Possible routes of drug elimination from the lungs in the tracheobronchial region [41].

2.1.3.1 Dissolution

Dissolution rate is an important attribute that influences drug bioavailability together with attributes such as drug saturation solubility, permeability, and dose and deposition pattern. Saturation solubility of a drug depends on the compound itself and its solid form as well as on the composition and volume of the lung fluid [42]. Dissolution rate depends in addition to solubility also on the cross sectional area of the drug particles, the drug surface properties, and the volume of the lung fluid, as well as on the hydrodynamics of mixing in the lungs, as given by the Noyes-Whitney/Nernst Brunner equation. This equation is in greater detail described in chapter 2.2. The total liquid volume in human lung is only around 10-70 mL [17,43]. This volume is, of course, spread over the large surface area of the lungs as a thin film rather than being a bulk volume,

which leads to very small volumes being effectively available for dissolution of the deposited drugs.

It could be assumed that similarly as for oral drug delivery, also inhalation drugs can be dissolution-rate and permeation-rate limited. However, dissolution-rate limitation is for several reasons not seen as often [13]. For one thing, the drug particle size is in pulmonary delivery, compared to oral delivery route, rather small, which aids faster dissolution due to increased specific surface area. For second thing, the required dose seen with most of the inhaled drugs, such as the short-acting and long-acting bronchodilators, is rather small (in micrograms range) (Figure 2.7).

Additionally, the knowledge about the aspects affecting drug dissolution in the lungs is still very limited due its complexity and the difficulty to study this drug delivery method [43].

2.1.3.1.1 Tracheobronchial region

The liquid layer volume and thickness ranges 10-30 mL and 5-10 µm, respectively, in the tracheobronchial region [44]. Most of the currently marketed small molecule drugs for inhalation, including the mentioned bronchodilators, target this lung region. These drugs are not dissolution limited as their saturation solubility in the 10-30 mL is sufficient for the required dose. These are the drugs located above the band in Figure 2.7.

Dissolution-rate limitation is seen with two groups of drugs: 1) corticosteroids such as fluticasone propionate (FP), beclomethasone dipropionate (BDP) or mometasone furoate (MF) due to their very low solubility, and 2) antiinfectives of limited solubility (< 100 µg/mL) such as ciprofloxacin betaine or amphotericin B, whose required dose is very high. These are the drugs below the band in Figure 2.7. Permeability-limited drugs, on the other hand, might be dissolving under lack of sink conditions due to their accumulation in the mucus layer.

The lung fluid composition could also have a positive effect on the drug solubilisation due to presence of various salts, phospholipids, proteins, and mucins [45].

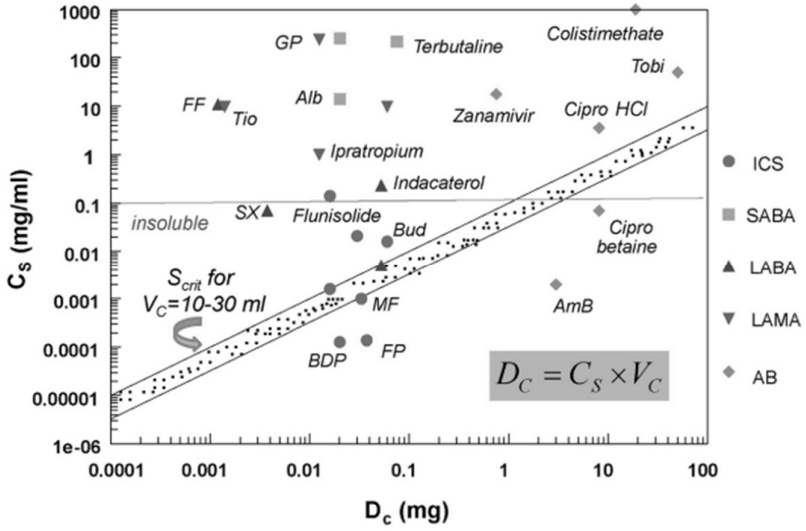

Figure 2.7 Solubility of pulmonary drugs vs. the required dose in the conducting airways [46].

2.1.3.1.2 Alveolar region

Drugs targeted to the alveolar region are usually intended for their absorption into the systemic circulation. As described earlier, the liquid layer thickness gradually decreases with increasing generation number and eventually reaches only 0.01-0.08 μm. However, this layer is surfactant-like in nature as it consists mostly of lipids. This potentially improves solubilisation of low molecular weight drugs (*i.e.* not macromolecules) that do reach this region. Thanks to the thin epithelial layer, the dissolved substances are likely quickly absorbed into the blood stream and thus sink conditions are easily maintained.

2.1.3.2 Transport to site of action

Lungs are used to treat both local as well as systemic diseases and thus the site of action a drug needs to reach depends on the disease that is being addressed. In general, compounds that dissolve upon deposition on the lung surface and are not cleared can be transported across the cell membrane via different pathways [47]:

- transcellular passive diffusion,
- paracellular passive diffusion,
- carrier-mediated uptake at the apical side followed by passive diffusion across the membrane,
- vesicle-mediated transcytosis, and
- transporter-mediated uptake or efflux.

It has been shown by Schanker et al. [48,49] that most low molecular weight compounds are absorbed by passive diffusion. They have also shown that the rate of absorption increases with lipophilicity for compounds with partition coefficient from -3 to 2. Nature of the drugs also affects the speed with which they are absorbed: as a rule of thumb, lipophilic drugs with a log $P > 0$ show rapid absorption times ($\approx$ 1 min), while hydrophilic drugs with a log $P < 0$ have notably longer absorption times of ca 1 h [46]. It has been also shown that the upper size limit for particles to be transported by clathrin-mediated endocytosis is approximately 200 nm, which is relevant for delivery of slowly soluble nanoparticles [50]. Current research of macromolecules suggests that proteins can be transported across the alveolar epithelium both transcellularly (*e.g.* endocytosis) and paracellularly with the molecular weight of the macromolecule affecting greatly the transport mechanism type [1].

2.1.3.2.1 Tracheobronchial region

The tracheobronchial region is targeted mostly for local treatment of diseases such as asthma, COPD, or cystic fibrosis. It is therefore the local bioavailability that is of interest when targeting this region. The drugs' mode of action is often of bronchodilative or mucolytic character. The drugs affect either the mucus composition or the smooth respiratory muscles, which are located between the epithelium and the blood vessels (Figure 2.6) [51]. Also antibiotics might be administered to the endobronchial region, usually for treatment of comorbid infections, such as by *Pseudomonas aeruginosa*, due to hypersecretion of mucous and its reduced removal in cystic fibrosis patients [52].

The receptors for these drugs are located either on the cell surface or inside of the cells. The drug solute thus has to pass through this cellular barrier, which is in the bronchi composed of a rather thick monolayer of columnar cells (Figure 2.8) [1,27]. Due to the thickness of the conducting airways, the distance to reach blood vessels is rather long and therefore only small portion of the drug enters the systemic blood circulation.

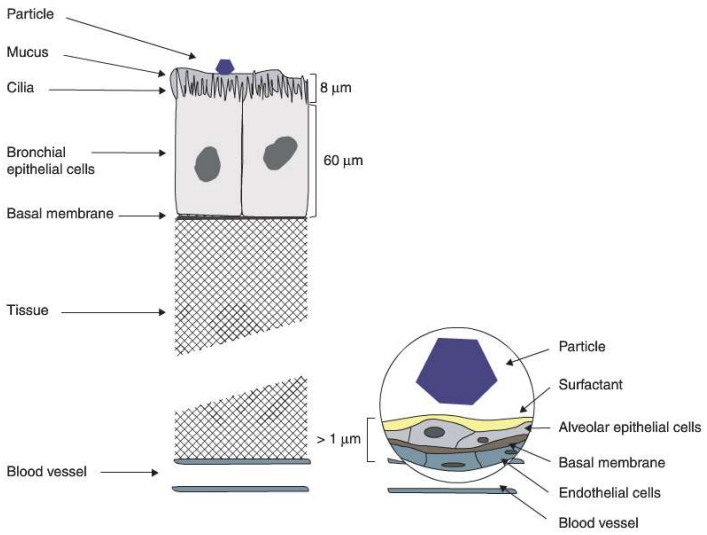

Figure 2.8 Schematic drawing of the bronchial and alveolar physical absorption barrier [53].

2.1.3.2.2 Alveolar region

On the other hand, the alveolar region is typically targeted to achieve systemic drug absorption thanks to the small thickness of alveolar epithelial barrier and the vast blood-capillary network. The cell monolayer is made of thin, broad cells with the distance between the respiratory tract and circulation being approximately 500 nm (Figure 2.8) [1,27]. The advantage of using lungs for systemic delivery of small molecules (*e.g.* nicotine, morphine, fentanyl) is that it offers fast action onset, non-invasiveness, low metabolism, and high systemic bioavailability [2,54]. For example, an inhaled levodopa formulation has been recently (2019) approved in Europe for use in Parkinson's disease, showcasing the attractiveness of this approach [55]. The systemic bioavailability can be considerable also for biological macromolecules (*e.g.* insulin, heparin, growth hormone), however this largely depends on the biomolecule's molecular weight. Up to 30 kDa, the bioavailability is 20 – 50%; however can be notably lower for some molecules due to degradation upon their deposition (*e.g.*by enzymatic hydrolysis, proteolysis). This might be addressed by formulation composition such as by the addition of absorption enhancers or protease inhibitors to the formulation. [56]

2.1.3.3 Clearance

As Hastedt et al. [46] well said "In contrast [to gut], the lungs are designed to *remove* foreign material in order to maintain gas exchange". Thus, instantaneously as an inhaled formulation starts to dissolve, the defence mechanisms try to remove it from the lung surface.

2.1.3.3.1 Tracheobronchial region

Particles deposited in the conducting airways are rapidly ($t_{½}$ ≈ 1-1.5h [57]) cleared by the movement of mucus up towards the trachea and subsequently pharynx, where they are either swallowed or spat out. This process is known as the mucociliary escalator and is ensured by coordinated beating of the ciliated cells. Coughing greatly enhances mucus clearance by moving the mucus faster to pharynx, while failing to clear mucus can lead to obstruction and infection [27].

2.1.3.3.2 Alveolar region

Since the composition of alveolar region is completely different from tracheobronchial region, also the defence mechanism against the foreign particles differs. Clearance of any insoluble or slowly soluble particles deposited in the alveoli is ensured by phagocytosis done by alveolar macrophages. On average, in each alveoli are 12-14 macrophages that ensure this clearance [58]. Their action is rather fast: majority of particles (50-75%) was shown to be phagocytised in 2-3 h, more than 90% by 12 h and almost 100% by 24 h [58,59]. After phagocytosis, the alveolar macrophages remove the particles by either enzymatic degradation, translocation into the lymphatic system, or by moving them towards the ciliated cells [60].

Interestingly, effectiveness of macrophage phagocytosis depends on the geometric particle size. It is most effective for particles with geometric size in the range between 1.5 and 3 μm, while particles with size < 1 μm and >4 μm were found to have reduced uptake [61]. For comparison, the average nuclear size of a human alveolar macrophage is ≈ 8 μm [62]. The particle surface composition also plays a role in the extent of phagocytic clearance. Makino et al. [63] studied the effect of functional groups on the microsphere surface on the macrophage uptake using 1 μm polystyrene particles with primary amine, sulfate, hydroxyl, or carboxyl groups on their surfaces. This study showed that microparticles with primary amine groups were phagocytosed to largest extent, microparticles with carboxyl groups to slightly lower, and other microparticles to much less extent.

2.2 Drug dissolution

Drug dissolution is generally a two-step process: in the first step, the drug molecules are solvated by the solvent at the solid-liquid interface, while in the second step are the solvated molecules transported from the interface into the bulk solution. The first step is controlled by the drug's solubility in the solvent. The second step is then controlled by the transport (diffusion and convection) of the drug molecules [64]. Diffusion rate is influenced by the diffusion coefficient, boundary layer thickness. It depends also on parameters such as dissolution medium agitation intensity, temperature and viscosity, particle size [65].

The dissolution rate (dm/dt) of a solid substance in a liquid medium can be described by the classical Noyes-Whitney/Nernst-Brunner equation [66,67]:

$$\frac{dm}{dt} = \frac{D\,S}{h}(C_s - C) \tag{2.12}$$

where m is dissolved drug amount, t is time, D is diffusion coefficient, S is surface area of solid substance, h is thickness of diffusion boundary layer, C_s is saturation solubility of drug in the medium, and C is concentration of dissolved drug in the medium.

The dissolution process can be limited by either of the two above-mentioned steps. However, it is usually the diffusion that limits the dissolution since molecules have to translocate across large distances compared to molecular dimensions, which are involved in the first solvation step [64]. However, for poorly soluble drugs also solvation can be the limiting step instead. This occurs when the equilibrium solubility (eq. (2.12) is very low in the given medium (Figure 2.7). The surface specific dissolution rate of such poorly soluble drugs can be positively influenced by the decrease in particle size, which directly increases the specific surface area. Additionally, it was

suggested that as well the particle shape can affect the dissolution rate in such a way that irregular particles show lower dissolution rates [68].

The most common techniques for dissolution rate enhancement of poorly-water soluble drugs either focus on chemical modification (*e.g.* salt or co-crystal formation, complexation with excipients) or on physical modification of the drug such as the particle size reduction or crystal habit change (*e.g.* polymorphic change, formation of amorphous solid dispersion) [69].

2.2.1 Particle size reduction

Particle size reduction by micro- and nanonisation is one of the frequently applied techniques for improvement of dissolution rate and is one of the few techniques that does not require change in chemical composition of the drug. Though when applied to create nanoparticles, it is often desirable to use stabilizers to prevent agglomeration and crystal growth, which occur as a results of the system trying to reduce its free Gibbs energy. This makes the nanocrystals thermodynamically unstable causing Ostwald ripening or particle agglomeration. [70] Particle size reduction to nanosize range is especially of interest for dissolution rate enhancement since the specific surface area dramatically increases below 1 µm (Figure 2.9) due to its inverse proportionality to particle size.

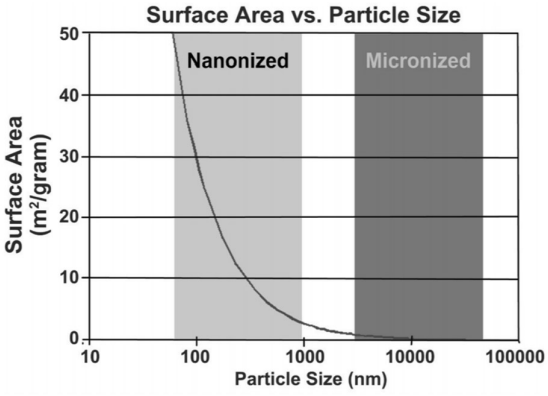

Figure 2.9 Specific surface area as a function of particle size [71].

The particle size reduction and to it related increase in the surface curvature can also marginally improve the dissolution rate by increasing the solubility of nanoparticles as described by the Ostwald-Freundlich equation:

$$C_r = C_\infty exp\left(\frac{2\gamma M}{r\rho RT}\right) \tag{2.13}$$

where C_r and C_∞ are the solubilities of a particle of radius r and of infinite size. γ, M, and ρ are interfacial tension at the particle surface, the molecular weight of the solute, and the density of the particle, respectively [72].

2.2.2 Drug nanoparticles

Drug nanoparticles have gained importance in pharmaceutical research and industry in the recent years, as evidenced *e.g.* by numerous wet media milled drug products for oral and parenteral use on the market [73].

The techniques for production of nanoparticles are of two characters: top down, where nanoparticles are created by breakage of larger particles, or bottom up, where nanoparticles are built from molecular scale [74]. Top down approaches include milling (*e.g.* wet media and jet milling) and homogenization (*e.g.* high pressure, jet stream, piston-gap). Bottom up approaches include solvent evaporation and precipitation techniques for example by dissolving the drug in a solvent to supersaturation level and inducing precipitation by adding an antisolvent [12,75,76]. Most commonly, the nanoparticles are maintained suspended in a liquid, forming a nanosuspension. Nanosuspensions have the potential to provide high drug load as they might contain as little as 10% of stabiliser [77]. Typical stabilisers used in wet media milling, which was employed within this work, are Poloxamer 188 and 407, Polysorbate 80, D-α-tocopherol polyethylene glycol 1000 succinate (TPGS), cellulosics, polyvinylalcohol, or sodium dodecylsulphate [78]. Stabilisers however usually provide only short or medium term stability. In order to achieve long term stability, it is desirable to dry the nanoparticles into a powder. This is usually done using the freeze or spray drying techniques (chapter 2.3.1.2.1).

2.2.2.1 Wet media milling

Wet media milling represents one of the commonly used top-down approaches for nanoparticle production. During the milling process, the suspended material is ground by shear and compression forces between the grinding media, which is given kinetic energy from a rotating shaft and stirring elements. The specific energy input ($E_{m,P}$) of the process is proportional to the number of milling stress events and their energy. The milling stress events are affected by the milling time and the grinding media's amount, density, size, and relative velocity [79]. The information on the specific energy input can be calculated by application of equation (2.14:

$$E_m = \frac{\int_0^t (M(t) - M_0)\omega dt}{m_p} \tag{2.14}$$

where *M(t)* is the torque measured during milling, M_0 is the no-load torque, ω is the stirrer angular velocity, and m_p is the product mass.

Knowledge of the specific energy is crucial for the outcome of the process, experiment repeatability, and process scale up. The milling result is affected also by the operation mode of the mill, by the formulation of the suspension as well as the mill geometry. Numerous poorly water-soluble drugs have been nanomilled in the last 15 years [80] with median particle sizes ranging from < 100 nm [81] to ≈ 650 nm [82] or even larger in screening studies [83]. Unfortunately, only few studies [84–87] related the obtained nanoparticle sizes to the $E_{m,P}$.

2.3 Dry powders for inhalation

Chapter 2.1 described the theory of aerosol deposition as well as subsequent fate of the particles in the lungs. However, an understanding of the aerosol formulation preparation and its properties as well as characterisation is still missing.

There are three major types of inhalers that can be used for delivery of drugs to the lungs: nebulisers, pressurised metered dose inhalers (pMDIs), and dry powder inhalers (DPIs). In nebulizers, the drug is suspended or dissolved in water, whereas in pMDIs it is suspended or dissolved in a liquid propellant. The propellant is typically a hydrofluoroalkane and is kept under pressure in a canister. Dry powder inhalers are devices where the drug powder or drug-containing powder is stored in a capsule or reservoir. In DPIs, the patient's inspiration provides

energy for aerosolisation of the powder bed. Unlike the pMDIs, they do not require coordination of actuation and inhalation. They are also environmentally friendlier due to lack of any propellant. However, the delivery greatly depends of patient's inspiratory flow and as in case of all the inhaler types, on correct inhaler use. [88]

Irrespective of the inhaler type, the formulation should have upon dispersion aerodynamic particle size distribution (APSD) favourable for successful deposition in the target area of the lungs (Figure 3.7.) As mentioned, it is widely accepted in the scientific community that the aerodynamic particle size range for efficient pulmonary delivery is 1-5 μm. This range has been assessed based mainly on *in vivo* studies of radiologically labelled formulations.[35] As indicated in equation 9, the aerodynamic particle size depends mostly on the equivalent volume diameter, which is then greatly guiding the formulation performance.

There are two approaches for preparation of dry powders for inhalation – traditional, carrier-based approach, and an engineering approach. Majority of the marketed DPI formulations use the traditional system where small drug particles cover surface of a much larger carrier, usually lactose. During inhalation part of the drug deagglomerates and enters the lungs. Since the drug particles have density close to or slightly greater than 1 g/cm^3, the aerodynamic particle size is larger than the geometric particle size of the drug particle.

The engineering approach is currently used only in very few marketed products (*e.g.* TOBI® Podhaler™, Colobreathe® Turbospin) [89] and relies on the large porous particles [6]. In this approach, the drug is embedded within an engineered particle, which usually comprises also other excipients. The density of such particles is typically a lot smaller than 1 g/cm^3, which allows the geometric particle size to be larger than in case of the traditional approach, while achieving same aerodynamic properties as smaller but denser particles.

2.3.1 Preparation of dry powders for inhalation

2.3.1.1 Traditional approach

Most traditional DPI formulations contain either drug particles alone or blend these with a carrier (Figure 2.10). The drug is usually micronised by jet milling to achieve the respirable particle size range of 1-5 μm. However, this process can yield highly cohesive powders and offers only limited control over the particle size distribution and morphology. To help deaggregation of the usually rather cohesive particles, the drug is often blended with a much larger carrier (*e.g.* lactose with median particle size ≈ 100-150 μm) to form an adhesive mixture. Here, the interactions between the drug and the carrier have to be balanced to ensure that the mixture is on the one hand stable and homogenous throughout the production process (such as blending, encapsulation, blistering) but on the other hand allows detachment of the drug from the carrier during inhalation. To improve even more the performance of these formulations, force control agents (*e.g.* magnesium stearate, lactose fines) are sometimes added to the blends [51,90,91].

Although well-established, this system does not allow high drug load and the fraction of drug delivered to the lungs is usually rather low (10-30%) [92,93].

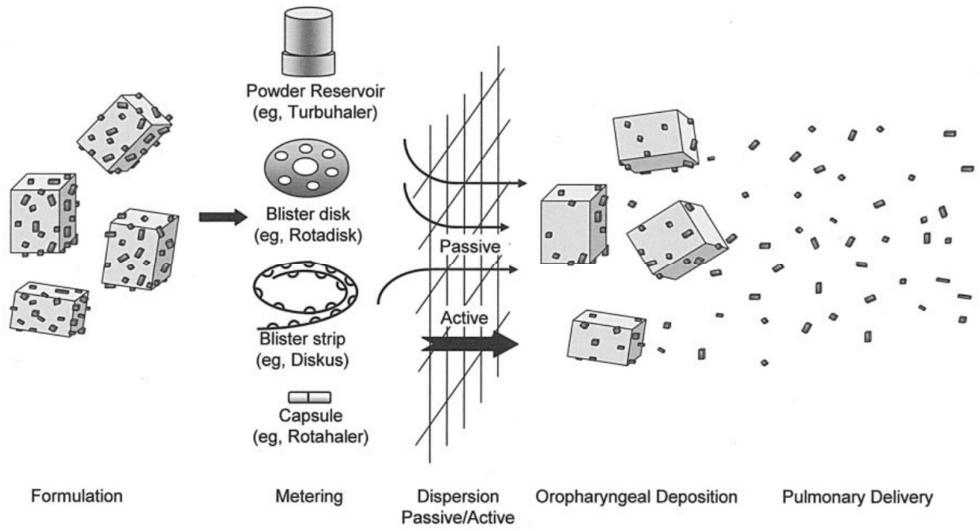

Figure 2.10 Principle of carrier-based, traditional dry powder inhaler formulation [88].

2.3.1.2 Engineering approach

Another approach for preparation of DPI formulations is to use bottom up techniques such as spray drying, freeze drying, or supercritical fluid technology. These techniques offer better control of the particle size distribution and morphology and allow also formulation of therapeutic biomolecules. For example freeze drying has been advantageously used for production of large porous particles that have large geometric size (up to 20 μm) but thanks to low density ≈ 0.1 g/cm^3) reach desirable aerodynamic sizes for high lung deposition (50-60%) [6]. Theoretically, geometrically large particles should also have smaller contact area and thus lower extent of cohesive forces between the particles [94], which should improve handling and dispersibility [95]. However, for this effect to be pronounced the difference in the particle size would likely have to be in the orders of magnitude rather than increase by units of micrometres. The drug loading of these particles as well as fraction of the delivered drug dose is usually higher (40-70%) [93]. Great benefit of this approach is also that one can embed drug nanoparticles within the microparticles and deliver them to the lungs. This is important especially for poorly water-soluble drugs, whose dissolution can be enhanced by the particle size reduction (chapter 2.2). Spray drying is often the process of choice for production of engineered particles [89].

2.3.1.2.1 Spray drying

Spray drying is a rather versatile, one-step process in which a liquid feedstock is within milliseconds transformed into dry powder. It has three distinct stages: atomisation of feedstock into droplets, droplet drying, and solid particle collection. Atomisation guides to a large extent the initial droplet particle size. Right after the atomisation, a droplet is formed and the solvent starts to evaporate. Initially, the droplet size does not decrease much as the droplet temperature increases to its wet-bulb temperature. After this, the solvent starts to rapidly evaporate and the droplet shrinks. Depending on the solutes' critical supersaturation concentration, a skin formation occurs and the particle quickly solidifies [96].

In spray drying, the droplet evaporation and particle formation kinetics are governed by coupled heat and mass exchange processes [96], which can be influenced directly or indirectly by the process and feedstock properties. Among the process properties belong inlet and outlet

temperature, drying gas flow, and atomising pressure. Feedstock properties are feedstock flow rate, solids content, as well as solutes' saturation levels.

The drying process can be described by a dimensionless Péclet number (Figure 2.11) [8]. This number (eq. 2.15) compares the rate of droplet surface reduction (*i.e.* evaporation rate κ) to the diffusion of the solutes in the droplet (D_i) [96]. The evaporation rate is directly related to the temperature of the drying gas and its relative humidity, while the diffusion coefficient controls how fast dissolved or suspended solutes redistribute inside of the shrinking droplet. [97]

$$Pe_i = \frac{\kappa}{8D_i} \tag{2.15}$$

Particle formation theoretically occurs at low or high Péclet numbers. In both cases, as the droplet shrinks, the solute concentration close to the droplet surface increases. The result of the drying however depends on the Péclet number:

a) Drying at low Péclet number (Pe < 1) occurs when the evaporation is slower compared to the diffusion of the solutes. During such drying process, the solutes have enough time to diffuse along the concentration gradient from the droplet surface towards inside of the droplet. Thus, solid particles with density close to the skeletal density of the solute are likely to form.

b) If the evaporation is faster than the diffusion of the solutes, the Péclet number is larger than 1. The solutes, which are in higher concentration close to the surface of the droplet, do not have time to diffuse and thus precipitate and create a shell. [8,98] Density of such particles is naturally smaller than the skeletal density. Also spray drying of suspended (nano)particles follows similar path because the suspended material can be considered immobile compared to the receding droplet surface [8]. When producing the low-density particles in this way, one can use either a high molecular weight solute, which intrinsically has a small diffusion coefficient, or a solute that precipitates quickly in the drying process and thus becomes immobile (form example leucine, trileucine [8]). Successful formation of a shell composed of nanoparticles has been proven to be possible numerous times [98–100].

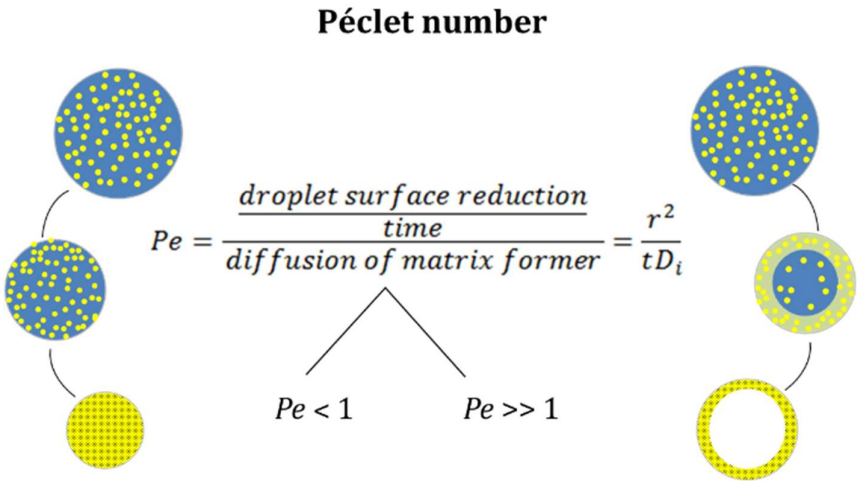

Figure 2.11 Péclet number representation (*r* is the droplet radius, *t* the droplet drying time, *Di* diffusion coefficient of solute).

However in reality, the diffusion coefficient of a component changes with concentration and composition of the solvent. Hence, the Péclet number changes as the droplet evaporates [8].

Application of particle engineering in spray drying thus allows tailoring both the geometric diameter as well as the particle density. The diameter can be tailored mostly by controlling the droplet size through atomising pressure in the spray nozzle and, to lower extent, by the feed solution concentration. Density, on the other hand, can be lowered by choice of drying conditions and formulation properties that support drying at high Péclet numbers [8].

2.3.2 Use of particle engineering for DPI formulation manufacturing

The possibility to control the resulting particle properties is very beneficial for tailored manufacturing of DPI formulations. Aside from an improved aerodynamic performance, the aerodynamic particle size can be tailored to some extent to target either more the bronchial or the alveolar region by changing the APSD profile.

Larger geometric particle size is also beneficial as the drag force increases linearly with geometric particle size (chapter 2.3.4.2). Compared to force of gravity, the drag force F_D of particles <10 μm is at least four orders of magnitude higher than F_G even at relatively low air velocities of 20m/s. Therefore, even at the same aerodynamic particle size, the chance to remove by an air stream a larger adherent particle from a surface is higher compared to a smaller one [101]. Additional benefit of larger geometric particle size can be the expected reduction of phagocytic clearance in the alveolar region, which as described earlier is a size-driven process (chapter 2.3.3.2).

Particle engineering by spray drying has been successfully utilized numerous times using many different drugs [102–107]. Duddu et al. [108] for example prepared PulmoSpheres™ (same technology as used in TOBI® Podhaler™) budesonide formulation that is able to deliver 57% of the nominal drug dose. Excipients such as phospholipids (distearoyl phosphatidylcholine, DPPC), lipids (cholesterol, lecithin), or amino acids (leucine, glycine) were often employed as well as various solvents (ethanol, methanol isopropanol, dichloromethane). The usage of the solvents is of concern since organic solvents have no therapeutic benefit, inherently have a certain level of toxicity, and cannot be fully removed from the product. Therefore, their usage should be limited as much as possible and their residual levels need to be closely monitored as instructed by the ICH Q3C guideline [109]. Thus, avoiding the organic solvents completely is the safest option at hand. Large porous particles have been mostly produced by spray drying of a double emulsion with various excipients as matrix formers (*e.g.* poly(lactic-co-glycolic) acid, cyclodextrins, DPPC in combination with hyaluronic acid or other excipient) [110]. Most often, the drug in such formulations was either dissolved in water or in any of the co-solvents, or used as drug suspension. Less frequently were the drugs, especially poorly water-soluble ones, pre-processed to nanosize range [111].

Despite the numerous advantages the engineering approach has, it is rarely used in the pharmaceutical industry since drying the technologies required for particle engineering are considerably more expensive than the techniques applied within the traditional approach. The high production costs would of course reflect in the commercial drug product price, which might not be competitive for the common respiratory diseases.

2.3.3 Pulmonary delivery of nanoparticles

The challenge in effective delivery of nanoparticles to the lungs is that, under normal circumstances, nanoparticles are too small to deposit in the lungs (Figure 2.5). Once inhaled,

nanoparticles are very likely to be exhaled as the time required for their deposition by diffusion is greater than the breath-holding time.

However, similarly as microparticles, nanoparticles can still be delivered into the lungs by inhalation of a colloidal suspension, or as dry powders. Nebulised formulations can consist of stabilised nanodispersion, powders for redispersion before usage, or drugs encapsulated in polymeric or lipid nanoparticles [75,112]. Solid formulations are usually preferable as they ensure better physical and chemical stability due to limited molecular mobility [112]. In the dry state, nanoparticles can be delivered to the lungs by using:

- composite microparticles with drug nanoparticles
- composite microparticles that contain nanoparticles with drug encapsulated within the nanoparticles,
- neat nanoparticles aggregated into microparticles.

2.3.3.1.1 Composite microparticles with drug nanoparticles

In this approach, which has been applied also within this work, the drug itself is in the form of a nanoparticle. The drug nanoparticles are then with help of excipients (amino acids, sugars or phospholipids) formulated in a subsequent process into microparticles [25]. Freeze- and spray drying are commonly used processes for microparticle formation. The advantage of this approach is that thanks to the nature of the nanoparticles the drug load can be maintained rather high and is not affect by encapsulation efficiency. The presence of excipients can on the other hand aid to dissolution of the microparticle once it lands on the lung surface.

2.3.3.1.2 Encapsulation of drug into nanoparticles

In this type of formulation the drug substance is encapsulated into nanoparticles. In the past, very often the drug was loaded into purchased or prepared nanoparticles made out of polystyrene, polyacrylate, colloidal silica, chitosan/tripolyphosphate, gelatin, or biodegradable polymers such as poly(butylcyanoacrylate) and poly(lactic-co-glycolic acid) [113–116]. Among the explored drug substances, which have been loaded into the polymeric nanoparticles, were for example aspirin and salbutamol sulphate [100], doxorubicin [114], ciprofloxacin [115], or macromolecules [117,118]. Loaded nanoparticles were usually dispersed in a matrix carrier (*e.g.* lactose, mannitol, trehalose) and spray dried. The encapsulation efficiency is however usually rather low, limiting greatly the amount of drug that can be delivered at once.

2.3.3.1.3 Nanoparticles aggregated into microparticles

As aggregated nanodrugs have been formulated mainly, but not only, poorly water-soluble drug substances, *e.g.* terbutaline sulfate [119], salbutamol sulfate [120], nifedipine [121], itraconazole [122], or paclitaxel [123]. Such formulations contain only the drug and possibly a stabiliser and are aimed to be hollow or porous. Thus, when prepared by spray drying, they adopt low density owing to very low mobility of the nanoparticles compared to evaporation rate.

2.3.4 Forces in powders

During manufacturing and administration of a DPI formulation, the powder particles are exposed to several forces irrespective of the adopted formulation approach. During the manufacturing, it is mostly the attractive interparticulate forces (of cohesive or adhesive character) that keep the particles together and possibly cause particle agglomeration to greater or lesser extent (chapter 2.3.4.1), while during usage forces that cause the particles' dispersion upon inspiration also play a key role (chapter 2.3.4.2). Fine balance between these forces needs to exist especially within

the traditional approach where the formulation has to remain homogenous and flowable throughout the manufacturing process but it also needs to successfully aerosolize during inhalation [124]. Homogeneity is less of a problem for the engineered formulations as each particle composition should be, theoretically, the same. However, as these formulations contain very fine particles (< 10 μm) flowability can pose a challenge during manufacturing.

2.3.4.1 Forces affecting particle cohesion/adhesion

Inhalation dry powders are formulations of ideally homogenous character in which attractive forces between the particles (drug-drug, drug-carrier, spray dried particle-spray dried particle) naturally exist. They can be of cohesive or adhesive character, depending on the surface energies of the system components. In the carrier-based formulations, they are responsible for adhesion of the drug particles to the carrier surface and it is desirable that they are strong enough to ensure formulation homogeneity. The extent of the attractive forces depends on many factors such as (but not only) particle size, shape, surface roughness and morphology, density and porosity, moisture content [125–127]. The cohesion forces are in fact directly proportional to the particle diameter (Figure 2.12).

Among the most common attractive interparticulate forces experienced by DPI formulations are van der Waals, electrostatic (which can be also repulsive), and capillary liquid forces. The van der Waals and capillary forces are major attractive forces for particle sizes < 10 μm [101]. The capillary forces are the dominant forces above a critical RH level (65-70%) [51,128]. As the relative humidity during formulation production can be controlled, it is mostly the van der Waals forces that cause agglomeration of small particles and lead to poor flowability and dispersibility of powders made of such particles. These forces are caused by the dipole-dipole interactions of the molecules and play role when the separation distance between the surfaces is below 50-100 nm [101,129]. The overall van der Waals forces will increase with increase in the surface contact area as in case of *e.g.* two flat surfaces [130]. For this reason, it is advantageous to formulate DPI formulations as spray dried powders, or blend the drug particles with carriers as done within the traditional approach, to prevent extensive agglomeration and improve dispersibility [131]. The dispersibility of the spray dried particles can be improved even further when the particles have corrugated surface as this lowers the contact area even more [101,132].

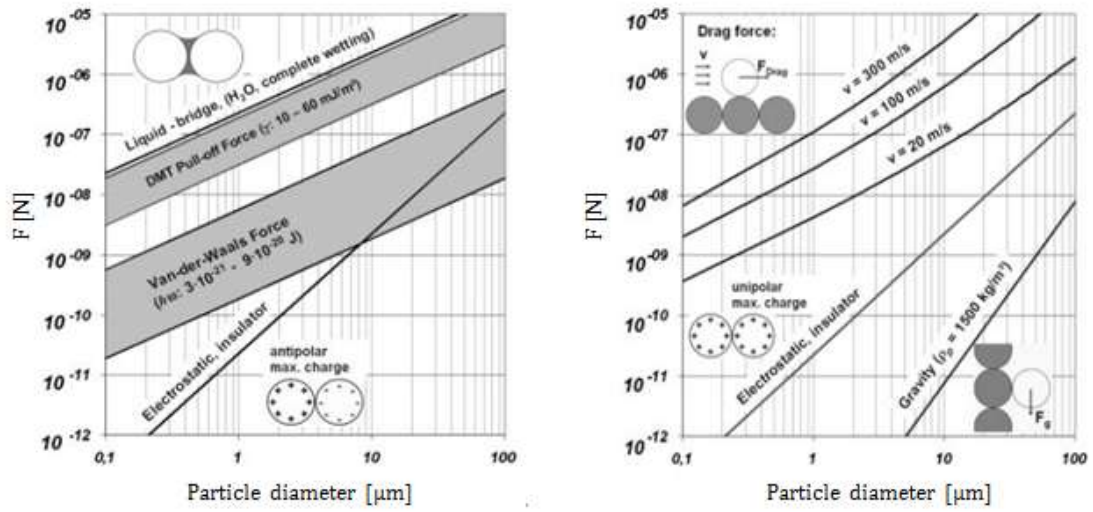

Figure 2.12 Left: Theoretical cohesion forces of two contacting, rigid, insulated, and spherical particles. Right: Theoretical forces influencing the separation of adhering spherical particles.[101]

2.3.4.2 *Forces affecting particle aerosolisation*

Particle of sizes < 10 µm are mostly influenced by the above-mentioned cohesive forces and gravitational forces are more pronounced only for particles in the upper micron-size range (Figure 2.12). Powder aerosolisation, caused most often by an air stream from patient's inspiration, puts energy into an otherwise static powder bed and leads to powder fluidisation. At the same time, a drag force acts on the adhered particles within the powder. When the drag force is greater than the attractive interparticulate forces, it leads to successful particle detachment and inhalation of the drug or drug-containing particle. The drag force increases linearly with particle size at *Re* < 0.5 and exponentially with higher *Re*. This leads to higher chance of particle detachment in case of larger particles compared to a smaller one [101]. However particles < 20 µm are difficult to aerosolise as they lift as an agglomerate due to the interparticulate forces being considerably larger than the drag forces [133,134]. The aerosolisation efficiency is in practise directly related to the inhaler's resistance and the inspiration flow rate [131].

2.4 Characterization of inhalation powders

Just as any pharmaceutical product, also powders for inhalation are tested to assess their quality and to ensure that the patient receives the expected drug dose. Health authorities commonly require monitoring of the delivered dose uniformity and fine particle dose in the inhaled drug products, as well as their adequate quality [135]. Other tests might be given by certain international bodies and their guidelines, such as the ICH [109].

Further tests like physical-chemical characterization (*e.g.* particle size distribution, water content, X-ray powder diffraction, *etc.*) or blend and content uniformity of the drug product might be performed to ensure control over some of the above-mentioned aspects. Other tests like a dissolution test might be done to not only control the product quality but also to study the drug's release kinetics and to potentially draw conclusion on bioavailability in case an *in vitro-in vivo* correlation (IVIVC) has been established. However, establishment of an IVIVC has been possible so far only for certain categories of oral drug products [136]. For this, different USP dissolution methods are being used, which mimic reasonably well the *in vivo* situation in the gastrointestinal

tract. An IVIVC for inhalation products has however not yet been established due to the many challenges the method establishment entails. A clinical bridging study is usually necessary to compare the safety and efficacy the products that wish to claim bioequivalence [137]. One of the crucial missing tools is the dissolution rate assessment possibility although it has been of researchers' as well as authorities' interest for many years now [15,16,46,138]. Yet up to now, there is no official pharmacopoeial dissolution method for inhalation products due to the many difficulties faced with the *in vitro* method establishment (chapter 2.4.2).

Another aspect of the IVIVC is also the response against which is the *in vitro* data correlated. This is often done against the drug's pharmacokinetic parameters such as the concentration or area under curve [139]. These can be obtained from clinical, safety, efficacy, or toxicological studies, which are conducted on humans and/or animals during the drug product development. Yet it is debatable how relevant are the plasma levels for locally acting drugs. The measured drug levels might have only very limited validity in terms of the therapeutic effect caused by the drug. Therefore the *in vitro* data might rather be correlated with a quantifiable effect that the drug has (*e.g.* forced expiratory volume in one second). However, precious resources are used in the studies and in case of the animal studies, the study subjects usually have to be sacrificed. For ethical reasons, the animal studies should then be limited to as few as possible and *in vitro* assays should be leveraged on more frequently [40]. For this, it is desirable that the models and techniques applied can provide results that are representative of those that would be obtained from *in vivo* or *ex vivo* studies. Also computational fluid dynamics is starting to greatly contribute to better understanding the complex lung system especially in terms of deposition but also this system still need an in vivo validation [140].

2.4.1 Aerodynamic evaluation

Pharmacopoeias require that all products intended for pulmonary delivery are assessed for delivered dose uniformity and aerodynamic particle size distribution [135]. For the former, for example a dosage unit sampling apparatus can be used, while for the latter it is mainly the impactors. An impactor is a device that classifies particles or droplets of a formulation according to their aerodynamic particle size (Figure 2.13). The European Pharmacopoeia lists four devices capable of such classification, namely the glass impinger, the multi-stage liquid impinger, the Andersen cascade impactor, and the next generation impactor [141].

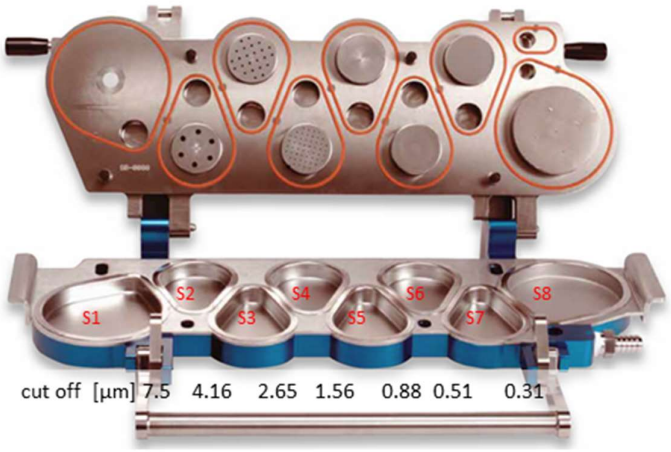

Figure 2.13 Next generation impactor (NGI) with indication of the cut off diameters at 68 L/min. Adapted based on [142].

These tools are indispensable in pulmonary formulation development as they characterize the formulation's aerodynamic properties by its classification according to aerodynamic particle size. Deposition mechanism employed during the classification is inertial impaction (discussed shortly in chapter 2.1.2.2) and its principle is schematically shown in Figure 2.14. The NGI body consist of eight sets of nozzles and impaction cups. As the air is drawn through the NGI, the number of nozzles gradually increases from one nozzle in stage 1, to 52 nozzles (stage 4), and eventually to 4032 nozzles in stage 8. At the same time, the nozzles' diameters decrease and thus the air velocity passing through the nozzles increases.

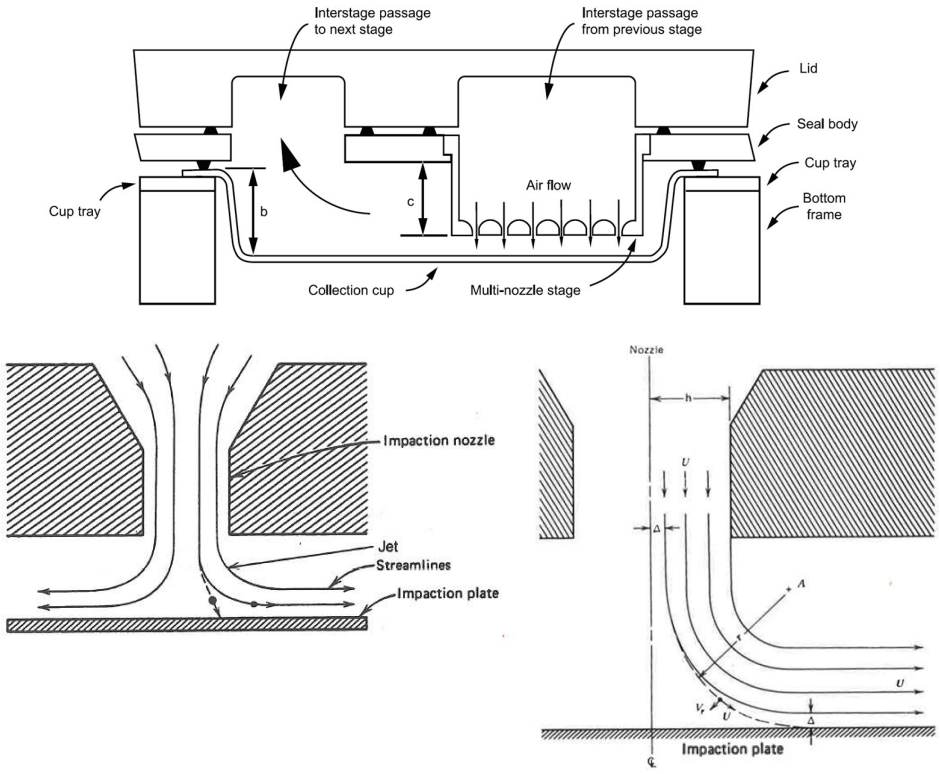

Figure 2.14 Configuration of interstage passage (top) [141] and the principle of classification by impaction (below) [4].

During the experiment, aerosol particles are aerosolised and carried by an air stream from the inhaler through the body of the impactor from stage 1 to stage 8. Due to the impactor's geometry, the streamlines suddenly change direction at almost right angle several times. Particles with too large inertia are unable to follow the streamlines, follow their trajectory and deposit on the impaction cup plate. Particles that follow the streamlines continue to the next stage at higher velocity and in the next stage same scenario occurs however at lower cut off diameter. The impaction and therefore also the collection efficiency is governed by the Stokes number (eq. (2.16), which is defined as "the ratio of particle's stopping distance at the average nozzle exit velocity (U) to the jet radius ($D_j/2$)":

$$Stk = \frac{\rho_P d_P^2 U C_c}{9\eta D_j} \tag{2.16}$$

where $\rho_P$is the particle density, $d_P$is the particle diameter, C_c *i*s the Cunningham correction factor, and η is the dynamic viscosity [4].

For evaluation of the aerodynamic performance, the so called fine particle mass (FPM) or fine particle fraction (FPF) are calculated. The FPM or FPF are the mass or ratio of the drug amount below the aerodynamic particle size of 5 µm, respectively. In case of FPF, the ratio can be related to the expected drug amount in the formulation (declared content) or drug amount recovered in the impactor components (delivered content). From the impaction measurement can be also calculated the mass median aerodynamic diameter, which is the aerodynamic diameter below which falls 50% of the drug amount [143].

2.4.2 *In vitro* dissolution testing of DPI formulations

As it was already mentioned, there have been several attempts to create suitable *in vitro* dissolution test setup for inhaled products [144]. Among the tests employed so far are modified versions of the paddle (USP2)/paddle-over-disk (USP5) apparatuses [145–147], flow-through cell apparatus [146,148], and diffusion-controlled systems, such as the Transwell insert [149–151] or the Franz cell [146]. However, great variability exists among the methods used, mainly in terms of dissolution media volume. In general, the methods might be split into two groups: one for which large media volumes are required (ranging between 100 mL and 1000 mL), usually given by size of the test equipment [152,153], and a second group where small volumes (< 5 mL) are sufficient. Little bit more unity exists in terms of dissolution medium: predominantly PBS at pH 7.4, with and without surfactants, was the dissolution medium of choice in both groups. This medium offers a good buffering capacity compared to the complex simulated lung fluids [147]. In the majority of cases, the tested powders were separated from the bulk liquid by a membrane forming a barrier between the particles and the liquid. Several polymeric membrane materials have been used, with polycarbonate being the most employed one [18]. The tested powders were often collected from an impactor, however either only from one impactor stage or only powder below certain aerodynamic size (*e.g.* 5 μm). Rarely have particles from more than one impactor stage been compared though it could be expected that due to the different geometric particle size these particles possess their dissolution behaviour might vary.

In a study comparing the different methods, May and co-workers [146] reported that the modified UPS2 paddle apparatus showed optimal reproducibility with the best discrimination power. On the other hand, the Transwell setup use has been advocated due to use of low liquid volumes as this resembles more closely the *in vivo* fluid volume. Yet, it does not mimic the absorption-induced concentration gradients and exchange of fluids that occur *in vivo* [18]. Also the need for surfactants in the small-volume receiver compartment introduces a degree of arbitrariness. The concentration gradient experienced *in vivo* might be mimicked better by having a compartment with low liquid volume where the drug dissolves and then permeates to a larger, sink-conditions maintaining compartment. Such setup has only recently been proposed, namely with the Inhalation Sciences' proprietary Dissolv*It*® module [154]. However, its usage in a standard laboratory setting is due to the proprietary nature of this system close to impossible.

2.4.3 *In vitro* ADME testing

In vitro tests are often very useful but they have a clear disadvantage of missing any input that could be gained from an interaction with a biological system. Without a clearly established IVIVC or a conducted clinical test, it is very difficult to judge on the permeability or metabolism, let alone the bioavailability of a drug upon its deposition. To shed light on drug's bioavailability, which is affected on the one hand by its dissolution, but on the other hand also by it absorption, distribution, metabolism, and excretion (ADME), experience with living cells (primary or immortalised cell lines) is often desirable [139]. Aside from a direct clinical experience and animal models, testing of the interactions of particles with lung cells is usually done on *ex vivo* models, mainly on the isolated perfused lungs [30]. The ultimate goal of many researchers is to develop model system with *in vitro* cell cultures to avoid the unnecessary, ethically problematic, and expensive animal or human testing. A great step ahead in this direction with a significant potential presents the lung-on-a-chip microfluidic device, which has the first time emerged around ten years ago and that is being used for disease modelling, drug development, or toxicological studies [24,155]. Though due to its complexity it is not a commonly used tool.

Indtead, pulmonary cells cultures are used by researchers to study and possibly also to predict the fate (*e.g.* ADME, dissolution) and toxicological effects of drug particles once they land on the lung surface. As stated earlier, the composition of the lungs varies with the increasing generation number. Therefore, also the cell culture models used for testing should reflect the region in which particles are expected to deposit. There are *in vitro* models for tracheobronchial as well as alveolar epithelium, with each of this group having the possibility to use primary cell cultures or immortalised cell lines.

2.4.3.1 Tracheobronchial cell cultures

The tracheobronchial primary cell cultures can be obtained from different species (mouse, hamster, rat, dog, pig, cow, human, *etc.*) [28]. Though the primary cells generally provide the best correlation to the real *in vivo* conditions, especially the human primary cell are very difficult to obtain in amounts sufficient for more comprehensive studies. For drug absorption studies, the primary cell cultures are unfortunately suitable only for couple of subcultures. Afterwards, they lose the ability to form tight junctions [28]. Generally, primary cultures areless convenient and economical than the immortalised cell lines. Aside from the reduced costs, the use of the cell lines is advantageous because of their lower variability. Most commonly used are the Calu-3 and the 16HBE14o- cell lines. Calu-3 is an adenocarcinoma cell line used mainly for permeation studies and employed for the investigation of metabolic processes, and was used also in a number of particle-cell interaction studies [156]. This cell line grows in monolayers, forms ciliated and secretory phenotypes but the cilia are highly irregular. It also produces a mucus layer when grown at ALI.

2.4.3.2 Alveolar cell cultures

Primary cultures of alveolar epithelium are usually isolated from animals such as mouse, rat, rabbit, and pig, and from humans undergoing lung resection surgeries. They are used for most studies of alveolar functions like solute transport and metabolism because the cell lines do not form as good tight junctions. In human alveolar epithelial cells (hAEpC) was also observed the presence of caveolin-1 and thus they may be beneficial for study of the caveolae-facilitated transport of macromolecules [14]. Unfortunately, the alveolar epithelial cells exhibit very limited proliferation profile and are not suitable for passaging. The most frequently used alveolar cell line is the A549. It is a cell line of adenocarcinomic human alveolar basal epithelial cells. This cell line has some important biological properties of alveolar epithelial type II cells such as the surfactant secretion when grown on air-liquid interface [30]. It is thus widely used as an *in vitro* model for a type II pulmonary epithelial cell model. Its primary use is for toxicity studies as it shows only a limited ability to generate functional tight junctions, although it stains positively for zonula occludens-3, occludin, and claudin-2 [22].

2.4.3.3 Use of cell cultures for DPI formulation assessment

Cell cultures are mostly used under submerged conditions, which is a suitable approach for most drug delivery routes. However, pulmonary drug delivery presents a challenge as the submerged conditions do not properly reflect the in vivo system where ALI exists. A thin surfactant layer on top of the cells can be achieved when using for example the A549 cells. The surfactant forms when the cells are exposed to air for at least 5h [22]. Mimicking the *in vivo* situation in terms of liquid amount and composition in the cell culture system is crucial when studying the interaction of deposited particles or droplets with the lung epithelium [46,157]. Even better might be the use of a 3D co-culture model consisting of epithelial cells (A549 or 16HBE14o-), alveolar

macrophages, and dendritic cells. In fact, *in vivo* the cells continuously cross-talk through intercellular signalling to maintain homeostasis and to coordinate immune responses [158]. Thus such am *in vitro* model resembles very closely the *in vivo* situation [30].

Studies that combine aerodynamically classified deposition and cell interaction are still rather rare. In some reports, pharmacopoeial instruments such as the twin-stage impinger [159,160], multistage liquid impinger [161,162], and Andersen cascade impactor [163,164] were transformed to accommodate a cell culture system. In one instance, also the NGI was used but without any description of the NGI transformation [165]. It is important to note that deposition in all these systems is based on impaction, which might induce certain cell stress [53]. More gentle deposition, however without aerodynamic classification, can be ensured using sedimentation-based systems, *e.g.*, the Pharmaceutical Aerosol Deposition Device on Cell Culture (PADDOCC) [166], Air-Liquid Interface Cell Exposure (ALICE) [167], or LTC-C Computer-Controlled Long-Term Cultivation (CULTEX®) system [168]. Alternatively, insufflators such as MicroSprayer IA-1C could also be utilized for bulk powder deposition [22,169]. In the above-mentioned experiments where deposition was combined with cell interaction, immortalised, bronchial Calu-3 cell line were most commonly used. These are thus mostly relevant for study of the particle fate in the bronchial region. So far, alveolar cell lines have not been used for deposition studies.

Chapter 3

3 Production of fast-dissolving low-density powders for improved lung deposition by spray drying of a nanosuspension

3.1 Summary

We combined high-energy wet media milling and spray drying to engineer dry powders for inhalation consisting of geometrically large, low-density particles with superior aerodynamic properties and fast dissolution. Péclet number proved to be a useful instrument to guide choice of the additives and process conditions for generating low-density powders by spray drying. Composite dry powders consisted of milled and stabilized budesonide nanoparticles, leucine or albumin as matrix formers, and ammonium carbonate as a pore former. Powders of different composition showed fairly large and comparable geometric particle sizes ($d_{e,50}$ > 4.4 µm) with effective densities strongly depending on the present matrix former. Powders with lowest density reached an aerosol performance of up to 60%, which is well above most commercial, carrier-based products. It was also demonstrated that the nanomilling step was indispensable to yield such good aerosol performance. Dissolution of aerodynamically classified particle fractions showed a very fast onset and was largely completed within 30 minutes irrespective of the formulation and the impactor stage. Mathematical kinetic modelling was used to deduce the API dissolution rate coefficient from the results obtained using a modified USP 2 apparatus. Dissolution rate was found to be determined by the properties of the API nanoparticles rather than those of the composite particles. The employment of industrially established, solely water-based processes allows introducing the presented approach as a platform technology for the development of well-performing pulmonary formulations.

3.2 Introduction

For many years, pulmonary drug delivery has been an established route of administration for drugs that tackle lung diseases (*e.g.* asthma, cystic fibrosis, COPD) and has recently become interesting for drugs of indications unrelated to lungs, such as diabetes or pain management; additionally it is explored for administration of vaccines and gene therapy [54]. The majority of the marketed dry powders for inhalation (DPIs) formulations are based on the conventional approach where the drug particles cover the surface of a much larger (median particle size ≈ 100 µm) carrier, usually lactose.

Although well-established, this system has several disadvantages such as poor control over the formulation performance, different drug delivery efficiency if formulated as mono compound or in combination with other drug(s), performance dependence on the inhalation flow rate, lack of high drug load possibility, and rather low fraction of drug delivered to the lungs (≈ 10-30%) [92,170]. These drawbacks can be overcome by using a particle engineering**,** carrier-free formulation approach. The use of industrially established and well-scalable manufacturing processes, such as spray drying, alone or in combination with other process(es), is important if such formulation approach should be applied in industrial setting.

Particle engineering *via* spray drying uses the understanding of particle formation process for production of structured microparticles. In spray drying, the droplet evaporation and particle formation kinetics are governed by coupled heat and mass exchange processes. The drying process can be described by the dimensionless Péclet number (*Pe,* eq.3.1), which compares the rate of droplet surface reduction (*i.e.* evaporation rate κ) to the diffusion of the solutes in the droplet (D) [171].

$$Pe_i = \frac{\kappa}{8D_i} \tag{3.1}$$

As the solvent evaporates and the droplet shrinks, the solute concentration close to the droplet surface increases. The result of the drying, however, depends on the Péclet number:

a) Drying at low Péclet number ($Pe < 1$) occurs when the evaporation in terms of surface area reduction is slower compared to the diffusion of the solutes. The solutes, therefore, diffuse along the concentration gradient from the surface towards the inside of the droplet provided that they do not reach saturation solubility and precipitate. Thus, solid particles with density close to the solute's true density are likely to form.

b) If the evaporation is faster than the diffusion of the solutes, *i.e.* for *Pe* larger than 1, the solutes reach a higher concentration close to the droplet's surface and will, therefore, precipitate when they reach saturation solubility and create a shell. Consequently, density of such particles is smaller than the true density. Also spray drying of suspended (nano)particles follows a similar path because the suspended material can be considered immobile compared to the receding droplet surface [8]. When producing low-density particles at high *Pe*, one can use either a high molecular weight solute, which intrinsically has a small diffusion coefficient, or a solute that precipitates quickly in the drying process due to its low solubility and becomes immobile.

Applying particle engineering in spray drying allows tailoring both the geometric diameter as well as particle density. The former can be tailored mostly by controlling the droplet size and, to lower extent, by the feed solution concentration, while the latter can be lowered by choice of drying conditions and formulation properties that support drying at high *Pe* [8]. The possibility to control particle production can be very beneficial for tailored manufacturing of DPIs since both geometric size and particle density greatly influence the aerodynamic particle size and thus the product performance. Furthermore, particle engineering can be advantageously used for production of so-called large porous particles (LPP), which have large geometric size but reach desirable aerodynamic size for lung deposition thanks to low density [6].

Production of fast-dissolving low-density powders for improved lung deposition by spray drying of a nanosuspension

Particle engineering by spray drying has been successfully utilized numerous times using many different drugs [102–107]. Excipients such as phospholipids (*e.g.* distearoyl phosphatidylcholine, dipalmitoyl phosphatidylcholine (DPPC), lecithin), other lipids such as cholesterol, or amino acids (*e.g.* leucine, glycine) were often employed as well as various solvents (*e.g.* ethanol, methanol isopropanol, dichloromethane). LPPs have been mostly produced by spray drying of a double emulsion with various excipients as matrix formers (*e.g.* poly(lactic-co-glycolic) acid, cyclodextrins, or DPPC in combination with hyaluronic acid or other excipients) [110,172]. Most often, the drug in such formulations was either dissolved in water or any of the co-solvents, or used as drug suspension. Less frequently have the drugs, especially poorly water-soluble ones, been pre-processed to nano range sizes [82].

Drug nanoparticles (NPs) have gained importance in pharmaceutical research and industry in the recent years, as seen *e.g.* by 14 wet media milled drug products for oral and parenteral use on the market [73]. Wet media milling (WMM) represents one of the commonly used top-down approaches for NP production. These possess unique properties such as higher saturation solubility and larger specific surface area and thus have improved dissolution kinetics [173]. During the milling process, the drug is ground by shear and compression forces between the grinding media, which is given kinetic energy from a rotating shaft and stirring elements. This specific energy input ($E_{m,P}$) of the process is proportional to the number of milling stress events and their energy, which are affected by the milling time and the grinding media's amount, density, size, and relative velocity [79]. The information on the specific energy input is therefore crucial for the outcome of the process, experiment repeatability, and process scale up.

Nanosuspensions have the potential to provide high drug load as they can contain as little as 10% of stabilizer [77]. Stabilizers are needed during WMM to prevent particle growth due to an increase of the surface area and free Gibbs energy achieved by milling. This makes the nanocrystals thermodynamically unstable causing Ostwald ripening or particle agglomeration (Van Eerdenbrugh et al., 2008). Typical stabilizers are, *e.g.*, Poloxamer 188 and 407, Polysorbate 80, D-α-tocopherol polyethylene glycol 1000 succinate (TPGS), cellulosics, polyvinylalcohol, or sodium dodecylsulphate [78].

Numerous poorly water-soluble drugs have been nanomilled in the last 15 years [80] with median particle sizes ranging from < 100 nm [81] to ≈ 650 nm [82], or even larger in screening studies [83]. Unfortunately, only few studies [85–87,174] related the obtained nanoparticle sizes to the $E_{m,P}$.

Only few studies have combined the WMM using a traditional equipment and spray drying for production of DPIs; their focus was rather on milling parameters (*e.g.* use of co-milling agent, exploration of different stabilizers) and the influence of drug substance properties [82,111,175].

Dissolution is a prerequisite for bioavailability [16] and can be challenging to bigger or lesser extent for a poorly water-soluble drug, depending on its solubility in the given biological fluid. Drug particles delivered to the lungs encounter several obstacles on their way from solid to dissolved state, including mucociliary clearance and alveolar phagocytosis. Therefore, for a drug to be effective it is important that it dissolves before it is cleared.

It is common to predict the *in vivo* release kinetics of oral dosage forms using data obtained from *in vitro* dissolution tests that employ various pharmacopoeial methods [176]. For inhaled products, however, there is still no pharmacopoeial technique that would allow confident assessing of the dissolution characteristics. There have been several attempts to create suitable

setups for *in vitro* dissolution tests of inhaled products [144]. Most common tests used are modified versions of the paddle/paddle-over-disk apparatus [146,147,177], flow-through cell apparatus [146,148], and diffusion-controlled systems, such as the Transwell insert [149–151] or the Franz cell [146]. However, great variability exists among the methods employed, mainly in terms of dissolution media volume. The methods might be split into two groups: one for which large media volumes are required (ranging between 100 mL and 1000 mL), usually given by size of the test equipment [152,153], and a second group where small volumes (< 5 mL) are sufficient.

Predominantly PBS at pH 7.4, with and without surfactants, was the dissolution medium of choice in both groups likely due to its good buffering capacity instead of the simulated lung fluid. In the majority of cases, the tested powders were separated from the bulk liquid by a membrane forming a barrier between the particles and the liquid. Several polymeric membrane materials have been used, with polycarbonate being the most employed one [18].

Usually, the tested powders were collected from an impactor, either from one impactor stage or powder below certain aerodynamic size (*e.g.* 5 µm). Only rarely have particles from more than one impactor stage been compared.

In a study comparing the different methods, May et al. [146]reported that the modified paddle apparatus showed optimal reproducibility with the best discrimination power. On the other hand, the Transwell setup use has been advocated due to use of low liquid volumes as this resembles more closely the *in vivo* fluid volume; however, it does not mimic the absorption-induced concentration gradients and exchange of fluids that occur *in vivo* [18], and the need for surfactants in the small volume receiver compartment introduces a degree of arbitrariness. The concentration gradient experienced *in vivo* might be mimicked better by having a compartment with low liquid volume where the drug dissolves and then permeates to a larger, sink-conditions maintaining compartment. Such setup has only recently been proposed, namely with the Inhalation Sciences' proprietary Dissolv*It*® module [154].

The objective of this work was to develop and manufacture formulations of low-density composite particles for pulmonary delivery using the combination of high-energy wet media mill for nanoparticle production with spray drying for particle engineering in order to harness the advantages of both processes. Spray drying at high *Pe* guided the choice of formulation composition and process parameters with the aim to obtain engineered powders exhibiting fast dissolution, maximal fine particle fraction for deep lung deposition, and maximal geometric size. This work involves industrially established processes to ultimately introduce this as platform technology for pulmonary formulation development. To the best of the authors' knowledge, this approach has not been proposed in the context of optimizing inhalation drug product performance before. Budesonide was used as a model drug substance and the obtained results were compared with a commercial product. Mathematical kinetic modelling was employed to deduce the dissolution rate of the API contained in the powders that were collected at different stages of the new generation impactor (NGI) from results obtained using a modified USP 2 apparatus.

3.3 Materials and methods

3.3.1 Materials

Budesonide and D-α-tocopherol polyethylene glycol 1000 succinate (TPGS) were purchased from Atomole Scientific (Wuhan, China). L-leucine (Leu), ammonium bicarbonate (AC), bovine serum albumin (Alb), sodium diphosphate dibasic, potassium phosphate monobasic, and sodium chloride were obtained from Sigma-Aldrich (Buchs, Switzerland). Ammonium formate, formic acid, and phosphoric acid were from Fluka (Switzerland). Ethanol and acetonitrile (both HPLC grade) were purchased from J.T.Baker (Deventer, The Netherlands). Ultrapure water (Milli-Q, Millipore) was used for all experiments. Budesonide was chosen as a model drug as it is poorly soluble in water and it is used as an inhalation therapy for asthma. All raw materials were used as received.

3.3.2 Methods

3.3.2.1 Preparation of budesonide nanosuspensions

First, budesonide (5% w/v) was dispersed in 800 mL of water containing TPGS at a concentration of 1.25% (w/v), and the suspension was stirred overnight using a propeller stirrer. Subsequently, the suspension was milled in wet media mill DYNO®-MILL MULTI LAB (Willy A. Bachofen Maschinenfabrik, Muttenz, Switzerland), equipped with a 561 mL net volume grinding chamber, at a suspension feed rate of 1 L/min. The stirrer tip speed applied was 12 m/s. Yttrium-stabilized zirconia (SiLibeads Type ZY Premium) with bead size 0.15 - 0.25 mm (Sigmund-Lindner (Warmensteinach, Germany)) was used as milling media at filling ratio of 60%. The resulting nanosuspension was sampled at 30, 60, 90, 120, 150, and 180 min. The particle size of the nanosuspension was analysed using photon correlation spectroscopy (cf. Chapter 2.2.3 Particle size determination). For characterization by X-ray diffraction, a droplet of nanosuspension was air dried on the specimen holder and measured without further preparation using a D2 Phaser diffractometer by Bruker AXS, (Karlsruhe, Germany).

3.3.2.2 Spray drying

Prior to spray drying, the nanosuspension was diluted to 300 mL with purified water generated by MilliQ system to reach a final active pharmaceutical ingredient (API) concentration of 0.5% (w/v). Leucine or albumin was added to the nanosuspension as matrix former to achieve final total solids concentration of 1% (w/v). Ammonium carbonate was added to some feedstocks at concentration of 2% (w/v) and it was expected to completely evaporate during drying. For comparison, a suspension of not milled budesonide containing the spray drying additives was also spray dried. Finally, a formulation of nanosuspension without any additives with a final API concentration of 1% (w/v) was prepared. Table 3.1 gives an overview of the formulations.

The feedstock was spray dried in a Mini Spray Dryer B-290 coupled with Dehumidifier B-296 and molecular sieve (all Büchi Labortechnik, Flawil, Switzerland) using a 0.7 mm two-fluid nozzle that was cleaned pneumatically every 30 seconds, with nitrogen as the spraying gas. For the manufacture of the different formulations, the inlet temperature, the feedstock flow rate, the atomizing pressure setting, and the aspirator flow rate were kept at 170°C, 9 mL/min, 35 mm, and 35 m^3/h, respectively. A yield of 70-80% was achieved. Initial experiments were performed to define these spray drying conditions. In these, the effect of the inlet temperature

(170°C/200°C), the atomizing pressure setting (35 mm through 55 mm), and the feedstock concentration (0.1%, 1%, and 4% (w/v)) on median geometric particle size and aerosol performance were studied. The outlet temperature depended on the inlet temperature and was around 63°C and 83°C for inlet temperatures of 170°C and 200°C, respectively. The humidity of the drying gas was kept below 5% during all experiments. The spray-dried powders were stored for one week at a temperature of 22 ± 2°C and relative humidity 50 ± 5% before characterization.

3.3.2.3 Particle size determination

Photon correlation spectroscopy (PCS)

The particle size of the nanomilled suspension was measured by photon correlation spectroscopy using a Zetasizer Nano ZS (Malvern Instruments, Worcestershire, United Kingdom) at a wavelength of 633 nm at 25 °C.

Laser diffraction (LD)

Laser diffraction (LD) was used to determine the particle size of the spray-dried powders. The instrument consisted of a HELOS sensor and the dispersing system RODOS, equipped with the micro dosing unit ASPIROS (all Sympatec (Clausthal-Zellerfeld, Germany)). The software Windox 5 (Sympatec, Switzerland) was used to evaluate the measured data. Approximately 150 mg of the powder was filled in a glass vial. Each spray-dried sample was measured in triplicate in the measurement range of 0.1/ 0.18 to 35 µm. All measurements were done at primary injector pressure of 1 bar.

3.3.2.4 Scanning electron microscopy (SEM)

Particle size and morphology of the spray-dried powders were determined with a Zeiss Supra VP 40 scanning electron microscope (SEM; Carl Zeiss, Jena, Germany). Prior to imaging, the samples were sputter-coated with gold for 45 s using a Polaron SC 7620 (ThermoVG Scientific, United Kingdom). The pictures were taken under high vacuum at a voltage of 5 kV and a working distance of 5 mm.

3.3.2.5 Specific surface area

The specific surface area was measured by gas adsorption using the BET method. For this, the surface area analyzer Gemini-2360 (Micrometrics, USA) was used. Powder samples were flushed overnight with helium and measured in triplicate using nitrogen in relative pressure range 0.05–0.25 (p/p0).

3.3.2.6 Mercury porosimetry

Micromeritics AutoPore IV 9500 system at maximum pressure of 212 MPa (corresponds to ca. 31000 psia) was used to measure the pore volume within the particles and to calculate the effective density of the particles. The effective density ρ_e was calculated using equation:

$$\rho_e = \rho\left(1 - \frac{V_{pores}}{V_{total}}\right) \tag{3.2}$$

Where, ρ is true density, V_{pores} is the volume of pores below 5 µm, and V_{total} is the total volume of the particles, *i.e.* the volume of the pores and the solid combined. Prior to loading into the measurement cell, the powder was slightly compressed to create a defined object to be analysed.

3.3.2.7 Aerodynamic performance

The Next Generation Impactor (NGI; Copley Scientific, United Kingdom) was used to determine the aerodynamic performance of the spray dried powders. Approximately 1 mg of the powder was manually filled into a two-piece hypromellose capsule of size 3 (gifted from CAPSUGEL®, France). The capsule was placed in a monodose dry powder inhaler (type RS01 Mod. 8, kindly donated by Plastiape S.p.a., Italy) and the powder was lead through the impactor for 3.5 s at an airflow that generated a 4 kPa pressure drop, namely 68 L/min. Prior to each measurement, the

collection cups were coated with a 1% (w/v) glycerol in ethanol (EtOH) solution. The deposited powders were recovered by ethanol extraction using an orbital shaker for 30 minutes; stages 1 and 8 were extracted due to their larger size using 25 mL of ethanol, while stages 2-7 were each extracted with 10 mL EtOH. The budesonide content of each of these ethanolic solutions was quantified using the above-mentioned HPLC-MS method.

The fine particle fraction (FPF) was calculated as the fraction of total budesonide amount recovered in particles with an aerodynamic diameter < 5 μm by interpolation within stage 2.

3.3.2.8 High-performance liquid chromatography/Mass spectrometry (HPLC-MS)

An HPLC-MS system consisting of a degasser G1379B, binary pump G1312A, autosampler G1367B, thermostat G1330B, column oven G1316A (series 1100), and a quadrupole MS detector G6130A (all Agilent Technologies, USA) was used to quantify budesonide content. A Kromasil C8 reversed phase column (100 x 2.1 mm, 5 μm (Phenomenex®, USA)) was used. The mobile phase consisted of 25 mM ammonium formate buffer (pH 3.2) and acetonitrile in ratio 1:1 and was used at flow rate of 0.2 mL/min. Sample injection volume of 50 μL was employed.

The ions were generated by atmospheric pressure electrospray ionization. MS detector was operated at positive polarity with fragmentor set to 100 V, capillary voltage 4000 V, drying gas flow 10 L/min, drying gas temperature 350°C, and nebulizer pressure 20 psig. Budesonide was detected in SIM mode as $[M+H]^+$ at *m/z* 431.

3.3.2.9 Dissolution testing

The technique for dissolution testing was based on that developed by Son et al. [147]. The powders from NGI stages 3, 4, and 5 (cutoff diameters 4.16, 2.64, and 1.56 μm, respectively) were taken for the dissolution tests using modified NGI collection cups (Copley Scientific, UK). This allowed small dose of aerodynamically classified powder to be tested. After powder deposition and insert removal from the impaction cup, 200 μL of dissolution medium were placed on the insert's surface near the powder and a polycarbonate membrane (pore size 0.05 μm, thickness 6 μm (Whatman Nuclepore™, USA)) was fixed on top of the powder. Such insert was placed as quickly as possible into a cylindrical dissolution vessel, which was subsequently filled with 300 mL of dissolution medium consisting of phosphate buffered saline (pH 7.4). The dissolution test, therefore, resembled the USP Apparatus 5 (paddle over disk) test setup (Figure 3.1). The dissolution was tested at 37.0 ± 0.5°C using the paddle stirrers at 50 rpm. Samples of 2 mL were taken from the 300 mL bulk solution after 5, 10, 15, 20, 25, 30, 40, 50, 60, 90, 120, 180, 240, 360, 480, and 1440 minutes. The sample volume was immediately replenished with new dissolution medium. At the end of the dissolution experiment, the membrane was cut open using a scalpel to allow dissolution of any undissolved powder in the bulk solution. Prior to analysis, all samples were centrifuged at 16100 × g for 10 minutes.

In addition to measuring the dissolution with powders deposited on different NGI stages, dissolution experiments using the complete (*i.e.* not aerodynamically classified) formulations were carried out. In these experiments, an exactly weighed amount of approximately 1 mg of each formulation was placed on the impaction insert and the test was subsequently performed in an identical fashion as for the NGI stages. Additionally, physical mixture (PM) of budesonide and leucine in ratio 1:1, prepared by low shear mixing, was tested.

The TPGS concentration in the 200 μL of dissolution medium was evaluated for each formulation based on the recovered drug amount and the nominal drug and stabilizer content of the powders

and compared to the critical micellar concentration of TPGS. Additionally, the solubility of the drug in the dissolution medium was evaluated by adding drug in excess into dissolution medium, stirring for at least 24 hours, centrifuging and determining drug concentration in the supernatant.

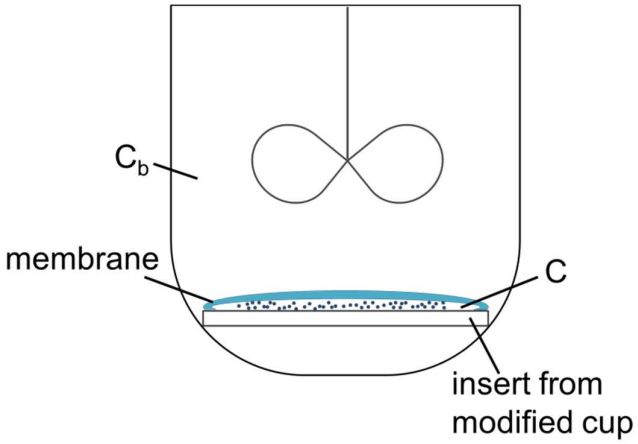

Figure 3.1 Dissolution test setup.

3.3.2.9.1 Kinetic model for the estimation of dissolution coefficient

In the dissolution setup used, inner and outer compartments were formed within the vessel. The dissolution took place in the inner compartment while the drug was quantified in the outer compartment after permeating through the membrane.

To estimate the dissolution coefficient of budesonide, a kinetic model was developed. The dissolution rate of a solid substance in a liquid medium is described by the classical Noyes-Whitney/Nernst-Brunner equation [66,67]:

$$\frac{dm}{dt} = \frac{D\,S}{h}(C_s - C) \tag{3.3}$$

where, m is dissolved drug amount, t is time, D is diffusion coefficient, S is surface area of solid substance, h is thickness of diffusion boundary layer, C_s is saturation solubility of drug in the medium, and C is concentration of dissolved drug substance in the medium.

For a particulate solid, the surface area of the particle assembly can be expressed by:

$$S = \frac{6\,\Gamma m_p}{\rho\, d_g} \tag{3.4}$$

where, m_p is mass of the drug substance particles, Γ is shape factor accounting for particles' surface area deviation from that of a sphere, ρ is particle density, and d_g is geometric particle diameter.

By introducing Eq. (3.4) into Eq. (3.3) and considering that particle mass and particle diameter decrease over time in the course of dissolution, Eq. (3.3) becomes:

$$\frac{dm}{dt} = \frac{D\;6\,\Gamma\left(m_p(0) - m\right)}{h\,\rho\, d_g(0)\sqrt[3]{\left(m_p(0) - m\right)/m_p(0)}}(C_s - C) \tag{3.5}$$

where, $m_p(0)$ is initial drug particle mass and $d_g(0)$ is initial geometric diameter of the particles.

If solid particles consist not only of drug substance but contain also excipients, Eq. (3.5) should read:

$$\frac{dm}{dt} = \frac{q\ D\ 6\ \Gamma\left(m_p(0) - m\right)}{h\ \rho\ d_g(0)\ \sqrt[3]{\left(m_p(0) - m\right)/m_p(0)}}\left(C_s - C\right) \tag{3.6}$$

where, $1/q$ is the mass fraction of drug substance in the particle and $m_p(0)$ is in this case the initial amount of drug substance contained in the particles, and $d_g(0)$ is initial geometric diameter of particles.

If, on the other hand, the total initial mass of particles rather than their drug substance content is known, then Eq. (3.6) is modified to:

$$\frac{dm}{dt} = \frac{D\ 6\ \Gamma\left(m_p(0) - q\ m\right)}{h\ \rho\ d_g(0)\ \sqrt[3]{\left(m_p(0) - q\ m\right)/m_p(0)}}\left(C_s - C\right) \tag{3.7}$$

where, $m_p(0)$ in this case represents the initial total mass of the particles consisting of drug substance and excipients.

For a particle size distribution, the dissolution rate is given by:

$$\frac{dm}{dt} = \sum_{i=1}^{n} \frac{D\ 6\ \Gamma}{h\ \rho} \frac{\left(m_p(0)(i) - q\ m(i)\right)}{d_g(0)(i)\ \sqrt[3]{\left(m_p(0)(i) - q\ m(i)\right)/m_p(0)(i)}}\left(C_s - C\right) \tag{3.8}$$

where, i denotes size fraction and n varied in this work between 24 and 27 depending on the formulation under investigation.

In the employed experimental arrangement, the studied drug formulation was contained in the inner compartment that was separated from the outer bulk solution of the vessel by a polymeric membrane (Figure 3.1). The rate of change of concentration, C, of dissolved drug substance in the medium of the inner compartment is given by:

$$\frac{dC}{dt} = \frac{1}{V}\frac{dm}{dt} - A_m\ P\ \ (C - C_b)/V \tag{3.9}$$

where, A_m is surface area of the membrane, P is permeability coefficient of the membrane for the drug substance, V is volume of the inner compartment, and C_b is drug substance concentration in the bulk solution of the vessel.

Finally, the rate of concentration change in the bulk solution is expressed by:

$$\frac{dC_b}{dt} = A_m\ P\ \ (C - C_b)/V_b - \dot{V}_{sampl}(t)\ \ C_b/V_b \tag{3.10}$$

where, V_b is volume of the bulk solution and $\dot{V}_{sampl}(t)$ is the rate of volume sampling from the bulk solution. This was approximated by the following empirical equation that was obtained by fitting to the withdrawn sample volume at the successive time points:

$$\dot{V}_{sampl}(t) = 0.559 - 1.17\ 10^{-2}t + 9.9\ 10^{-5}t^2 - 3.93\ 10^{-7}t^3 + 7.31\ 10^{-10}t^4 - 5.13\ 10^{-13}t^5 \quad (3.11)$$

The following boundary conditions were applied:

$t = 0, m = 0, C = C(0), C_b = 0$

To allow for $C(0) \geq C_s$, the following additional condition was implemented:

$$\frac{dm}{dt} = \begin{cases} 0, [0, t_{ch}) \\ as\ in\ Eq.\ (13)\ or\ Eq.\ (8), [t_{ch}, \infty) \end{cases} \quad (3.12)$$

where t_{ch} was treated as an adjustable parameter, and Eq. (3.6) was modified to:

$$\frac{dm}{dt} = \frac{q\ D\ 6\ \Gamma\left(m_p(0) - C(0)V - m\right)}{h\ \rho\ d_g(0)\ \sqrt[3]{\left(m_p(0) - C(0)V - m\right)/\left(m_p(0) - C(0)V\right)}}(C_s - C) \quad (3.13)$$

The system of eq. (3.9), (3.10) and (3.12) with either Eq. (3.13) for the individual deposition stages of the NGI or eq. (3.8) for the complete formulation were fitted to the measured concentration values in the bulk solution by least-square regression analysis following numerical solution of the differential equations using the software EASY-FIT® [178]. From the fit, optimal values of the following parameters were deduced:

$k_{diss} = \frac{D\ 6\ \Gamma}{h\ \rho}, C(0), P\ and\ t_{ch}$

The value of q was estimated from the total dissolved drug substance amount at the end of the experiment with the complete formulations and the same q value was also used in the dissolution experiments with the NGI stages. For $m_p(0)(i)$ and $d_g(0)(i)$ in eq. (3.8) the relative volume distribution and the equivalent particle size d_e, respectively, were used, which were taken from the particle size distribution of the complete formulation determined by LD. For $m_p(0)$ and $d_g(0)$ in eq. (3.13), the total dissolved drug substance amount at the end of the experiment and the average aerodynamic particle size of the respective deposition stage, respectively, were used.

3.4 Results

3.4.1 Characterization of raw material

The budesonide drug particles prior to milling are shown in Figure 3.2 (left); the particles had cuboid shape and formed rather large agglomerates. The median particle size was 2.83 µm with largest particles reaching ≈ 20 µm and around 25% of particles were very fine (< 1 µm) (Figure 3.2, right).

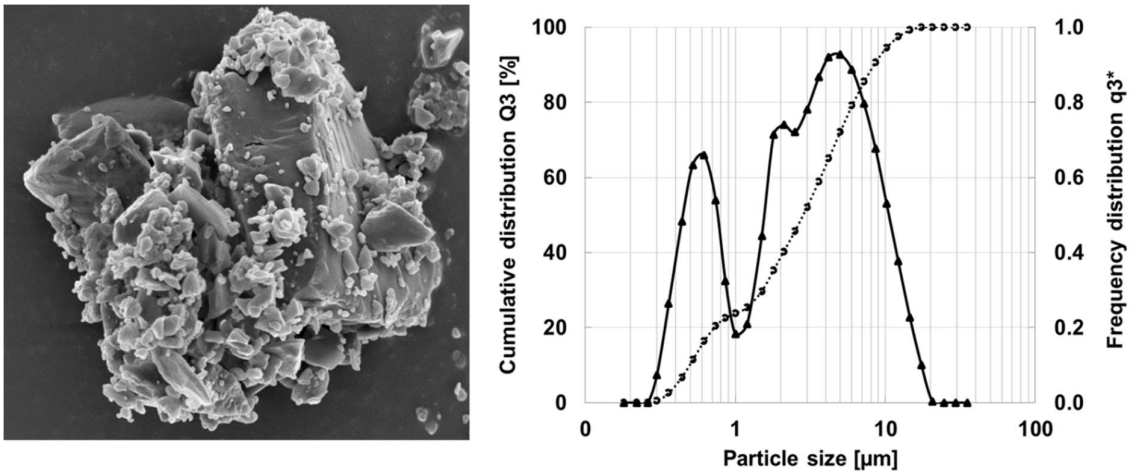

Figure 3.2 SEM micrograph (left) and particle size distribution by LD (right) of raw budesonide.

3.4.2 Wet media milling

Based on a screening study [179], which tested the ability of different stabilizers such as polysorbate 80, poloxamer 188 and 407, and TPGS to stabilize the nanoparticulate system (data not shown), TPGS was chosen as the preferred stabilizer as smallest nanoparticle size and narrowest distribution was achieved. TPGS, a GRAS listed compound, included in NF and approved by the FDA for per-oral administration is used here as research reagent. WMM with this stabilizer was performed for 150 minutes and generated nanoparticles of median particle size 263 ± 39 nm at specific energy input of 137 ± 3 MJ/kg.

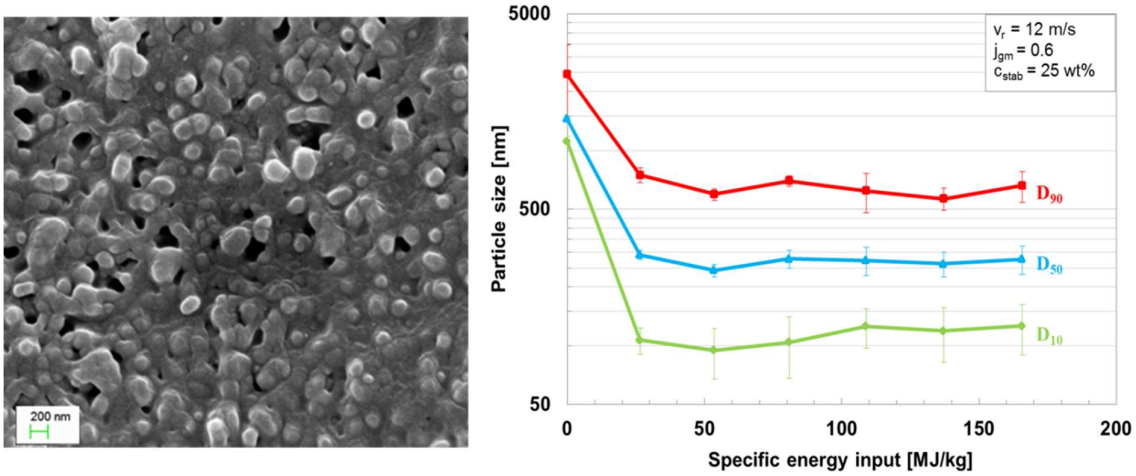

Figure 3.3 Left: SEM micrograph of budesonide nanoparticles after WMM at specific energy input of 137 MJ/kg. Right: Particle size reduction during wet media milling.

3.4.3 Spray drying conditions

The spray drying conditions used for production of the final powders in Table 3.1 were chosen based on a series of initial experiments. In these, the influence of inlet temperature and formulation composition (Figure 3.4), atomizing pressure (Figure 3.5), and concentration of feedstock (data not shown) on median geometric particle size (de,50) and FPF was studied. In general, the larger the geometric particle size the lower the FPF. Formulations containing ammonium carbonate, for instance, exhibited smaller geometric size and higher FPF than the ones without this excipient. As a notable exception, powders produced at 170°C with leucine had a larger geometric size and a higher FPF than the formulation with albumin. Also, at 200°C formulations with leucine and albumin exhibited a larger or the same geometric size as the formulation with glycine but a higher FPF. The use of higher inlet temperature led to smaller $d_{e,50}$ for powders with all used additives except for albumin (Figure 3.4 left) while this larger geometric size was accompanied by an increase of FPF for the albumin formulation (Figure 3.4 right).

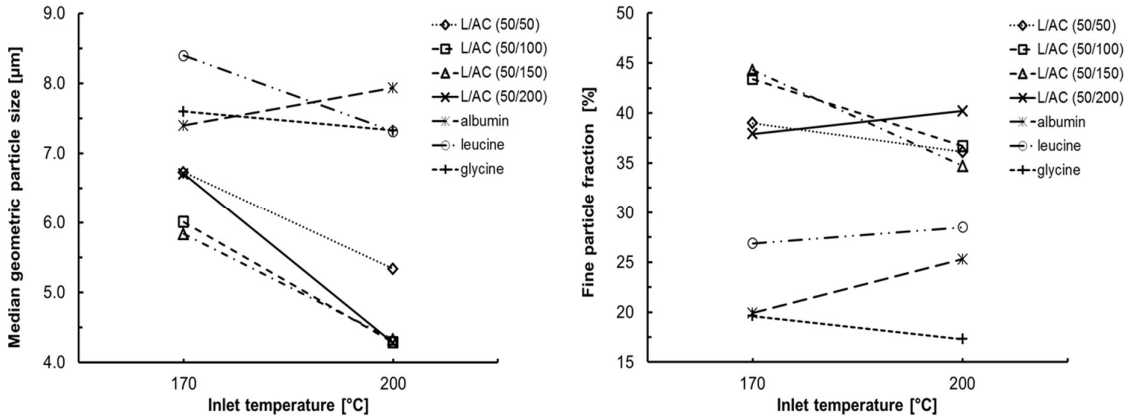

Figure 3.4 Median geometric particle size (left) and FPF (right) as a function of inlet temperature of powders containing varying ratios of leucine (L)/ammonium carbonate (AC), albumin, leucine, or glycine as spray drying additives.

Increase of atomizing pressure, one of the main factors influencing the droplet size, had a clear negative effect on the median geometric particle size while it simultaneously caused an increase of FPF (Figure 3.5).

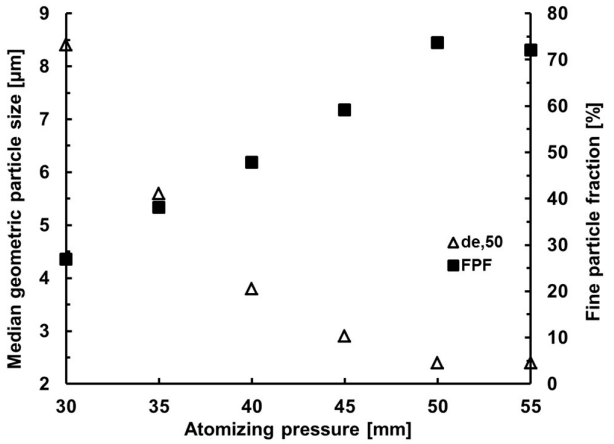

Figure 3.5 Median geometric particle size and FPF as a function of atomizing pressure of powders with leucine as spray drying additive.

Since the aim of this study was to create geometrically large particles with good aerodynamic performance, the following spray drying conditions were selected based on these results: Atomizing pressure setting of 35 mm and inlet temperature of 170°C. Based on previous experience, feedstock flow rate of 9 mL/min and total solids concentration (excluding AC) of 1% w/v were chosen. The ratio of leucine to ammonium carbonate, when used in a mixture, was set to 50/200.

3.4.4 Manufactured powders

The physical properties of the 5 spray dried formulations are shown in Table 3.1. In 4 cases, the feedstock contained the WMM budesonide in form of a nanosuspension (NS), while in the fifth case budesonide was not milled and was spray dried as a suspension (S) containing the additives.

Table 3.1 Overview of compositions of spray drying feedstocks with the resulting median geometric particle size, specific surface area, and effective density of the produced powders.[a]

Formulation notation	Feedstock basis	Spray drying additive	$d_{e,50}$ [µm]	Specific surface area [m^2/g]	Effective density [g/mL]
NS/–	Nanosuspension	-	5.30 ± 0.06	2.1 ± 0.1	0.74
NS/Alb	Nanosuspension	Albumin	5.01 ± 0.10	3.5 ± 0.1	0.52
NS/Leu	Nanosuspension	Leucine	5.30 ± 0.03	19.0 ± 0.4	0.34
NS/Leu+AC	Nanosuspension	Leucine Am. carbonate	4.39 ± 0.02	14.3 ± 0.1	0.39
S/Leu+AC	Non-milled suspension	Leucine Am. carbonate	5.04 ± 0.02	6.9 ± 0.2	0.54

[a] Values represent average ± SD (n=3)

The median geometric particle size was similar for all formulations and ranged between 4.39 µm and 5.30 µm. Considerable differences were seen in the specific surface areas, formulations with nanosuspension and leucine as an additive yielded much higher surface area than the other formulations. The same formulations produced particles with the lowest effective density. The additives had also an influence on the shape and morphology of the particles (Figure 3.6). For example, powders of formulation NS/Alb crumpled during drying and formed raisin-like particles (Figure 3.6A) while formulations containing leucine appeared sponge-like (Figure 3.6B).

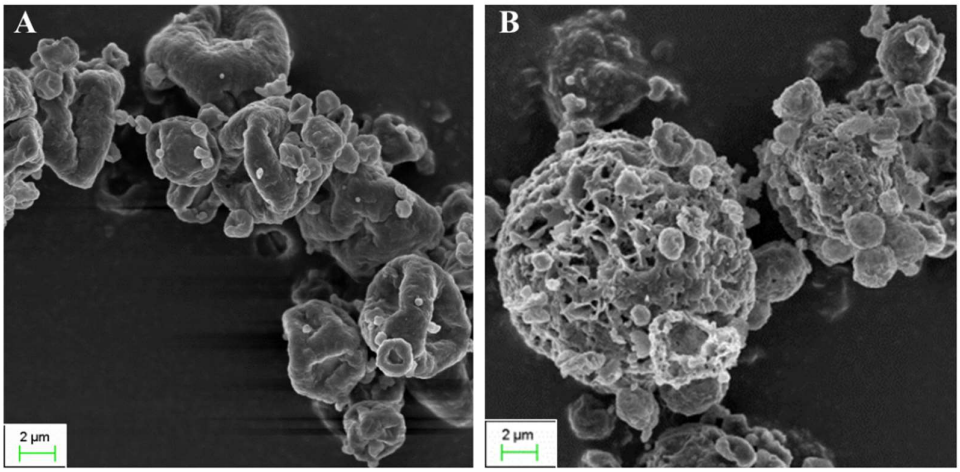

Figure 3.6 SEM micrographs of spray-dried powders with albumin (A, formulation NS/Alb) and leucine (B, formulation NS/Leu) as spray drying additive.

3.4.4.1 Aerodynamic properties

The additives affected also considerably the aerodynamic particle size distribution of the powders (Figure 3.7). Formulation NS/Leu+AC containing nanosuspension, leucine, and AC (red line) showed very good aerodynamic performance, which can be judged by the high deposition in stages below 7.49 µm cutoff diameter and low deposition above this cut-off. On the other hand, formulations NS/– (green line) and S/Leu+AC (black line) had highest deposition in the induction port, which mimics the throat and where large particles or agglomerates deposit. The poor aerodynamic performance of these formulations was reflected also in the low FPF values they reached (Figure 3.8).

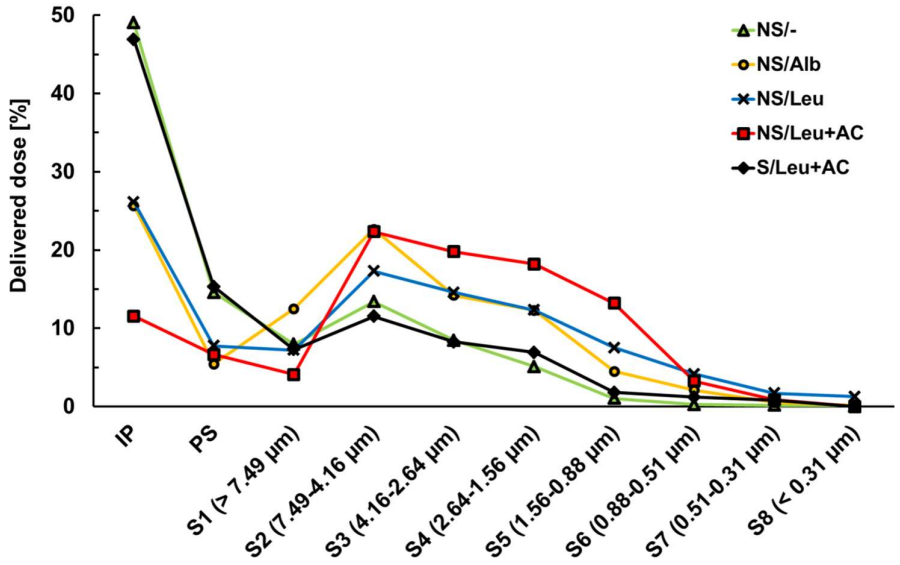

Figure 3.7 Aerodynamic particle size distribution of different formulations of spray-dried powders in the NGI with the cutoff diameters of each stage (IP = induction port, PS = pre-separator).

Formulation NS/Leu+AC reached the highest FPF of around 61%, while the lowest FPF (around 18%) was obtained with formulation NS/–, which contained the nanomilled drug alone (Figure 3.8). Interestingly, formulation S/Leu+AC containing also leucine and ammonium carbonate as additives but drug suspension rather than nanosuspension as the feedstock basis reached a rather low FPF of only around 22%. Between the two additives Leu and Alb, the former had a more positive effect on FPF. By comparison, aerodynamic performance of a commercially available budesonide product (Miflonide® 400 µg, Novartis AG) reached a FPF of 21%. This was evaluated using the Aerolizer device supplied with the packaging. Notably, formulations produced in this work applying the particle engineering approach outperformed the commercial product.

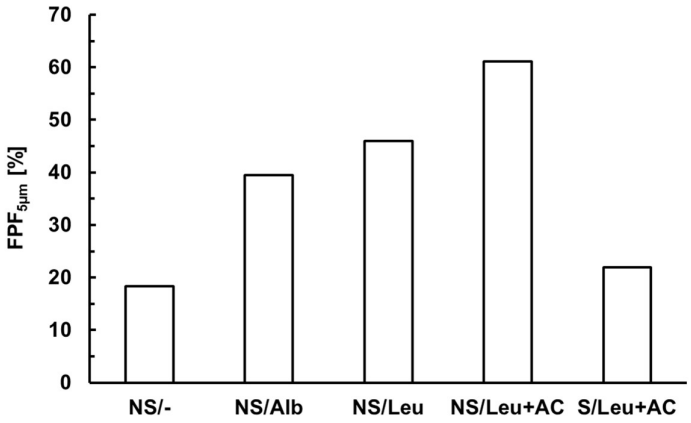

Figure 3.8 Fine particle fraction of different formulations of spray-dried powders.

The effective density measured by mercury porosimetry was lowest for formulations NS/Leu+AC and NS/Leu. These formulations exhibited as seen above the highest FPF. Hence, addition of leucine to the nanosuspension formulations is shown to aid the formation of low-density porous particles with smaller aerodynamic diameters than the other formulations although the

geometric diameter remained largely unaffected. Ammonium carbonate had a positive effect on FPF but not on the effective density and lowered somewhat the geometric diameter. Bulk density was expectedly much lower than the effective density. Interestingly, this quite more simple measurement produced in general a similar trend for the studied formulations as the effective density with the exception of S/Leu+AC (Figure 3.9).

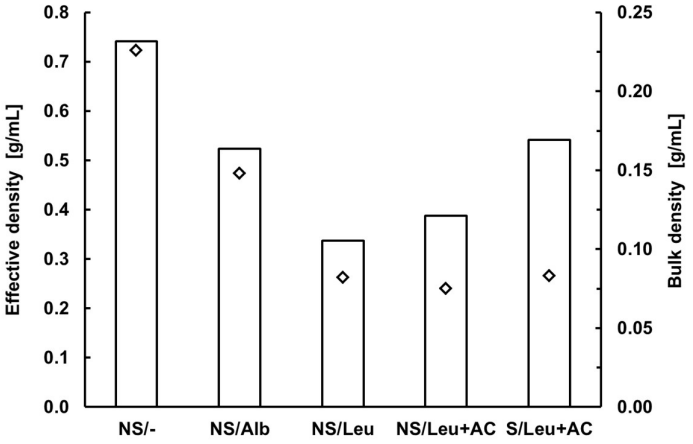

Figure 3.9 Effective (bars) and bulk (diamonds) densities of the spray-dried powders.

3.4.4.2 Dissolution rate

Figure 3.10 shows an example of concentration data in the bulk solution and the corresponding line obtained by model fitting (according to Chapter 3.3.2.9.1) for powder from stages 3 through 5 of formulation NS/Leu+AC. We observed a very fast onset of dissolution that was largely completed within 30 minutes. No differences were observed among the individual NGI stages. Comparable results were obtained for the remaining four formulations (Appendix 8.1).

The model fitting to the dissolution results of NGI stages 3, 4, and 5 of all formulations yielded values for the dissolution rate parameter kdiss shown in Figure 3.11. Significant values of initial concentration *C(0)* were deduced. These were larger for formulations NS/Alb, NS/Leu and NS/Leu+AC than for S/Leu+AC and the physical mixture and they decreased for the three stages generally in the order 3 > 4 >5. The C(0) values ranged between 0.15 and 0.2 mg/mL (in stage 3) and 0.05 and 0.1 mg/mL (in stage 5) for the former formulations, and between 0.05 and 0.1 mg/mL and 0 and 0.05 mg/mL in these stages for the latter formulations. Notably, these *C(0)* values of the first group of formulations lie above drug substance solubility in the dissolution medium. For the permeability coefficient *P*, an average estimate of 1.65×10^{-3} cm/min (standard error = 3.61×10^{-4} cm/min, n = 23) was obtained. Goodness of Fit (GOF) was in all cases satisfactory (GOF > 0.999) [178].

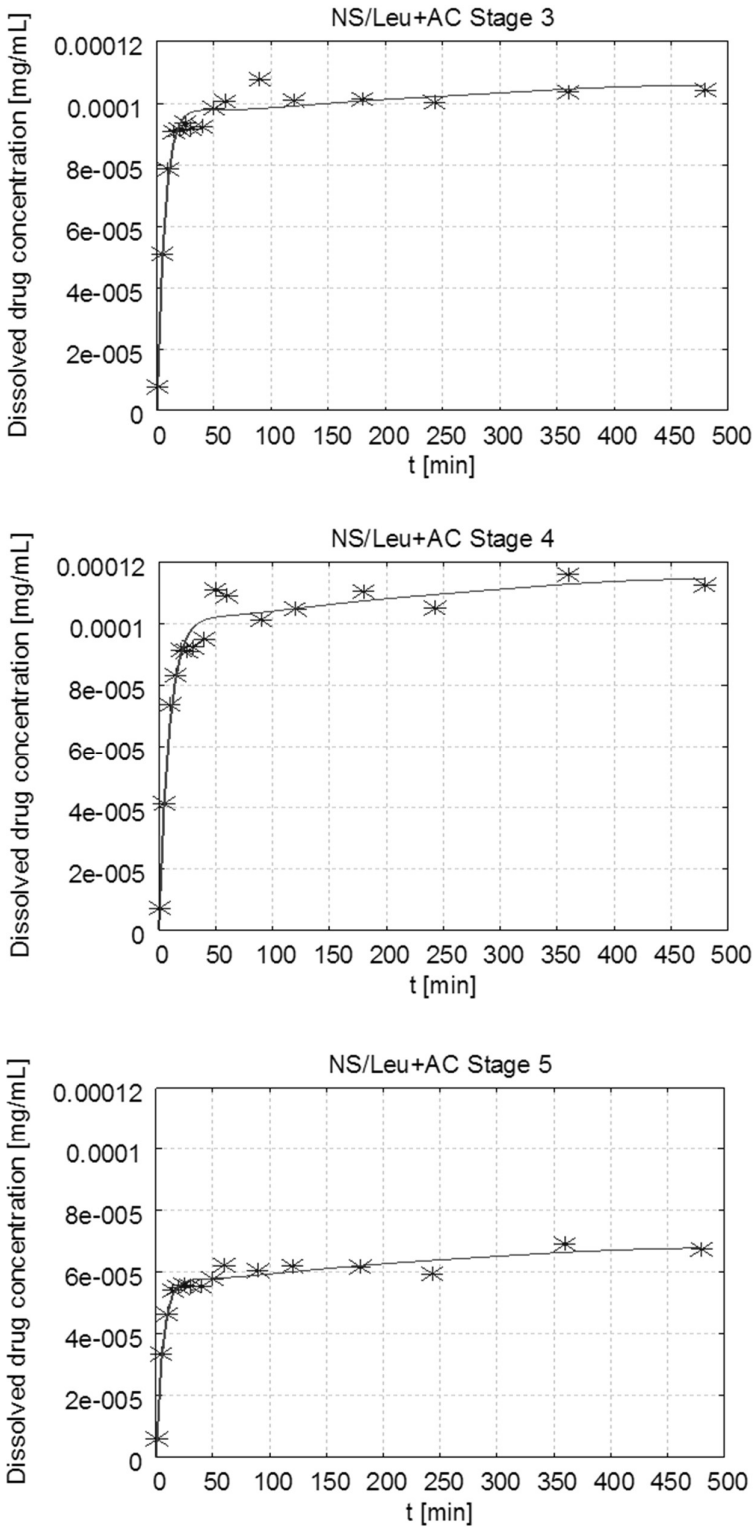

Figure 3.10 Example of dissolution test result of formulation NS/Leu + AC. Crosses represent the measured drug concentration in the bulk solution (Cb), lines represent fitted dissolution profile; (top) dissolution of powder from stage 3, (middle) dissolution of powder from stage 4, (bottom) dissolution of powder from stage 5.

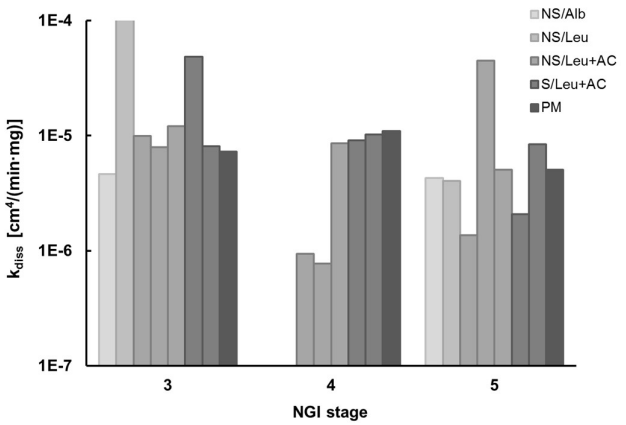

Figure 3.11 Overview of dissolution rate parameters kdiss for deposition stages 3, 4 and 5 deduced by model fitting. Order of formulations from left to right corresponds to that in the legend from top to bottom.

No clear difference in k_{diss} for the different formulations in the three NGI stages is observed (Figure 3.11). Also, no trend between the NGI stages can be postulated, since the value of k_{diss} appears to fluctuate with some exceptions around 10^{-5} cm^4/(min · mg). Furthermore, the deduced value of *P* did not seem to depend on formulation or stage.

The complete formulations exhibited by comparison a more gradual dissolution. Experimental data and fitted line are shown for NS/Leu+AC as typical example in Figure 3.12 (and Appendix 8.1). The deduced parameter values by model fitting are given in Table 3.2. Only the dissolution parameter k_{diss} could be determined with certainty, while the other three adjustable parameters, *i.e.*, *C(0)*, *P*, and t_{ch}, had a large standard error (SE) and their confidence interval at the 5% level included the zero point. They were therefore assigned low priority and eliminated [178]. The values of *q* (Eqs. 6-8, 13) were estimated from the total dissolved drug substance amount at the end of the experiment and corresponded to a mass fraction of drug substance, *1/q*, for the different formulations of 0.3356 to 0.3954. The GOF was in all cases better that 0.999 underscoring the high significance of the model approximation.

Hence, the use of parameter k_{diss} alone was sufficient to explain the experimental data of the complete formulations. Notably, fixing membrane permeability coefficient, *P*, to values < 0.01 cm/min markedly reduced the GOF while larger fixed values of *P* did not alter the goodness of the approximation or the deduced value of k_{diss}. For the physical mixture exceptionally, a fixed value of $P \approx 0.01$ cm/min or larger had to be used *a priori* in order to obtain a reliable estimate of k_{diss} with a small SE while much smaller values for *P* yielded k_{diss} values whose confidence interval included the zero point and ultimately worsened the GOF.

Table 3.2 Dissolution rate parameter k_{diss} in cm^4/(min·mg) of complete formulation powders deduced by model fitting.

NS/Alb	NS/Leu	NS/Leu+AC	S/Leu+AC	Physical mixture
3.18E-5 ± 3.93E-6	2.37E-5 ± 1.48E-6	2.73E-5 ± 4.45E-6	2.04E-5 ± 2.01E-6	2.06E-6 ± 2.41E-7

[a] Estimated values ± SE of estimate

Interestingly, no significant difference (at p = 0.05) in the dissolution parameter is found between the four spray dried formulations considering the error of estimate (p = 0.01 only for the pair NS/Alb and S/Leu+AC). The resulting k_{diss} values are of the same order of magnitude as the values deduced for the powders deposited at the different NGI stages. Solely the physical mixture yielded a 10-fold smaller k_{diss} compared to the other complete formulations, this difference being highly significant (p = 0.00).

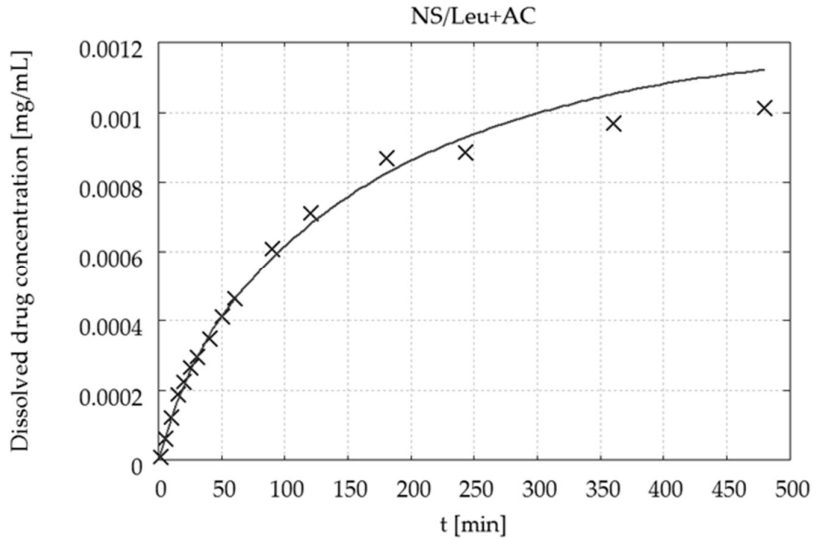

Figure 3.12 Example of dissolution test result of complete formulation NS/Leu + AC. Crosses represent the measured drug concentration in the bulk solution (Cb), lines represent fitted dissolution profile.

3.5 Discussion

3.5.1 Spray drying process conditions

Generation of geometrically smaller particles (Figure 3.4) at higher inlet and therefore higher outlet temperature could be explained by fast diffusion of dissolved excipient from the surface towards the interior of the droplet during drying. Higher temperature results in faster solvent evaporation and therefore faster concentration increase of excipient at the surface. High diffusion coefficient excipients will be transported in larger amounts along the concentration gradient towards the centre before precipitating in the receding perimeter of the droplet, leading to the formation of particles with smaller geometric size and higher density. This likely occurs in all leucine-containing formulations in the used temperature values reflecting relatively small *Pe* numbers. For albumin on the other hand, a high molecular weight, low diffusion coefficient excipient, increased solvent evaporation rate and faster concentration rise caused by the higher temperature probably elicits a sooner precipitation at the perimeter resulting in larger and less dense particles in accordance with a large *Pe* number. Interestingly, leucine as an excipient gave geometrically larger particles than albumin at 170°C whereas the opposite was true at 200°C. Hence, the different *Pe* number of the two compounds alone does not explain their behaviour and additionally their different solubility and therefore time to reach saturation plays an important role in the particle formation process.

Reduced geometric diameter at higher temperature is expected to correspond to an increased FPF provided that the density of the particles remains roughly the same. This was not observed in three of the formulations with L/AC suggesting that particle density at the higher drying temperature was higher than at the lower temperature. Hence, the phenomena described above led for these formulations to the generation of particles whose density increased as their size decreased. The addition of ammonium carbonate that was envisaged to improve particle porosity upon its removal did not fulfil this intention possibly because sublimation of this additive caused bursts and/or breaking apart of the particles. The formulation containing only leucine and the formulation with the highest ammonium carbonate content seemed to have slightly improved FPF at the higher temperature. Notably, use of albumin as an additive produced a higher FPF that was accompanied by a larger geometric particle size, strongly indicating that particle density was reduced at the high drying temperature (Figure 3.4). At 170°C, on the other hand, the density of leucine-containing particles was lower than that of albumin-containing particles as both geometric size and FPF of the former were larger than of the latter. Thus, the response of the albumin-containing formulation to temperature increase is shown to be more pronounced and favourable from a pulmonary delivery point of view than the one of the leucine-containing formulation. These results demonstrate the principle invoked for particle engineering at large *Pe* numbers.

The observed trend in Figure 3.5 of smaller $d_{e,50}$ with increasing atomizing pressure setting was expected since higher atomizing pressure leads to creation of smaller droplets and thus smaller particles. The simultaneous strong increase in FPF with increasing atomizing pressure setting, on the other hand, would suggest that the particle density was largely unaffected by the atomizing pressure as *Pe* is expected to remain almost the same with changes of atomizing pressure.

3.5.2 Performance of manufactured powder formulations

The geometric particle size of the powders was similar throughout all the formulations at the employed process conditions. Formulation NS/Leu+AC only exhibited a somewhat smaller $d_{e,50}$, which may be ascribed to bursts of the droplets and/or particles as ammonium carbonate sublimes, leading to the creation of smaller particles.

Significantly, marked differences in the aerodynamic performance were evident between formulations. The use of leucine as an additive together with the nanosuspension in the feed yielded considerably higher FPF than the other formulations. Given that the variation in geometric particle size between formulations was rather small (Table 3.1), the difference in aerodynamic performance was most likely due to differences in particle density. This was confirmed by the effective density measurements (Table 3.1). These results demonstrate that the addition of leucine elicited the formation of porous particles with decreased aerodynamic particle size. The latter was ultimately affected by precipitation of leucine in the perimeter of the drying droplets. Leucine is shown to be somewhat more efficient in this respect than albumin under the employed process conditions (Figure 3.7 and Figure 3.8) probably on account of the shorter time it requires to reach saturation concentration. At a higher inlet temperature (200°C), on the other hand, used in the investigation of the spray drying conditions (Figure 3.4), albumin-containing compositions were found to improve their performance relative to their leucine counterparts reflecting a process at larger *Pe* number for albumin. Ammonium carbonate did not contribute to the generation of increased porosity in the particles causing instead a geometric size reduction possibly because of burst during sublimation. Therefore, the improved FPF of the NS/Leu+AC

formulation is likely related to its even smaller geometric particle size as its particle density was not reduced compared to NS/Leu.

It is intriguing to note that formulation S/Leu+AC despite having the same composition as NS/Leu+AC exhibited a higher effective density and a much smaller FPF. This indicates that nanomilled API particles are necessary in order to obtain the porous composite particles providing enhanced aerodynamic performance. The reason for this can be that the distribution of the original drug microparticles within the droplets, and therefore also in the dried particles, is not as homogeneous as when nanosuspension feedstock is used. This could be expected due to the fact that the drug substance particles reach rather large sizes with $d_{e,90}$ of 8.4 µm (Figure 3.2). It is, therefore, unlikely that small composite particles will contain these large drug substance particles. Therefore, we assume that the particles of formulation S/Leu+AC that reach the lower NGI stages (stage 2 and below) contain only small drug particles, which account for ca 25% of the raw material particles.

Hence, careful choice of process and formulation parameters as well as raw material preparation/pre-processing are required to allow particle engineering by spray drying that insures production of powders with optimal aerodynamic properties. It was shown that applying the particle engineering approach has large potential to improve the product performance compared to the commercial product. In addition, once deposited in the deep lung, it can be expected the engineered particles to be less susceptible to phagocytosis due to their larger geometric size [63].

The different additives used affected the particles' specific surface areas. As SEM imaging indicated (Figure 3.6), leucine facilitated formation of a sponge-like particles, within which the drug nanoparticles were embedded. Such structures inherently have an increased surface area with nanosuspension in the feedstock showing stronger effect than the suspension (Table 3.1). This was in agreement with the effective density measurements, which showed similar but opposite trend. Effective density of most formulations followed the trend of the bulk density except for S/Leu+AC.

3.5.3 Dissolution rate

Dissolution rate measurements were performed in order to characterize the developed formulations after deep lung deposition as determined by the NGI. The employed experimental setup was chosen to closely mimic the *in vivo* conditions after drug inhalation when particles are deposited on mucus or a surfactant layer of very limited volume (10-30 mL) that is not subject to mechanical agitation. In the employed setup, dissolution takes place in a very small fluid volume and the drug substance then diffuses through a membrane to a large compartment representing the sink of the bloodstream.

No clear difference in the dissolution rate parameter k_{diss} between the NGI stages was found by data analysis using kinetic modelling that took into account the size of composite particles. Also, no difference of k_{diss} between the formulations was detectable. Significant non-zero values of the starting concentration $C(0)$ were found in all cases. This is a compelling result of the analysis indicating that a considerable amount of drug powder that was deposited on the insert of the modified NGI cup dissolved already in the course of the sample preparation for the dissolution test. More interestingly, the deduced concentration values were in most cases above the solubility of the drug substance in the dissolution medium. The latter was determined in separate

experiments to be equal to 0.03 mg/mL. It was furthermore verified that the TPGS content of the samples, originating from WMM, produced concentrations in the dissolution media that did not exceed the critical micellar concentration of this excipient. This leads to the conclusion that the drug substance was probably present at least in part in an amorphous state in the deposited powder. This conclusion is supported by XRPD measurements showing that the API is partially amorphous after WMM as well as after spray drying (Appendix 8.1). It is also consistent with the observed fast onset of dissolution. *C(0)* values for the different NGI stages correlated positively with the drug amount deposited in the respective stages. *C(0)* values were further higher for those formulations that were produced by spray drying of nanosuspensions than for the formulation containing the non-milled drug and for the physical mixture, this being in agreement with the proposed reasoning for $C(0) > 0$.

As a large proportion of the deposited drug was already dissolved at the beginning of the dissolution test, the deduced k_{diss} explained only a small part of the measured dissolution profile. This can be the reason for the observed variability of the k_{diss} results (Figure 3.11). It must be pointed out that the applied model-based data analysis made it possible to discern the contribution of the drug dissolved in the beginning and during the dissolution test. No differences in k_{diss} were found between the NGI stages for any of the formulations within experimental variability that would reflect variation in shape and/or surface roughness of particles. Also, no differences of k_{diss} between formulations were found despite the fact that the studied formulations differed considerably in their physical characteristics (Table 3.1). Additionally, similar k_{diss} values as for the engineered powders were found for the commercial product.

To better understand this finding, dissolution experiments with the complete formulations of each formulation were carried out. The deduced values of dissolution rate parameter k_{diss} were not significantly different from each other in a statistical paired test with the exception of the two extreme values (Table 3.2). This is largely in agreement with the result of the dissolution test with the samples of the NGI stages. Only the physical mixture yielded a ten-fold smaller k_{diss} value. Thus, all spray dried formulations exhibited a dissolution rate that was consistent with the size distribution of the composite particles while their specific surface area, which differed greatly among formulations, did not seem to influence their dissolution rate. We suggest that this may be because composite particles of all formulations contained the same primary API nanoparticles. This would mean that dissolution rate is actually defined by the surface area of the API particles, which is the same in all formulations. From a dissolution point of view, no difference in the outer accessible surface area of the composite particles of the different formulations seems evident although their specific surface area differs (see also below). The same argument can be applied to the powders of the NGI stages that differ in particle size but exhibit no difference in dissolution rate, the latter being defined by the surface area of the primary API nanoparticles. No difference in dissolution rate of formulation S/Leu+AC could be explained by the likely presence of very small drug particle sizes in the powder of the different stages caused by the homogeneity challenges described in Chapter 3.5.2.

In the kinetic model that was developed for evaluating dissolution behaviour, dissolution of the solid drug substance in the inner compartment containing the inhalable formulation and permeation of the substance through the membrane are treated as consecutive processes entailing additionally a homogeneous substance concentration in the inner unstirred compartment. Model-based analysis allows delineation of the contribution of each kinetic step to the overall mass transport process. In the experiments with the individual NGI stages, values for

k_{diss} reflecting dissolution and P reflecting membrane permeation were independently estimated. P was relevant chiefly in connection with the permeation of drug that was already dissolved in the inner compartment in the beginning of the measurement. For the complete formulation powders, the dissolution parameter k_{diss} alone adequately explained the measured concentration data while the membrane permeability coefficient, P, was found not to be significant for describing the data. This was further substantiated by the performed analysis showing that the fit was not sensitive to the value of P at large P values while at small P values no good approximation was attained. Dissolved drug substance amount in the beginning of the measurement was negligible compared to the much larger amount contained in the used complete formulation powder. Hence, in the experiment of the complete formulation powders, dissolution appears to be the kinetically controlling process.

Notably, k_{diss} values obtained on the one hand with powders from the NGI stages and on the other hand with the complete formulations were comparable, thus supporting the validity of the used model analysis. To further challenge the model, the plausibility of the k_{diss} values deduced from the fit of the model to the experimental data was examined. This parameter comprises the quantities given in the following equation:

$$k_{diss} = \frac{D\ 6\ \Gamma}{h\ \rho} \tag{3.14}$$

where all symbols were defined above.

It should be first pointed out that a constant thickness of the diffusion boundary layer, which was independent of particle size, was used in the present model. The effect of diffusion boundary layer on particle dissolution kinetics in stirred and unstirred media has been the subject of research in recent decades [180–182]. Dissolution has been treated as a chiefly diffusion-controlled process whereas in case of convective diffusion the effective thickness of the diffusion boundary layer required to adequately describe dissolution kinetics was shown to depend on the size of the dissolving particles. For particle size in the range of a few micrometres up to tens of micrometres this thickness was demonstrated on theoretical grounds, and confirmed experimentally, to be comparable to the respective radius of the particles [68,183,184]. In the stirred USP II dissolution apparatus, a difference between the tangential fluid velocity and particle velocity was documented under non-slip conditions that increased at higher stirring rates, substantiating convective diffusion as dissolution controlling mechanism [185]. However, in the experimental arrangement employed in the present study, the dissolving particles are separated from the stirred outer bulk solution by a polymeric membrane and were therefore not subject to agitation. For this reason, the thickness of the diffusion boundary layer was not assumed to depend on particle size and a constant thickness was used in the dissolution model instead.

For the diffusion coefficient, D, a typical value for a low molecular weight drug substance of approximately 5×10^{-6} cm^2/s [182–184], and for particle density, ρ, a representative value of the effective density measurement of 0.45 g/cm^3, may be used. The shape factor, Γ, denotes the deviation of the specific surface area of the particles from that of smooth spheres. The manufactured particles had an uneven surface (Figure 3.6) and a large specific surface area that depended on the formulation (Table 3.1). The effect of surface morphology on processes taking place at the solid surface such as dissolution and chemical reaction has been previously described by the use of fractal geometry [186,187] and time-dependent rate coefficients [188]. It has been recognized, however, that frequently the surface fractal dimension reflects an active surface of

the particle participating in the process that does not coincide with the total surface area of the particle but rather corresponds to an outer exposed region of the surface. Also, a distinction between the total (as determined by BET analysis) and the external surface area has been made, the latter being actively involved in the dissolution process [68]. For this reason, the simplifying assumption of assigning Γ the smallest possible value of $\Gamma = 1$ was made for the following discussion. This is further consistent with the observation that there is no difference in k_{diss} between formulations despite their different specific surface areas.

Using the above values for these quantities and a typical value of $k_{diss} = 2\times10^{-5}$ cm⁴/(mg·min) deduced from the fitting, a thickness of the diffusion boundary layer of h=0.2 cm is estimated from eq. 3.14. This thickness, which is apparently consistent with the deduced dissolution kinetics, is far larger than values commonly reported for dissolution process controlled by convective diffusion. This discrepancy is attributed to the confined and unstirred inner compartment delimited by the polymeric membrane, in which dissolution takes place. Dissolution of solid particles in a stagnant unbounded (infinite) or bounded (confined) fluid has been treated theoretically and the effect of bulk concentration arising from confinement due to impermeable boundaries has been demonstrated [182,189]. The present situation, however, of dissolution in a confined and stagnant medium with permeable boundaries at which flux boundary conditions apply has, to the best of the authors' knowledge, not been resolved. It is hypothesized that the unrealistically large thickness of the diffusion boundary layer found in this study is a result of the heterogeneity of the dissolved drug concentration due to the lack of convection in the compartment that contains the dissolving particles. Nevertheless, it should be pointed out that model-based analysis has been instrumental for unravelling the contribution of the processes that play a role in the dissolution experiment with the present experimental setup.

3.6 Conclusion

In this work, we have demonstrated the feasibility of preparation of low-density particles with superior aerodynamic properties and fast dissolution by wet media milling and subsequent application of particle engineering *via* spray drying. Interestingly, omission of the milling step greatly decreased fine particle fraction of the formulation. The FPF of a commercial product of the same API yielded very similar results as when WMM was not used. Therefore, equal importance should be given to drug pre-processing by particle size reduction and to spray drying when formulating engineered powders for inhalation to achieve advantageous performance over carrier-based formulations. The geometric size of the spray-dried particles was larger than that of micronized drug, additionally offering the advantage of evading phagocytosis. The choice of additives can largely influence the physical properties of the spray dried powders. Leucine facilitated formation of low-density powders irrespective of the use of WMM. However, it is important to note that the ability of an excipient to facilitate formation of low-density particles depends, in addition to the saturation solubility of the excipient, on the applied spray drying conditions under which the use of albumin as excipient may present a valid alternative.

Very fast drug dissolution of deposited powders with no clear difference among individual NGI stages of each formulation or among the formulations was found by the model-based data analysis despite the large differences in particle shape and morphology among the formulations. We conclude that the primary drug particle properties govern dissolution rate and that processing can accelerate dissolution for example by amorphization.

The proposed combination of processes has the potential to become a platform technology for processing of poorly water-soluble drugs for inhalation. Advantageously, it is solely water-based and readily scalable. It was shown to be suitable for high drug load formulations and may also be attractive for multiple drug formulations.

Chapter 4

4 Investigation of drug dissolution and uptake from low-density DPI formulations in an impactor integrated cell culture model

Besides deposition, pulmonary bioavailability is determined by dissolution of particles in the scarce epithelial fluid and by cellular API uptake. In the present work, we have developed an experimental *in vitro* model, which is combining the state-of-the-art next generation impactor (NGI), used for aerodynamic performance assessment of inhalation products, with a culture of human alveolar A549 epithelial cells to study the fate of inhaled drugs following lung deposition. The goal was to investigate five previously developed nano-milled and spray-dried budesonide formulations and to examine the suitability of the *in vitro* test model. The NGI dissolution cups of stages 3, 4, and 5 were transformed to accommodate cell culture inserts while assuring minimal interference with the air flow. A549 cells were cultivated at the air-liquid interface on Corning® Matrigel® -coated inserts. After deposition of aerodynamically classified powders on the cell cultures, budesonide amount was determined on the cell surface, in the interior of the cell monolayer, and in the basal solution for four to eight hours. Significant differences in the total deposited drug amount and the amount remaining on the cell surface at the end of the experiment were found between different formulations and NGI stages. Roughly 50% of budesonide was taken up by the cells and converted to a large extent to its metabolic conjugate with oleic acid for all formulations and stages. Prolonged time required for complete drug dissolution and cell uptake in case of large deposited powder amounts suggested initial drug saturation of the surfactant layer of the cell surface. Discrimination between formulations with respect to time scale of dissolution and cell uptake was possible with the present test model providing useful insights into the biopharmaceutical performance of developed formulations that may be relevant for predicting local bioavailability. The absolute quantitative result of cell uptake and permeation into the systemic compartment is unreliable, though, because of partly compromised cell membrane integrity due to particle impaction and professed leakiness of A549 monolayer tight junctions, respectively.

4.1 Introduction

Bioavailability of a drug is given, among others, by its interaction with the absorption epithelium under *in vivo* conditions [139]. This is commonly studied using *in vitro* cell culture systems. Cell cultures are mostly used under submerged conditions, which is a suitable approach for most drug delivery routes. However, pulmonary drug delivery presents a challenge as the submerged conditions do not properly reflect the *in vivo* system where air-liquid interface (ALI) exists.

Mimicking the *in vivo* situation in terms of liquid amount and composition in the cell culture system is therefore crucial when studying the interaction of deposited particles or droplets with the lung epithelium [46,157].

For evaluation of inhalation drugs' performance *in vitro*, several established deposition systems exist, *e.g.* multistage liquid impinger, Andersen cascade impactor, or next generation impactor. They are indispensable in formulation development as they characterize the aerodynamic properties of a formulation by its classification according to aerodynamic particle size. In addition, it is highly desirable for complete and relevant characterization of the performance of a pulmonary formulation to study the behaviour of the inhalable fraction of particles with cells that simulate the *in vivo* state with respect to ALI.

Studies that combine aerodynamically classified deposition and cell interaction are still rather rare. In some reports, pharmacopoeial instruments such as the twin-stage impinger [159,160], multistage liquid impinger [161,190], and Andersen cascade impactor [163,191] were transformed to accommodate a cell culture system. In one instance, also the NGI was used but without clear description of the NGI transformation [165]. It is important to note that deposition in all these systems is based on impaction, which induces certain cell stress [53]. More gentle deposition, however without aerodynamic classification, can be ensured using sedimentation-based systems, *e.g.*, the Pharmaceutical Aerosol Deposition Device on Cell Culture (PADDOCC) [166], Air-Liquid Interface Cell Exposure (ALICE) System [167], or LTC-C Computer-Controlled Long-Term Cultivation (CULTEX®) system [168]. Alternatively, insufflators such as MicroSprayer® Aerosolizer IA-1C can also be utilized [22,169].

In these experiments of deposition combined with cell interaction, immortalized, bronchial Calu-3 cell line has been most commonly used. This cell line is generally appropriate for permeation studies that concern drug delivery to the bronchial region and produces a mucus layer when grown at ALI. Grown in submerged conditions, this cell line forms tight junctions with high transepithelial electrical resistance (TEER) values (≈ 1000 Ωcm^2), which are quite lower (≈ 300 Ωcm^2) when grown at ALI [192]. Notably, the ALI TEER values are comparable to values reported for the rabbit airway epithelium [192].

In the present work, we transformed the NGI to include the immortalized, alveolar A549 cell line for studying particle dissolution and drug uptake of aerodynamically classified powders from dry powder inhalers (DPI). The A549 cell line was used due to the focus on deep lung delivery. It currently represents a broadly used cell culture model for the alveolar epithelium [193] and has not been used in combination with aerodynamic powder classification before. These cells possess phenotype of epithelial type II cells – one of the two major cell type present in the alveolar region [53]. A549 cells have been extensively characterized both under submerged and ALI conditions and it was shown that TEER, even though generally low (≈ 150 Ωcm^2), does not depend on the conditions used. Also, the cells were shown to produce surfactant when grown on ALI. Additionally, positive staining of these cells for zonula occludens-3, occluding, and claudin-2 suggests the formation of tight junctions in the epithelial barrier [22,194]. It is acknowledged that A549 culture exhibits lower TEER compared to submerged primary alveolar type II cells (*e.g.* hAEpC [195,196]); however, no *in vivo* TEER values are available as a reference. Still this cell line may not be suitable for permeation studies of drugs across the epithelium to predict systemic bioavailability as indicated before [53,197].

In this work, the next generation impactor, which is the state-of-the-art pharmacopoeial method for aerodynamic testing of inhalation formulations in the industry, was employed and its cups were adapted to incorporate low-profile Millicell® cell culture insert for deposition of aerodynamically classified powders on the surface of A549 cells. The purpose of this work was to develop an *in vitro* experimental model for investigating factors that are relevant for local bioavailability of pulmonary formulations under conditions closely reflecting the *in vivo* situation. With this model, the effect of formulation properties and the potential role of the impactor stage should be elucidated.

Our aim was to a) evaluate dissolution upon deposition and cellular drug uptake of previously developed low-density powders for inhalation with improved lung deposition [198], and b) examine suitability of this experimental arrangement that combines NGI with the A549 cells to evaluate bioavailability and performance of pulmonary formulations intended for local delivery such as to treat bacterial infection, inflammation, or lung cancer. Drug products for these indications represent the majority of inhalation products on the market [199].

4.2 Materials and methods

4.2.1 Materials

Matrigel® matrix (growth factor reduced; Corning®, Germany) was used at a concentration of ≈ 4 g/L. *In vitro* toxicology assay kit and Millicell® cell culture inserts PICM0RG50 (30 mm diameter, 0.4 µm pore size, 4.2 cm^2 surface area; Millipore by Merck, Germany) with PTFE membrane were purchased from Sigma-Aldrich (Switzerland). LIVE/DEAD™ cell imaging kit was obtained from ThermoFisher Scientific (USA). Ammonium formate and formic acid were from Fluka (Switzerland). Ethanol (EtOH) and acetonitrile (both HPLC grade) were purchased from J.T.Baker (The Netherlands). Ultrapure water (Milli-Q®, Millipore, Switzerland) was used for all experiments.

4.2.1.1 A549 cell culture

Experiments were done with the human alveolar epithelial type II cell line A549, which was kindly donated by B. Rothen-Rutishauser (Adolphe Merkle Institute, University of Fribourg, Switzerland). The cells were cultured in RPMI 1640 (Gibco, Life Technologies Europe B.V., Switzerland) supplemented with 10% (v/v) fetal bovine serum (FBS; PAA Laboratories, Chemie Brunschwig AG, Switzerland), 1% (v/v) L-Glutamine (Life Technologies Europe, Switzerland) and 1% (v/v) penicillin/streptomycin (Gibco, Switzerland). The cells were kept in a humidified incubator at 37°C and 5% CO_2. Cell concentration was calculated using Trypan blue exclusion method. For the powder deposition experiments, cells of passage numbers 6 - 10 were seeded in low height cell culture inserts (PICM0RG50) at a density of 1.19×10^5 cells/cm^2. These inserts were selected having low sidewalls in order for them to fit in the transformed dissolution cup.

4.2.2 Methods

4.2.2.1 Matrigel® bioprinting

Due to the hydrophobic nature of the PTFE membrane, it was necessary to treat the inserts with a protein matrix such as Matrigel® before application of the cells on the membrane. The bioprinter BioFactory™ (regenHU Ltd., Switzerland) equipped with a contact dispensing microvalve CF300

(MVC03-006; regenHU Ltd.; nozzle diameter 0.3 mm) was used to print Matrigel® matrix on the Millicell® cell culture inserts using modified method of Horváth et al. [200]. Bioprinter parts that were in contact with Matrigel® were cooled in advance down to 5°C to prevent Matrigel® gelling during bioprinting. The applied bioprinting parameters were dispensing pressure of 0.27 kPa, dosing distance of 0.2 mm, and valve opening time of 110 µs.

4.2.2.2 Cell growth on Matrigel®-coated inserts

One mL of A549 cell suspension was evenly distributed on wetted, Matrigel®-coated insert membrane and the inserts were placed into a 6-well plate where each well contained 1 mL of supplemented RPMI medium. The cells were grown in the incubator until confluency for 3 days while exchanging the medium in both apical and basal chamber on day 2. On day 3, the apical medium was removed and the cells were kept exposed to air, creating an air-liquid interface (ALI). The cells were at ALI for 12 - 18 hours prior to further use, which ensured surfactant layer formation. The presence of surfactant layer on the cells was verified by the droplet method as reported before [22].

4.2.2.3 Powder deposition on cell cultures

In order to deposit powder on the cell surface, the NGI dissolution cups (Copley Scientific, UK) had to be first transformed to allow accommodation of a cell culture insert. Figure 4.1 illustrates the changes made to the NGI dissolution cup. The aerodynamic particle size distribution of a powder before and after these changes was assessed.

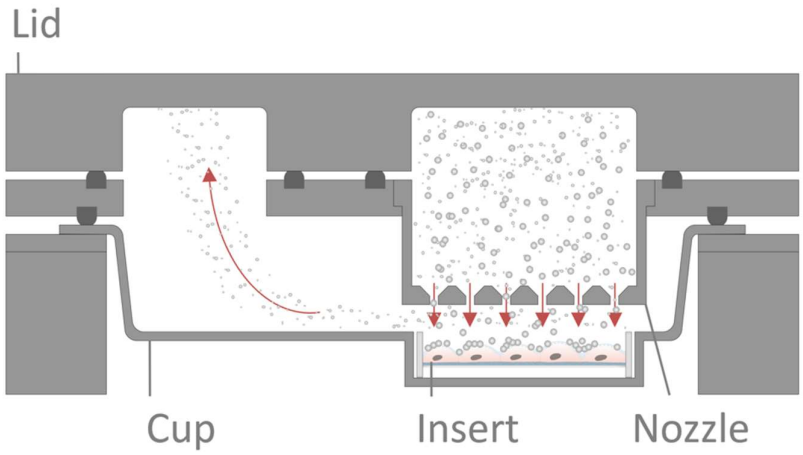

Figure 4.1 Schematics of NGI dissolution cup transformed to allow placement of a cell culture insert.

For the deposition experiment, insert with cells at ALI was placed into the transformed NGI cup in either stage 3, 4, or 5, which at 68 L/min have aerodynamic cut off diameters of 4.16 - 2.64 µm, 2.64 - 1.56 µm, and 1.56 - 0.88 µm, respectively. The transformed NGI was operated as described earlier [198] using the RS01 Mod. 8 (Plastiape S.p.a., Italy) dry powder inhaler; only the powder fill weight in the capsules was decreased to ≈ 0.2 mg in order to reduce number of particles depositing on the cell surface. The small powder amounts were weighted using an analytical balance (type XP2U Mettler Toledo, Switzerland) with precision of 0.1 µg. After the exposure, the insert was placed into a 6-well plate filled with 1 mL of RPMI 1640 medium supplemented with 1% (v/v) L-Glutamine and 1% (v/v) penicillin/streptomycin and kept in an incubator. Samples

of 100 µL were taken from the basal medium for up to eight hours and this volume was immediately replenished with fresh medium. At the end of the experiment, samples' cell surface was washed with 1 mL of cold EtOH:H_2O (50:50) mixture to collect and quantify any remaining budesonide on the apical side. After this step, the cells were lysed with 1% Triton™ X-100 (Sigma Aldrich, Switzerland) in water (0.75 mL) for 30 minutes at 37°C while gently stirring on an orbital shaker.

The *stage drug amount* was calculated as the sum of the drug amounts found in all three compartments, *i.e.*, the wash from cell surface, in the cell interior, and the basal medium at the end of the experiment. The *total drug amount* was calculated as the sum of the stage drug amounts from stage 3 - 5. The terms defined here will be used hereinafter.

Table 4.1 summarizes the formulations with nominal drug load of 43% used for the cell exposure experiments. Preparation of the formulations is in detail described in [198].

Table 4.1 Overview of formulations used for cell exposure experiments

Formulation notation	Feedstock basis	Spray drying additive	Mean geometric diameter [µm]	FPF [%]
NS/Leu+AmC	Nanosuspension	Leucine Am. carbonate	4.39 ± 0.02	61
S/Leu+AmC	Non-milled suspension	Leucine Am. carbonate	5.04 ± 0.02	22
NS/Leu	Nanosuspension	Leucine	5.30 ± 0.03	46
NS/Alb	Nanosuspension	Albumin	5.01 ± 0.10	39
NS/–	Nanosuspension	-	5.30 ± 0.06	18

4.2.2.4 HPLC-UV-MS

Budesonide (B) and budesonide oleate (BO) were analysed by HPLC-UV-MS series 1200 equipped with a degasser G1379B, a binary pump G1312A, an autosampler G1367B, a thermostat G1330B, a column oven G1316A, a variable wavelength detector G1314B, and a single quadrupole MS detector G6130A (all Agilent Technologies, USA). A C-8 reversed phase column (Kromasil® 100, 5 µm, 100 × 2.1 mm; Dr. Maisch, Germany) and mobile phase consisting of (A) ammonium formate buffer (25 mM, pH 3.2) : ACN (50:50) and (B) ammonium formate buffer (125 mM, pH 3.2) : ACN (10:90) were used. To analyse the calibrants of the first experiment, an isocratic mode was used with A:B = 100:0 a flow rate of 0.2 mL/min and a run time of 10 min. The composition of the mobile phase was varied in a gradient mode for all samples and the calibrants of the second experiment with a flow rate of 0.2 mL/min and a runtime of 50 min: 0 - 5 min A:B = 100:0, 5 - 15 min linear change to A:B = 0:100, 15 - 40 min A:B = 0:100, 40 - 41 min linear change to A:B

= 100:0, and 41 - 50 min A:B = 100:0. The samples were cooled in the autosampler to 4°C and the column temperature was set to 25°C. The ions were generated by atmospheric pressure electrospray ionization and the MS detector was run in SIM mode at positive polarity with capillary voltage 4000 V, fragmentor 100 V, drying gas flow 10 L/min, drying gas temperature 350°C, and nebulizer pressure 30 psig. Budesonide and budesonide oleate were detected at 240 nm in UV. Budesonide was detected at m/z 413.2 and 431.2 and budesonide oleate at m/z 677.5 and m/z 685.5 in MS corresponding to their protonated fragments and parent compounds, respectively. The metabolite was quantified with the calibration curve of budesonide in UV. The LOQ of budesonide for an injection volume of 50 µL was 0.07 µM in UV.

4.2.2.5 Cell integrity measurement

The cell damage induced during the experiment was assessed using a TOX7 cytotoxicity kit based on lactate dehydrogenase (LDH) quantification in the basal medium (Sigma Aldrich, Switzerland). An insert submerged in 5 mL of serum-free RPMI 1640 containing 10% Triton™ X-100® was used as a positive control. As a negative control, insert placed on the serum-free medium without any further treatment or exposure was used. Samples of the basal medium as well as positive control were diluted 10x with water prior to processing. LDH was quantified in triplicate spectrophotometrically in a 96-well plate at 490 nm. Background absorbance was measured at 690 nm and subtracted from the primary absorbance measurement at 490 nm. Additionally, absorbance of the serum-free RPMI 1640 medium was subtracted from all averaged values. Cell damage was calculated using the following equation (eq. 4.1):

$$Cell\ damage\ (\%) = \frac{Abs_{sample} - Abs_{neg\ control}}{Abs_{pos\ control} - Abs_{neg\ control}} \times 100 \qquad (4.1)$$

4.2.2.6 LIVE/DEAD™ assay

Right after deposition of the formulation NS/Leu+AmC on stage 3, 4, and 5, the cells were stained with the commercially available LIVE/DEAD™ Cell Imaging Kit (Invitrogen™ by Thermo Fisher Scientific, USA). According to the manufacturer, the Live Green was mixed with the Dead Red and 1 mL was added on the apical side of the insert and incubated for 30 min at room temperature. The staining was removed, PBS was added to the basal side and the cells were imaged with a fluorescence microscope (Olympus IX83, Japan). As controls non-stained and stained living cells and stained dead cells (30 min treatment of living cells with 70% MeOH) were used. The controls did not undergo deposition in the NGI.

4.2.2.7 Kinetic modelling

The process of drug uptake into the cells after particle deposition, drug metabolism and release into the basal solution was modelled in order to estimate kinetic parameters that would allow a quantitative description of the process. The time-dependent change of drug amount on the cell surface (eq. 4.2), drug and metabolite amount in the cells, (eq. 4.3) and (eq. 4.4), respectively, and drug amount in basal solution (eq. 4.5) was described by the following system of ordinary differential equations:

$$\frac{dB_A}{dt} = -k_u B_A \qquad (4.2)$$

$$\frac{dB_C}{dt} = k_u B_A - k_m B_c - k_r(B_C - K \cdot B_B) \quad (4.3)$$

$$\frac{dBO_C}{dt} = k_m B_C \quad (4.4)$$

$$\frac{dB_B}{dt} = k_r(B_C - K \cdot B_B) \quad (4.2)$$

where, B_A is budesonide mass in the apical compartment *i.e.*, on cell surface, B_C is budesonide mass in the cell, BO_C is budesonide oleate mass in the cell, B_B is budesonide mass in the basal solution, k_u is uptake rate constant of drug from the cell surface into the cell, k_m is metabolic rate constant of drug to its oleate metabolite, k_r is release rate constant of the drug from the cell into the basal solution, K is partition coefficient of drug between the cell interior and the basal solution, and t is time. All mass transfer and conversion steps were treated as first order processes and equilibrium of dissolved drug mass was assumed to ensue between the cell interior and the basal compartment.

The above equations were solved using numerical differentiation and the system was at the same time fitted by least square approximation simultaneously to all experimental data for B_A, B_C, BO_C, and B_B whereby optimal values of the parameters k_u, k_m, k_r and K were estimated. The software EASY-FIT® [178] was employed. Boundary conditions at t=0 of $B_A=B_A(0)$ and $B_C=BO_C=B_B=0$ were applied, whereas $B_A(0)$ was set equal to the sum of recovered drug amounts in all compartments including the metabolite at the end of the experiment.

4.2.2.8 Statistical analysis

Statistical analysis of the data was done using Excel's two-way ANOVA (Microsoft, USA). Stage drug amount was analysed as absolute amount, while budesonide and budesonide oleate in the compartments were analysed as relative amounts.

4.3 Results and discussion

4.3.1 Powder deposition and its pattern in transformed NGI

Powder was deposited on an insert placed either in stage 3, 4, or 5, which are the stages contributing to the largest extent to so-called fine particle fraction (FPF). The FPF is the percentage of the powder with an aerodynamic diameter below 5 µm and it provides an estimate of the drug dose effectively delivered to the lungs. The used formulations were found to differ markedly in their FPFs using the original, non-transformed NGI (Table 4.1); their properties that are responsible for this behaviour are extensively discussed elsewhere [198].

In the present work utilizing transformed NGI, the stage drug amount was determined as the sum of the quantities of budesonide and its metabolic product measured in the three investigated cell compartments, *i.e.*, the apical compartment constituting the cell surface, the cellular compartment, and the basal solution, at the end of the experiment. Deposited drug amount differed significantly between formulations and between stages of the NGI, the effect of both the formulation and the stage being very significant ($p<0.01$) as determined by two-way ANOVA (Figure 4.2, Table 4.2).

Table 4.2 ANOVA Total deposited budesonide amount (nmol) (significant factors are highlighted in bold)

Source of variation	Sum of squares (SS)	df	Mean square (MS)	F-ratio	p-value	Critical F-value
NGI stage	156.97	2	78.49	40.12	**0.0000**	3.68
Formulation	88.85	4	22.21	11.35	**0.0002**	3.06
Interaction	32.03	8	4.00	2.05	0.1103	2.64
Error	29.34	15	1.96			
Total	307.20	29				

Total drug amount decreased among formulations in the order:

NS/Leu+AmC > NS/Leu > NS/Alb > NS/– > S/Leu+AmC

The amount deposited in individual stages decreased for all formulations in the order stage 3 > stage 4 > stage 5, this trend being stronger for the formulations NS/Alb, NS/–, and S/Leu+AmC (Figure 4.2). These results are fully consistent with powder deposition measured with the NGI prior to its transformation for accommodating the inserts with the cell culture [198], demonstrating that this transformation did not influence the deposition/classification performance of the NGI. Ranking of the total drug amount in the three stages for the studied formulations was virtually the same before and after NGI transformation (columns, Figure 4.2), which additionally confirmed the negligible influence of this transformation on deposition. It should be noted that this comparison can only be performed in terms of ranking as the amount of powder in the capsules and the surface area of deposition varied between the two situations.

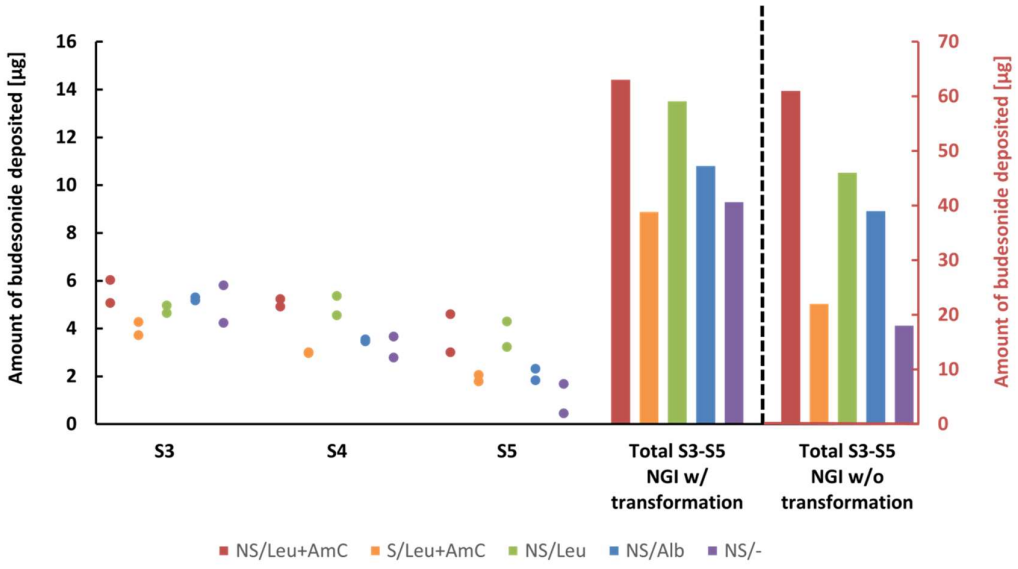

Figure 4.2 Budesonide deposition in transformed NGI in stages 3, 4, and 5 given as raw data (dots) and mean total drug amount of the three stages of all formulations (left set of columns) depicted on left y-

axis. Total drug amount of the three stages of all formulations in non-transformed NGI (right set of columns) depicted on right y-axis.

This verification was essential for making sure that the aerodynamics and hence powder deposition pattern were not markedly affected by the transformation of the NGI. In fact, the surface of the cell monolayer lay somewhat lower than the surface of the impaction cup of the non-transformed NGI in order to prevent the upper edge of the insert sidewall from protruding above the cup's surface (Figure 4.1).

4.3.2 Budesonide compartment distribution

Budesonide was detected in significant amounts in all compartments of the cell culture for all formulations (Figure 4.2, Figure 4.3). The percent drug amount recovered from the cell surface at the end of the experiment depended very significantly ($p<0.01$) on the formulation (Table 4.3), NS/Leu+AmC and NS/Leu exhibiting larger recovery amounts compared to the other formulations (Figure 4.3). This amount was larger for stage 3 compared to stages 4 and 5 (Figure 4.3), the effect of stage being also statistically very significant ($p<0.01$) by the two-way ANOVA (Table 4.3).

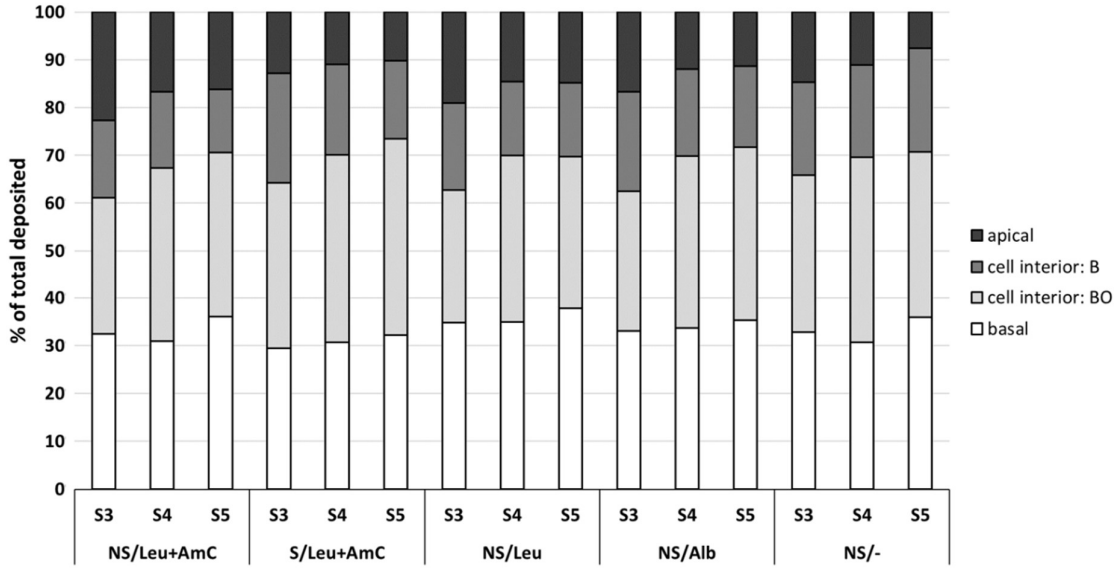

Figure 4.3 Mean percent drug distribution in the compartments of the in vitro test system (B = budesonide, BO = budesonide oleate) for the different formulations and NGI stages 3, 4 and 5 (n=2).

Table 4.3 ANOVA Budesonide amount in apical compartment (%) (significant factors are highlighted in bold)

Source of variation	Sum of squares (SS)	df	Mean square (MS)	F-ratio	p-value	Critical F-value
NGI stage	151.22	2	75.61	8.61	**0.0032**	3.68
Formulation	246.55	4	61.64	7.02	**0.0022**	3.06
Interaction	20.04	8	2.50	0.29	0.9607	2.64
Error	131.79	15	8.79			
Total	549.60	29				

On the contrary, the percent amount of budesonide determined at the end of the experiment in the interior of the cells and in the basal solution did not depend on the formulation or the stage under consideration (

Table 4.4 and Table 4.5).

Table 4.4 ANOVA Budesonide amount in cell compartment (%) (significant factors are highlighted in bold)

Source of variation	Sum of squares (SS)	df	Mean square (MS)	F-ratio	p-value	Critical F-value
NGI stage	39.76	2	19.88	0.66	0.5305	3.68
Formulation	107.89	4	26.97	0.90	0.4898	3.06
Interaction	48.13	8	6.02	0.20	0.9863	2.64
Error	450.80	15	30.05			
Total	646.59	29				

Table 4.5 ANOVA Budesonide amount in basal solution (%) (significant factors are highlighted in bold)

Source of variation	Sum of squares (SS)	df	Mean square (MS)	F-ratio	p-value	Critical F-value
NGI stage	62.55	2	31.28	1.07	0.3690	3.68
Formulation	82.40	4	20.60	0.70	0.6024	3.06
Interaction	15.20	8	1.90	0.06	0.9997	2.64
Error	439.97	15	29.33			
Total	600.12	29				

The release of drug into the basal solution exhibited a similar pattern as a function of time for all formulations and impactor stages, seemingly reaching an equilibrium within approximately two hours (Figure 4.4). In addition, large amounts of budesonide oleate, a drug metabolite reported previously to be formed in lung cells [201,202] were detected in the cell interior (Figure 4.3). The relative metabolite amount depended on the stage ($p<0.05$) (Table 4.6) with stage 3 exhibiting generally smaller amounts than the other two stages. The total cell content (B+BO) (in %) depended on the formulation ($p<0.01$) (Table 4.7Table 7), NS/Leu+AmC and NS/Leu exhibited a smaller amount than the other formulations. The ANOVA in Table 4.3 to Table 4.7 were carried out with the relative drug amount for the different compartments expressed in percent of the total amount deposited in the respective impactor stage.

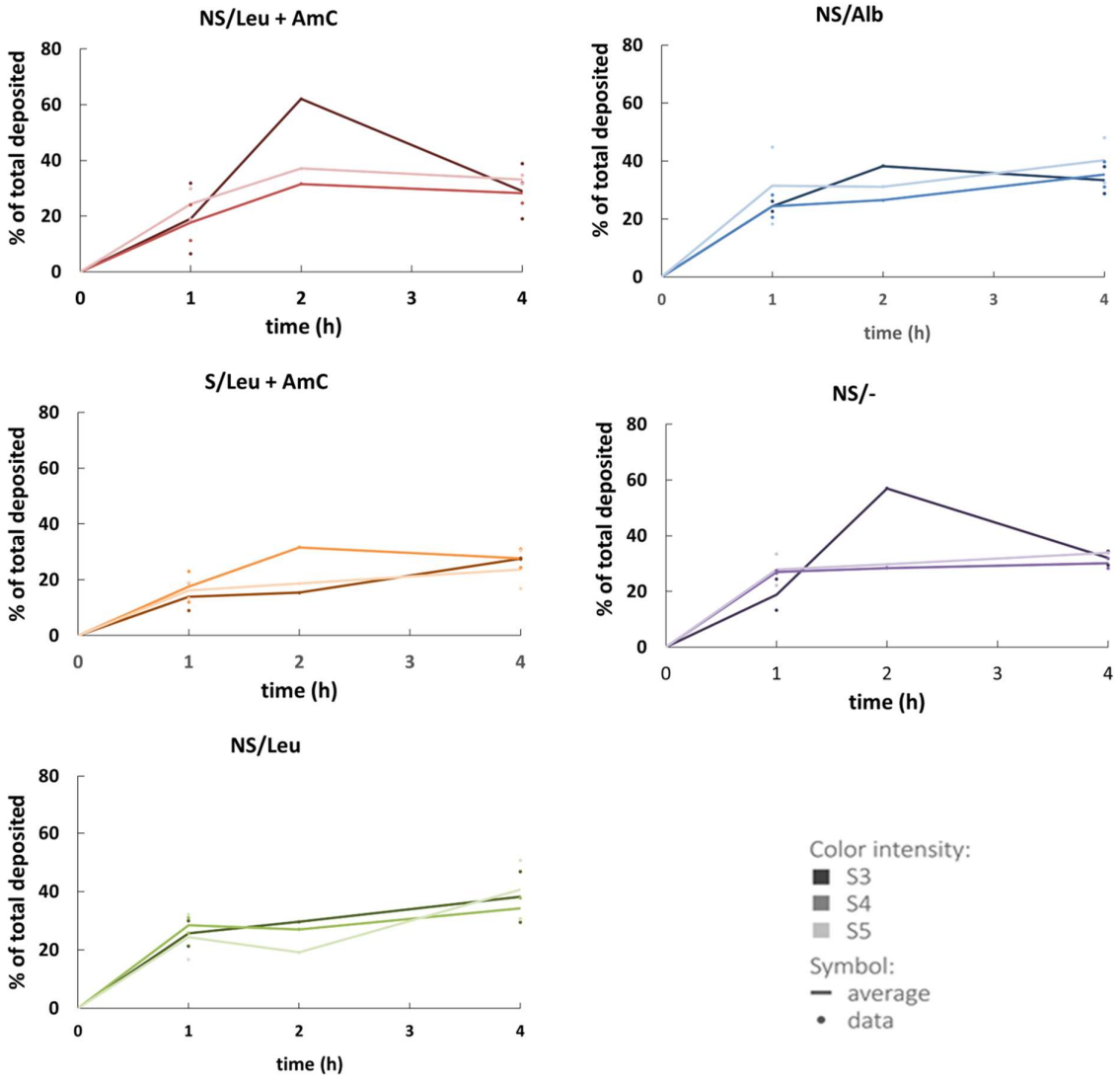

Figure 4.4 Budesonide concentration in the basal compartment as a function of time for the different formulations and NGI stages 3, 4 and 5. Dot symbols give individual raw data and lines connect average points.

Table 4.6 ANOVA Budesonide oleate amount in cell compartment (%) (significant factors are highlighted in bold)

Source of variation	Sum of squares (SS)	df	Mean square (MS)	F-ratio	p-value	Critical F-value
NGI stage	229.11	2	114.56	5.56	**0.0156**	3.68
Formulation	167.25	4	41.81	2.03	0.1418	3.06
Interaction	33.13	8	4.14	0.20	0.9862	2.64
Error	309.14	15	20.61			
Total	738.63	29				

Table 4.7 ANOVA Total drug amount in cell compartment (%) (significant factors are highlighted in bold)

Source of variation	Sum of squares (SS)	df	Mean square (MS)	F-ratio	p-value	Critical F-value
NGI stage	101.30	2	50.65	2.28	0.1364	3.68
Formulation	469.46	4	117.36	5.29	**0.0074**	3.06
Interaction	30.51	8	3.81	0.17	0.9916	2.64
Error	333.01	15	22.20			
Total	934.28	29				

4.3.3 Drug dissolution and cell uptake

It can be inferred from the above analysis that upon powder deposition, no complete dissolution of drug particles took place in the course of the experiment for formulations NS/Leu+AmC and NS/Leu, particularly on stage 3, which could be attributed to the comparatively large amount of deposited powder in the noted instances. The observed disproportionate distribution of drug in the investigated compartments between formulations and stages is illustrated in Figure 4.5 showing that the percentage recovered from the cell surface increased with increasing deposition while the percentage released in the basal solution did not, and is considered to be due to saturation of the surfactant-rich fluid lining of the alveolar cells with drug. This layer consists primarily of phospholipids including saturated and unsaturated phosphatidylcholine, and water [203] and has been described to have a thickness on average of 0.1 µm [204]. The solubility of budesonide in the model lung surfactant preparation Survanta™ was reported to be 32 mg/mL [205]. For the used inserts with a surface area of 4.2 cm^2, a volume of the surfactant cell lining of 0.042 µL and a maximal dissolvable drug amount in this volume of 3.12 nmol (1.34 µg) can be estimated based on these data. The drug amount deposited on the cells was for all formulations and nearly all stages well above this margin (Figure 4.2). The drug amount recovered from the cell surface at the end of the experiment was for formulations NS/Leu+AmC, NS/Leu, and NS/Alb in stage 3 roughly equal to or somewhat below this margin (Figure 4.2 and Figure 4.3) supporting the proposed interpretation of saturation of the surfactant layer and hence no complete

dissolution of deposited drug until the very end. In all other cases, considerably smaller drug amounts were recovered from the apical compartment. The larger relative drug amount remaining on the cell surface correlated with the smaller relative amount of metabolite found in the interior of the cells in the same inserts. No other effect of formulation or difference between stages with respect to drug dissolution or cell uptake was detected. Also, no interaction between the stage and formulation in respect to any of the dependent variables was found to be significant in the two-way ANOVA (Table 4.2 to Table 4.7).

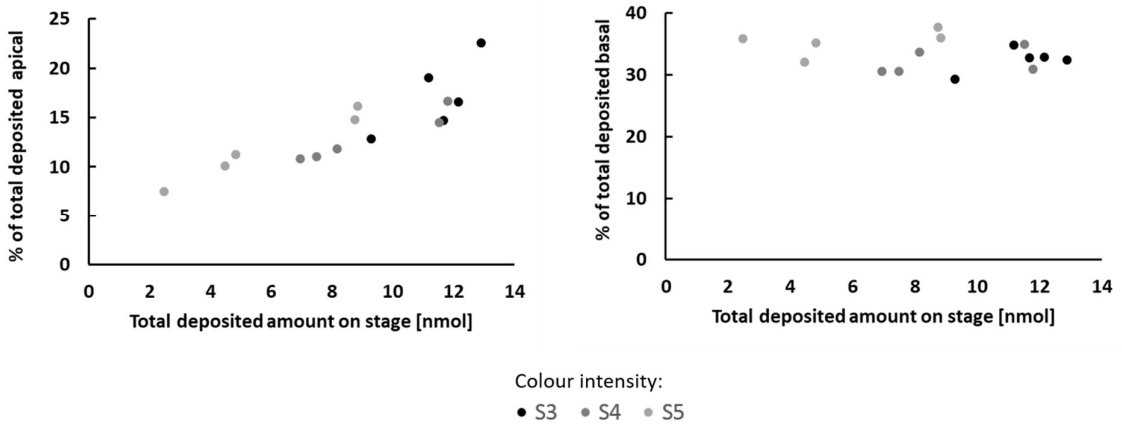

Figure 4.5 Dependence of relative drug amount at the end of the experiment in the apical compartment (left panel) and in the basal solution (right panel) on the total deposited absolute drug amount. Black symbols, dark grey symbols and light grey symbols depict results of stage 3, stage 4 and stage 5, respectively, each for the five formulations. Dot symbols give individual raw data.

These results therefore imply that while for small deposition amounts dissolution was rather quick and equilibrium of drug distribution among the investigated compartments was reached, dissolution of comparatively large deposited drug amounts took place almost throughout the duration of the experiment, *i.e.* four to eight hours. Hence, dissolved drug appeared to be distributed in the same fashion for all formulations and stages among the compartments as indicated by the very similar release profiles into the basal solution (Figure 4.4), while undissolved drug, if any, remained on the cell surface (Figure 4.5). Incidentally, no particle uptake by phagocytosis by the epithelial cells was assumed to take place [22]. Kinetic analysis of the results supports this view. An empirical first order rate constant k_u was used in the kinetic model to describe the appearance of drug in the interior of the cell (Figure 4.6). This is a combined rate constant capturing the consecutive steps of dissolution and cell entry of the drug since it was not feasible in the performed experiments to delineate these two steps. This rate constant acquired its smallest values for formulations NS/Leu+AmC and NS/Leu, particularly in stage 3, and was higher for the other formulations in this stage and in stages 4 and 5. This is consistent with the proposed interpretation of the data based on the two-way ANOVA, suggesting a protracted dissolution and uptake of the drug by the cells for the larger amounts of deposited powder. No systematic variation of the other two fitted parameters (k_r, K) was found (not shown).

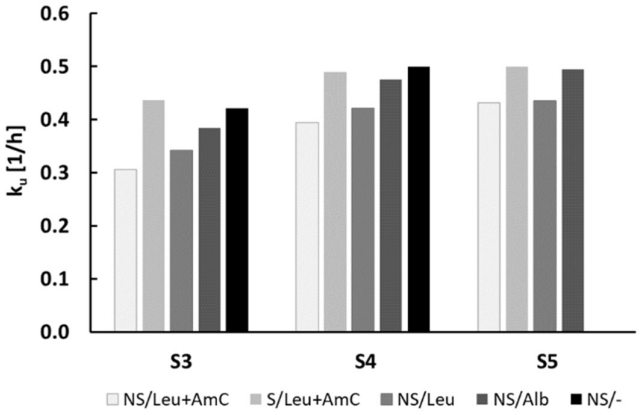

Figure 4.6 Uptake rate constant for NGI stages and formulations.

The rate of particle dissolution on the lung epithelium is relevant not only in the context of the onset of pharmacological action but the time a particle takes to dissolve is of essence because particles may be cleared by scavenger macrophages [206], which are present on the alveolar surface, potentially resulting in diminished bioavailability. Phagocytic activity depends on particle size with a maximum around 1 µm [63] and has a half-life of roughly two to three hours [58]. The time required for complete dissolution estimated from this study and the half-life calculated from the constant k_u for high drug deposition amounts are comparable to the phagocytosis half-life, indicating that indeed phagocytosis can impair bioavailability. These considerations point out the relevance of the present measurements for predicting performance of pulmonary delivery.

Earlier work using the NGI dissolution cups and a modified USP2 dissolution apparatus [198] demonstrated almost instantaneous dissolution of deposited budesonide and no differences of dissolution rate between formulations or stages. The different result of the present study is most likely because of the above-mentioned very limited fluid volume that is available for dissolution on the cell surface. Although the drug amount in the present study was one fifth of that in the earlier work, the fluid volume on the alveolar surface is still a lot smaller than the one used in the modified USP2 apparatus with the NGI dissolution cups.

Budesonide entering the cells was efficiently metabolized to budesonide oleate. The metabolite amount was at the end of the experiment roughly twice as much as the amount of budesonide in the cells. The two species found in the cell interior generally accounted together for more than half of the deposited drug amount. The accumulation of drug in the cells is probably related to the relatively high lipophilicity of budesonide (log(octanol/water partition coefficient) = 2.67) [207] and the estimated two to four orders of magnitude higher lipophilicity of its metabolite [201]. Budesonide oleate was not detected in any other compartment. The total amount in the cell interior was followed by the drug amount in the basal solution and the amount on the cell surface. Hence, in the duration of the experiment, the vast majority of deposited drug can be considered to become bioavailable in the pulmonary tissue.

However, the drug amount detected in the basal solution cannot be used as a measure of absorption or systemic bioavailability because the used A549 cell line forms tight junctions that are much leakier than those of primary alveolar cells [30,53] and presumably of the *in vivo* alveolar epithelium. On the other hand, the transport of budesonide through the cell monolayer

likely follows a transcellular pathway as evidenced by the large accumulation of drug in the cells and therefore would not be expected to be influenced by the leakiness of tight junctions. Still, the A549 cell model is for the above reason not universally appropriate for predicting systemic pulmonary bioavailability, much less so for rather hydrophilic drug molecules. Nevertheless, cell uptake of the drug may be considered to be relevant when local bioavailability is of the essence as in the present situation, since the site of budesonide drug action is located in the epithelial cells [208]. The extent of cellular accumulation will likely decrease when the basal compartment represents a sink such as in the *in vivo* situation. Yet, the presented experiments provide valuable insights into the process and kinetics of drug dissolution and cell uptake following powder deposition onto the cell surface. The obtained result is instructive of the efficiency of local delivery by pulmonary administration.

Transfer of the present results to the *in vivo* situation in the context of an *in vitro – in vivo* correlation, IVIVC, would comprise the estimation of local drug concentration in the lung. This would be valuable as the difficulty of measuring drug levels in the epithelial lining and tissue has been acknowledged as major obstacle in pulmonary IVIVC [139]. In this respect, the site of local pharmacologic action and hence the target site of drug delivery play an important role. Conductive airways have a comparatively small surface area and are covered by a small volume of aqueous mucus while the alveolar area is covered by a comparatively larger volume of surfactant-rich fluid. The volume and nature of the fluid that is available for drug dissolution should be referred to the dose reaching the lung region of interest for an IVIVC on the background of the results of the present study. While IVIVC is beyond the scope of this article and volumes of the involved physiological fluids are still a matter of debate, this discussion indicates the predictive potential of the work.

It should be finally pointed out that the present analysis revealed no differences between the studied formulations with respect to cellular processing such as uptake, metabolism and release into the basal medium other than what is elicited by the differences in the deposited amount. Also, a comparable behaviour among the studied NGI deposition stages was discovered. Given that for all formulations and different deposition stages the underlying drug substance nano-suspension was identical, this then leads to the conclusion that this is performance-determining.

4.3.4 Cell integrity

Cell integrity in the developed experimental setup was evaluated by lactate dehydrogenase assay (LDH) and LIVE/DEAD™ cell imaging assay using optical fluorescence microscopy. LDH results obtained at the end of the experiment (Table 4.8) indicate that the experimental procedure had an adverse effect on the cultured cell monolayer. This presumably occurred by the action of particle deposition on the cell surface causing some degree of damage to the cell membrane, which led to the leakage of the intracellular enzyme. No systematic effect of formulation or impactor stage on LDH was ascertained by two-way ANOVA (not shown). It should be pointed out that these measurements reflect the largest possible adverse effect as they were taken at the end of the experiment at a duration of four to eight hours. Blank experiments performed without the powder formulation interestingly showed that the air stream alone also affected the integrity of the cell membrane but to a much smaller extent.

Table 4.8 Cell damage induced in the course of the experiment according to stage and formulation a

	S3 (%)	S4 (%)	S5 (%)
NS/Leu+AmC	8.9 ± 6.3	13.4 ± 2.6	18.4 ± 5.4
S/Leu+AmC	10.0 ± 3.4	13.9 ± 2.9	15.3 ± 4.0
NS/Leu	19.1 ± 12.8	15.9 ± 10.9	14.9 ± 8.1
NS/Alb	20.9 ± 6.1	24.3 ± 2.9	31.3 ± 5.8
NS/-	20.5 ± 14.6	5.9 ± 3.5	15.5 ± 1.5
Air stream	0.6	2.0	1.9

[a] values represent average ± absolute standard error (n=3 except for air stream where n=1)

Optical microscopy demonstrated a confluent cell monolayer that remained largely intact in the course of the experiment (Figure 4.7). This figure depicts typical results obtained with one of the formulations. The employed staining revealed that the vast majority of the cells remained attached and in a live state, while a relatively small number of cells appeared dead. For impactor stages 3 and 4, the dead cells seemed to be randomly distributed across the monolayer whereas, interestingly, for stage 5 dead cells were concentrated in specific spots. These spots corresponded exactly to the nozzles of this stage of the NGI, which are smaller and more frequently distributed over the cup than the nozzles of the other two stages. These images, therefore, provide indirect evidence that the impact of particles is responsible for damage of the cell monolayer. Overall, however, the extent of damage detected by the microscopic assay seemed rather modest. This assessment is corroborated by the fact that the cells maintained a strong metabolic activity throughout the experiment as evidenced by the formation of large quantity of the oleate metabolite of the drug.

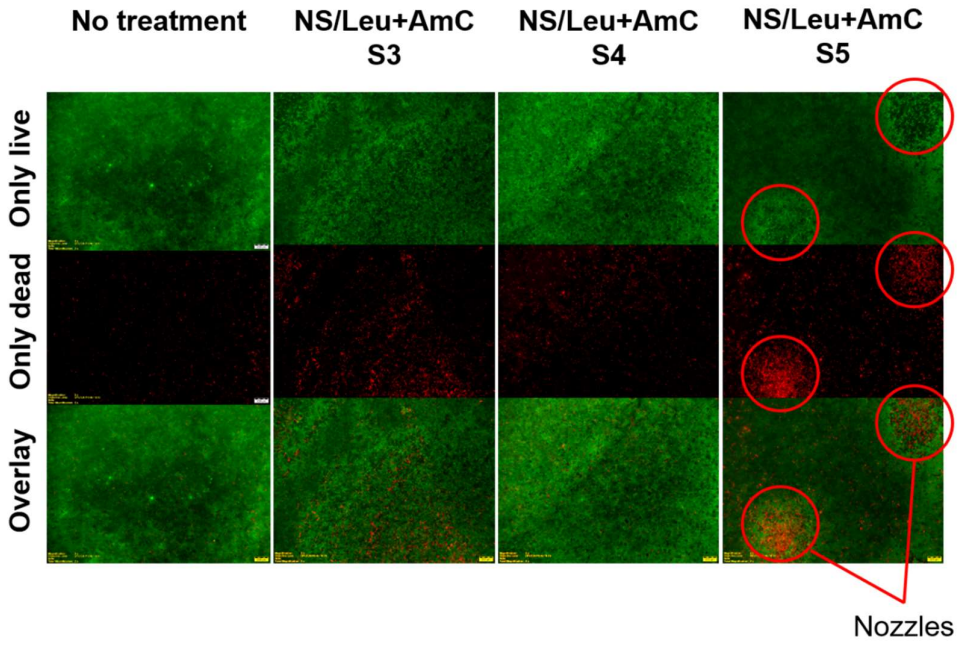

Figure 4.7 Images of cells stained using a LIVE/DEAD™ Cell Imaging kit (live and dead cells are shown in green and red, respectively). Images recorded after deposition of one formulation in different NGI stages versus control. In stage 5 the position of the nozzles above the cell monolayer is suggested. Scale bar represents 200 µm.

Taken together, the adverse effect on the cell monolayer caused by the experimental procedure appeared stronger when assessed by the LDH assay compared to microscopic imaging. It should be noted, however, that the LDH assay detects membrane injury which is not necessarily linked to cell death. Since cell membrane integrity is defining for molecular trafficking in and out of the cell, the cellular uptake of the drug determined in this work may be overestimated. On the other hand, the impact of partial loss of membrane integrity on cell uptake may arguably be less severe for lipophilic compounds, such as budesonide that readily partition into the lipid domain of the membrane than for hydrophilic drugs. In any case, utmost caution is required when transferring these results to the in vivo situation. The combination of NGI with A549 cell culture appears hence to be subject to similar drawback with respect to cell stress as suggested for other impingers in combination with cell lines [53]. Its usefulness therefore for assessing local pulmonary bioavailability in absolute terms may be compromised. Yet the model of the present study provided valuable insights into the comparative evaluation of stage-dependent formulation performance concerning particle dissolution and cell drug uptake and metabolism.

4.4 Conclusion

Transformation of the NGI to allow combination of aerodynamic formulation performance evaluation with powder – alveolar cell interaction was successful. This provided insights into NGI stage-dependent particle deposition on cell surface, dissolution, and subsequent drug uptake and metabolism by the cells. Cell damage by the impaction, however, could not be entirely avoided. Drug processing by the cells did not depend on stage or formulation. Discrimination between formulations was possible due to the difference of deposited powder amount. Deduced time frame of drug dissolution in the surfactant layer surface was shown to be dependent on deposition amount and be rather long (≥4 hours) for larger amounts of deposited powder despite the nano-range size of API particles, and to be in fact longer than reported before, implying potential negative impact on bioavailability. Drug transport in the A549 cell monolayer appeared to take place transcellularly and strong drug metabolism was evident. Stage-specific distribution of drug in different cell compartments and drug amount in each compartment are relevant for drug delivery and therapeutic effect, respectively, and have not been described in an *in vitro* system before. The developed experimental model provides useful insights and ought to be further improved as a tool for performance prediction in pulmonary formulation R&D.

Chapter 5

5 Final conclusion and Outlook

Modern dry powder pulmonary drug delivery has seen its advent in the 1940s with the first lactose-based powders, however rather little advancement, compared to for example oral delivery, has been done in this field in the decades since then. [1,209] Yet, the field remains an important one for local drug delivery, as it is widely used for treatment of chronic diseases such as asthma or COPD. It is also becoming an increasingly interesting alternative to intravenous administration due to the possibility to deliver drugs systemically *via* the alveolar region. Nonetheless, most of the marketed locally acting products still use decades-old technologies such as dry blending to create formulations of only moderate pharmaceutical performance.

This work employed and combined industry-viable manufacturing processes to create inhalation powders of superior pharmaceutical performance and prolonged residence time due to favourable physical-chemical powder properties. For this, wet media milling was used to process a poorly water-soluble model drug substance (budesonide), which led to creation of drug nanosuspension. The nanoparticles were stabilised by TPGS, which was selected from an array of investigated stabilisers based on the possibility to achieve smallest median particle size and span. Subsequently the nanosuspension was spray dried together with additives selected for their potential to favour drying at high Péclet numbers. Particle engineering approach was applied through careful selection of process parameters and formulation composition. Powders containing particles of large geometric particle size and low density were successfully prepared. Several powders showed notably superior aerodynamic properties compared to the commercial product and fast dissolution was achieved for all powders. Thanks to the larger particle size, the powders would also have the potential of prolonged residence time due to lower probability of being removed by phagocytic clearance. An important finding of this work was that only by combining both manufacturing processes powders of all the above-mentioned properties could be achieved. When wet media milling was omitted, aerodynamic performance was similar to that of the commercial, carrier-based budesonide drug product. Dissolution of aerodynamically classified powders has been studied in detail using a modified USP2 system to better understand the advantages drug nanoparticles bring into the formulation and to study the different dissolution kinetics based on secondary (*i.e.* microparticle) size. However, despite the notable differences in particle shape and morphology among the formulations, very fast drug dissolution of deposited powders was observed. No clear difference among individual impactor stages of each formulation or among the formulations was found by the model-based data analysis. This observation was likely the result of several contributing factors: a) the primary drug particle

properties, foremost the nanoparticle size, was the same in all tested formulations and therefore the same factor governed the dissolution rate; b) the chosen additives had good solubility in given medium; c) further processing by spray drying could had led to amorphisation of part of the material and thus could had accelerated the dissolution.

Further on within the work, the NGI impactor system was adapted to allow deposition of the aerodynamically classified powders on a surfactant layer of alveolar A549 cells. Such *in vitro* setup has been used for the first time ever and allowed to mimic the dissolution conditions much closer than the modified USP2 setup used previously within the work. This new setup allowed deposition of very small powder quantities, which varied based on the tested formulation and the deposition stage, on the cell surface. Further on, the appearance of the drug in the basal medium was monitored over time. Kinetic analysis was performed to evaluate the kinetics of drug uptake into the cells, metabolism into its oleate metabolite, and release into the basal solution. This method made it possible to assess the dissolution kinetics of particles in a lung surfactant, thus closely mimicking the *in vivo* fluid composition. Compared to tests in the modified USP2, this method was able to discriminate between the different formulations and stages. Differences among the formulations' dissolution kinetics were observed likely due to notably smaller dissolution medium amount, which further emphasised the need for a representative study setup when developing an *in vitro* system for example within the attempts of pulmonary *in vitro-in vivo* correlation establishment. Further, this experimental model enabled quantification of the drug distribution among the different cell compartments and to assess the extent of drug conjugation with oleic acid. It also clearly showed that the dissolution kinetics can be influenced by the saturation of the surface lining fluid when large powder amounts deposit on a cell surface, which could have potential negative impact on local bioavailability. Possibility to mimic the dissolution-rate limitation in a representative setup would be very valuable especially for very poorly water-soluble drugs.

It is hopefully not too bold to claim that the proposed combination of processes would have the potential to become even in an industrial setting a platform technology for processing of any poorly water-soluble drug for creation of pharmaceutical powders. For inhalation powders, such formulation approach would have clear advantages thanks to the improved aerodynamic performance, high and/or multiple drug load possibility. For majority of the drugs, it would possibly bring an even faster onset of action thanks to the very fast drug dissolution and it could shorten the half time of the very poorly water-soluble drugs such as fluticasone propionate. All these would potentially lead to cost savings due to increase of drug amount that reaches the patient's lungs. Also better compliance could be achieved if the improved delivery would for example lead to need of reduced dosing regimen. Further, the hereby used processes of wet media milling and spray drying are already well established on their own in the pharmaceutical industry and both are readily scalable. Moreover, within the frame of this work, solely water was used as a solvent, reducing any concerns due to residual solvents content in the resulting powder.

However, spray drying is known to be an expensive pharmaceutical process and the yield of wet media milling is often suboptimal due to product retention in the milling media. Unless the processes would be further optimized, it might be questionable whether the formulation benefits, which such technological combination could bring, would outweigh the higher price tag that would inevitably come along with it compared to the conventional processes. It is possible that for the traditional, locally acting drugs such as corticosteroids, it would not be justifiable to use such complex and pricey process chain. Yet, the need to deliver systemically acting drugs to the

alveolar region would ask for use of either very small-sized or engineered particles. As very small micronized particles would likely show poor aerodynamic performance, it can be assumed that engineered particles with their numerous beneficial psychical-chemical properties would offer considerably more reliable delivery option. Engineered particles could also provide a way forward for drugs that cannot be micronized and thus processed in the conventional manner. Furthermore, spray drying alone is becoming a very attractive process for formulation of biological molecules intended for pulmonary delivery, as done for example within the PulmoSol® technology [110]. Thanks to spray drying, the otherwise solution-based biological drug substance can be formulated into a powder, which generally provides better stability over a liquid formulation. For such expensive drug substances, which biomolecules undoubtedly are, using a more complex and expensive process that however provides superior product performance and stability is possibly justifiable. Given the rise in biotechnology and its products, alongside with an increasing interest for development of patient-centric products, it can be expected that the spray drying technology will find its place among the key pharmaceutical processes. And for such cases, the possibility to characterize and understand on a deeper level the spray dried product properties within an *in vitro* setting will play an indispensable role in pharmaceutical product development.

6 Literature

[1] H.D.C. Smyth, A.J. Hickey, eds., Controlled Pulmonary Drug Delivery, Springer New York, New York, NY, 2011. https://doi.org/10.1007/978-1-4419-9745-6.

[2] J.S. Patton, P.R. Byron, Inhaling medicines: delivering drugs to the body through the lungs, Nat. Rev. Drug Discov. 6 (2007) 67–74. https://doi.org/10.1038/nrd2153.

[3] M. Lippmann, R.E. Albert, The Effect of Particle Size on the Regional Deposition of Inhaled Aerosols in the Human Respiratory Tract, Am. Ind. Hyg. Assoc. J. 30 (1969) 257–275. http://www.tandfonline.com/doi/abs/10.1080/00028896909343120#.Ve2tsRG8PRY (accessed September 7, 2015).

[4] W.C. Hinds, Aerosol technology: properties, behavior, and measurement of airborne particles, 2nd ed., Wiley, 1999. https://books.google.ch/books/about/Aerosol_technology.html?id=ORxSAAAAMAAJ&pgis=1 (accessed April 12, 2016).

[5] H.W. Frijlink, A.H. De Boer, Dry powder inhalers for pulmonary drug delivery, Expert Opin. Drug Deliv. 1 (2004) 67–86. http://dx.doi.org/10.1517/17425247.1.1.67.

[6] D.A. Edwards, J. Hanes, G. Caponetti, J. Hrkach, A. Ben-Jebria, M.L. Eskew, J. Mintzes, D. Deaver, N. Lotan, R. Langer, Large Porous Particles for Pulmonary Drug Delivery, Science (80-.). 276 (1997) 1868–1872. https://doi.org/10.1126/science.276.5320.1868.

[7] D.A. Edwards, A. Ben-Jebria, R. Langer, Recent advances in pulmonary drug delivery using large, porous inhaled particles, J Appl Physiol. 85 (1998) 379–385. http://jap.physiology.org/content/85/2/379.full-text.pdf+html (accessed August 18, 2015).

[8] R. Vehring, Pharmaceutical Particle Engineering via Spray Drying, Pharm. Res. 25 (2008) 999–1022. https://doi.org/10.1007/s11095-007-9475-1.

[9] A.H.L. Chow, H.H.Y. Tong, P. Chattopadhyay, B.Y. Shekunov, Particle Engineering for Pulmonary Drug Delivery, Pharm. Res. 24 (2007) 411–437. https://doi.org/10.1007/s11095-006-9174-3.

[10] C. Moon, H.D.C. Smyth, A.B. Watts, R.O. Williams, Delivery Technologies for Orally Inhaled Products: an Update, AAPS PharmSciTech. 20 (2019) 1–17. https://doi.org/10.1208/s12249-019-1314-2.

[11] C. Lipinski, Drug-like properties and the causes of poor solubility and poor permeability, Curr. Dir. Drug Discov. Rev. Mod. Tech. 44 (2000) 235–249. http://www.sciencedirect.com/science/article/pii/S1056871900001076.

[12] R. Shegokar, R.H. Müller, Nanocrystals: Industrially feasible multifunctional formulation technology for poorly soluble actives, Int. J. Pharm. 399 (2010) 129–139. https://doi.org/10.1016/j.ijpharm.2010.07.044.

[13] J.S. Patton, S.C. Fishburn, J.G. Weers, The Lungs as a Portal of Entry for Systemic Drug Delivery, in: Proc. Am. Thorac. Soc. BT - Proc. Am. Thorac. Soc., 2004: pp. 338–344. http://dx.doi.org/10.1513/pats.200409-049TA.

[14] W. Yang, J.I. Peters, R.O. Williams III, Inhaled nanoparticles—A current review, Int. J. Pharm. 356 (2008) 239–247. http://www.sciencedirect.com/science/article/pii/S0378517308001257.

[15] W.P. Adams, R.C. Ahrens, M.-L. Chen, D. Christopher, B.A. Chowdhury, D.P. Conner, R. Dalby, K. Fitzgerald, L. Hendeles, A.J. Hickey, G. Hochhaus, B.L. Laube, P. Lucas, S.L. Lee, S. Lyapustina, B. Li, D. O'Connor, N. Parikh, D.A. Parkins, P. Peri, G.R. Pitcairn, M. Riebe, P. Roy, T. Shah, G.J.P. Singh, S.S. Sharp, J.D. Suman, M. Weda, J. Woodcock, L. Yu, Demonstrating Bioequivalence of Locally Acting Orally Inhaled Drug Products (OIPs): Workshop Summary Report., J. Aerosol Med. Pulm. Drug Deliv. 23 (2010) 1–29. https://doi.org/10.1089/jamp.2009.0803.

[16] T. Riley, D. Christopher, J. Arp, A. Casazza, A. Colombani, A. Cooper, M. Dey, J. Maas, J. Mitchell, M. Reiners, N. Sigari, T. Tougas, S. Lyapustina, Challenges with developing in vitro dissolution tests for orally inhaled products (OIPs), AAPS PharmSciTech. 13 (2012) 978–89. https://doi.org/10.1208/s12249-012-9822-3.

[17] E.R. Weibel, Morphometry of the Human Lung, Springer Berlin Heidelberg, Berlin, Heidelberg, 1963. https://doi.org/10.1007/978-3-642-87553-3.

[18] A. Floroiu, M. Klein, J. Krämer, C.-M. Lehr, Towards Standardized Dissolution Techniques for In Vitro Performance Testing of Dry Powder Inhalers, Dissolution Technol. 25 (2018) 6–18.

https://doi.org/10.14227/DT250318P6.

[19] J.S. Patton, J.D. Brain, L. a Davies, J. Fiegel, M. Gumbleton, K.-J. Kim, M. Sakagami, R. Vanbever, C. Ehrhardt, The Particle has Landed—Characterizing the Fate of Inhaled Pharmaceuticals, J. Aerosol Med. Pulm. Drug Deliv. 23 (2010) 71. https://doi.org/10.1089/jamp.2010.0836.

[20] G. Hochhaus, C. Davis-Cutting, M. Oliver, S.L. Lee, S. Lyapustina, Current Scientific and Regulatory Approaches for Development of Orally Inhaled and Nasal Drug Products: Overview of the IPAC-RS/University of Florida Orlando Inhalation Conference, AAPS J. 17 (2015) 1305–1311. https://doi.org/10.1208/s12248-015-9791-z.

[21] E. Fröhlich, Biological Obstacles for Identifying In Vitro-In Vivo Correlations of Orally Inhaled Formulations, Pharmaceutics. 11 (2019) 316. https://doi.org/10.3390/pharmaceutics11070316.

[22] F. Blank, B.M. Rothen-Rutishauser, S. Schurch, P. Gehr, An optimized in vitro model of the respiratory tract wall to study particle cell interactions., J. Aerosol Med. 19 (2006) 392–405. https://doi.org/10.1089/jam.2006.19.392.

[23] A.D. Lehmann, N. Daum, M. Bur, C.-M. Lehr, P. Gehr, B.M. Rothen-Rutishauser, An in vitro triple cell co-culture model with primary cells mimicking the human alveolar epithelial barrier, Eur. J. Pharm. Biopharm. 77 (2011) 398–406. https://doi.org/10.1016/j.ejpb.2010.10.014.

[24] J. Shrestha, S. Razavi Bazaz, H. Aboulkheyr Es, D. Yaghobian Azari, B. Thierry, M. Ebrahimi Warkiani, M. Ghadiri, Lung-on-a-chip: the future of respiratory disease models and pharmacological studies, Crit. Rev. Biotechnol. 40 (2020) 213–230. https://doi.org/10.1080/07388551.2019.1710458.

[25] J.C. Sung, B.L. Pulliam, D.A. Edwards, Nanoparticles for drug delivery to the lungs, Trends Biotechnol. 25 (2007) 563–570. http://dx.doi.org/10.1016/j.tibtech.2007.09.005.

[26] P. Gehr, M. Bachofen, E.R. Weibel, The normal human lung: ultrastructure and morphometric estimation of diffusion capacity, Respir. Physiol. 32 (1978) 121–140. https://doi.org/10.1016/0034-5687(78)90104-4.

[27] A.J. Hickey, D.C. Thompson, Physiology of the Airways, in: A.J. Hickey (Ed.), Pharm. Inhal. Aerosol Technol. Second Ed., 2nd ed., Marcel Dekker Inc., 2004: pp. 1–29. https://books.google.ch/books/about/Pharmaceutical_Inhalation_Aerosol_Techno.html?id=h33mIkVSpY0C&pgis=1 (accessed February 23, 2016).

[28] J.L. Sporty, C. Ehrhardt, L. Horálková, In vitro cell culture models for the assessment of pulmonary drug disposition, Expert Opin. Drug Metab. Toxicol. 4 (2008) 333–345. http://dx.doi.org/10.1517/17425255.4.4.333.

[29] J.S. Patton, Mechanisms of macromolecule absorption by the lungs, Adv. Drug Deliv. Rev. 19 (1996) 3–36. http://www.sciencedirect.com/science/article/pii/0169409X9500113L (accessed November 25, 2013).

[30] B. Rothen-Rutishauser, F. Blank, C. Mühlfeld, P. Gehr, In vitro models of the human epithelial airway barrier to study the toxic potential of particulate matter, Expert Opin. Drug Metab. Toxicol. (2008) 1075–1089.

[31] G. Scheuch, W. Zimlich, R. Siekmeier, Biophysical Parameters Determining Pulmonary Drug Delivery, in: K. Bechtold-Peters, H. Luessen (Eds.), Pulm. Drug Deliv., Editio Cantor Verlag, 2007: pp. 46–54.

[32] F. Possmayer, K. Nag, K. Rodriguez, R. Qanbar, S. Schürch, Surface activity in vitro: role of surfactant proteins, Comp. Biochem. Physiol. Part A Mol. Integr. Physiol. 129 (2001) 209–220. http://dx.doi.org/10.1016/S1095-6433(01)00317-8.

[33] T.S. Wiedmann, R. Bhatia, L.W. Wattenberg, Drug solubilization in lung surfactant, J. Control. Release. 65 (2000) 43–47. https://doi.org/10.1016/S0168-3659(99)00230-8.

[34] A. Nokhodchi, G.P. Martin, eds., Pulmonary Drug Delivery, John Wiley & Sons, Ltd, Chichester, UK, 2015. https://doi.org/10.1002/9781118799536.

[35] M. Lippmann, D.B. Yeates, R.E. Albert, Deposition, retention, and clearance of inhaled particles., Br. J. Ind. Med. 37 (1980) 337–62. http://www.pubmedcentral.nih.gov/articlerender.fcgi?artid=1008751&tool=pmcentrez&rendertype=abstract (accessed November 21, 2013).

[36] I. Gonda, Targeting by Deposition, in: A.J. Hickey (Ed.), Pharm. Inhal. Aerosol Technol. Second Ed., 2nd ed., Marcel Dekker Inc., New York, 2004: pp. 65–88. https://books.google.com/books?id=h33mIkVSpY0C&pgis=1 (accessed April 29, 2016).

[37] T.B. Martonen, I.M. Katz, Deposition Patterns of Aerosolized Drugs Within Human Lungs: Effects of Ventilatory Parameters, Pharm. Res. 10 (1993) 871–878. http://dx.doi.org/10.1023/A:1018913311788.

[38] R. Kobrich, G. Rudolf, W. Stahlhofen, A Mathematical Model of Mass Deposition in Man, Ann. Occup. Hyg. 38 (1994) 15–23. https://doi.org/10.1093/annhyg/38.inhaled_particles_VII.15.

[39] G.L. Amidon, H. Lennernäs, V.P. Shah, J.R. Crison, A Theoretical Basis for a Biopharmaceutic Drug Classification: The Correlation of in Vitro Drug Product Dissolution and in Vivo Bioavailability, Pharm. Res. An Off. J. Am. Assoc. Pharm. Sci. 12 (1995) 413–420. https://doi.org/10.1023/A:1016212804288.

[40] H. Eixarch, E. Haltner-Ukomadu, C. Beisswenger, U. Bock, Drug Delivery to the Lung: Permeability and Physicochemical Character-istics of Drugs as the Basis for a Pulmonary Biopharmaceutical Classification System (pBCS), 2010. https://pdfs.semanticscholar.org/3c4e/923e5ea77f26d42f599e527e2b6c6fc3010e.pdf (accessed September 30, 2018).

[41] S. Edsbäcker, C.-J. Johansson, S. Edsbacker, Airway Selectivity: An Update of Pharmacokinetic Factors Affecting Local and Systemic Disposition of Inhaled Steroids, Basic Clin. Pharmacol. Toxicol. 98 (2006) 523–536. https://doi.org/10.1111/j.1742-7843.2006.pto_355.x.

[42] B. Olsson, E. Bondesson, L. Borgström, S. Edsbäcker, S. Eirefelt, K. Ekelund, L. Gustavsson, T. Hegelund-Myrbäck, Pulmonary Drug Metabolism, Clearance, and Absorption, in: Control. Pulm. Drug Deliv., Springer New York, 2011: pp. 21–50. https://doi.org/10.1007/978-1-4419-9745-6_2.

[43] J.E. Hastedt, The lung as a dissolution vessel? Dissolution testing, Inhalation. 8 (2014) 1–5. www.inhalationmag.com (accessed May 4, 2020).

[44] J.H. Widdicombe, J.G. Widdicombe, Regulation of human airway surface liquid, Respir. Physiol. 99 (1995) 3–12. http://www.sciencedirect.com/science/article/pii/003456879400095H.

[45] H. Fischer, J.H. Widdicombe, Mechanisms of acid and base secretion by the airway epithelium., J. Membr. Biol. 211 (2006) 139–50. https://doi.org/10.1007/s00232-006-0861-0.

[46] J.E. Hastedt, P. Bäckman, A.R. Clark, W. Doub, A. Hickey, G. Hochhaus, P.J. Kuehl, C.-M. Lehr, P. Mauser, J. McConville, R. Niven, M. Sakagami, J.G. Weers, Scope and relevance of a pulmonary biopharmaceutical classification system AAPS/FDA/USP Workshop March 16-17th, 2015 in Baltimore, MD, AAPS Open. 2 (2016) 1–20. https://doi.org/10.1186/s41120-015-0002-x.

[47] M. Bur, U. Bock, E. Haltner-Ukomadu, C. Lehr, In vitro Models for Pulmonary Drug Absorption, in: K. Bechtold-Peters, H. Luessen (Eds.), Pulm. Drug Deliv., Editio Cantor Verlag, 2007: pp. 58–81.

[48] L.S. Schanker, J.A. Hemberger, Relation between molecular weight and pulmonary absorption rate of lipid-insoluble compounds in neonatal and adult rats, 1983. http://www.sciencedirect.com/science/article/pii/0006295283900254 (accessed November 26, 2013).

[49] R.A. Brown, L.S. Schanker, Absorption of aerosolized drugs from the rat lung., Drug Metab. Dispos. 11 (1983).

[50] J. Rejman, V. Oberle, I.S. Zuhorn, D. Hoekstra, Size-dependent internalization of particles via the pathways of clathrin- and caveolae-mediated endocytosis, Biochem. J. 377 (2004) 159. https://doi.org/10.1042/BJ20031253.

[51] A.J. Hickey, Pharmaceutical inhalation aerosol technology, M. Dekker, 2004.

[52] D.E. Geller, Aerosol Antibiotics in Cystic Fibrosis Rationale for Use of Inhaled Antibiotics Antibiotic Selection : Factors to Consider, Respir. Care. 54 (2009) 658–669.

[53] M. Bur, C.-M. Lehr, Pulmonary cell culture models to study the safety and efficacy of innovative aerosol medicines., Expert Opin. Drug Deliv. 5 (2008) 641–52. https://doi.org/10.1517/17425247.5.6.641.

[54] D. Cipolla, Will pulmonary drug delivery for systemic application ever fulfill its rich promise?, Expert Opin. Drug Deliv. 13 (2016) 1337–1340. https://doi.org/10.1080/17425247.2016.1218466.

[55] European Medicines Agency, Inbrija, 2019. (n.d.). https://www.ema.europa.eu/en/medicines/human/EPAR/inbrija (accessed February 15, 2021).

[56] R. Siekmeier, G. Scheuch, Systemic treatment by inhalation of macromolecules--principles, problems, and examples., J. Physiol. Pharmacol. 59 Suppl 6 (2008) 53–79. https://doi.org/10.1115/1.4026364.

[57] J.E. Agnew, P.P. Sutton, D. Pavia, S.W. Clarke, Radioaerosol assessment of mucociliary clearance: Towards definition of normal range, Br. J. Radiol. 59 (1986) 147–151. https://doi.org/10.1259/0007-1285-59-698-147.

[58] M. Geiser, Update on macrophage clearance of inhaled micro- and nanoparticles., J. Aerosol Med. Pulm. Drug Deliv. 23 (2010) 207–17. https://doi.org/10.1089/jamp.2009.0797.

[59] G. OBERDÖRSTER, Lung Clearance of Inhaled Insoluble and Soluble Particles, J. Aerosol Med. 1 (1988) 289–330. https://doi.org/10.1089/jam.1988.1.289.

[60] N.R. Labiris, M.B. Dolovich, Pulmonary drug delivery. Part I: Physiological factors affecting therapeutic effectiveness of aerosolized medications, Br. J. Clin. Pharmacol. 56 (n.d.). http://www.ncbi.nlm.nih.gov/pmc/articles/PMC1884307/pdf/bcp0056-0588.pdf.

[61] Y. Tabata, Y. Ikada, Effect of the size and surface charge of polymer microspheres on their phagocytosis by macrophage, Biomaterials. 9 (1988) 356–362. https://doi.org/10.1016/0142-9612(88)90033-6.

[62] K.C. Stone, R.R. Mercer, P. Gehr, B. Stockstill, J.D. Crapo, Allometric relationships of cell numbers and size in the mammalian lung., Am. J. Respir. Cell Mol. Biol. 6 (1992) 235–243. https://doi.org/10.1165/ajrcmb/6.2.235.

[63] K. Makino, N. Yamamoto, K. Higuchi, N. Harada, H. Ohshima, H. Terada, Phagocytic uptake of polystyrene microspheres by alveolar macrophages: effects of the size and surface properties of the microspheres, Colloids Surfaces B Biointerfaces. 27 (2003) 33–39. http://www.sciencedirect.com/science/article/pii/S0927776502000425.

[64] J. Wang, D.R. Flanagan, Fundamentals of Dissolution, in: Dev. Solid Oral Dos. Forms, Elsevier Inc., 2009: pp. 309–318. https://doi.org/10.1016/B978-0-444-53242-8.00013-8.

[65] M. Bisrat, E.K. Anderberg, M.I. Barnett, C. Nyström, Physicochemical aspects of drug release. XV. Investigation of diffusional transport in dissolution of suspended, sparingly soluble drugs, Int. J. Pharm. 80 (1992) 191–201. https://doi.org/10.1016/0378-5173(92)90277-9.

[66] W. Nernst, Theorie der Reaktionsgeschwindigkeit in heterogenen Systemen, Zeitschrift Für Phys. Chemie. 47U (1904) 52–55. https://doi.org/10.1515/zpch-1904-4704.

[67] E. Brunner, Reaktionsgeschwindigkeit in heterogenen Systemen, Zeitschrift Für Phys. Chemie. 47U (1904) 56–102. https://doi.org/10.1515/zpch-1904-4705.

[68] M. Mosharraf, C. Nyström, The effect of particle size and shape on the surface specific dissolution rate of microsized practically insoluble drugs, Int. J. Pharm. 122 (1995) 35–47. https://doi.org/10.1016/0378-5173(95)00033-F.

[69] P. Khadka, J. Ro, H. Kim, I. Kim, J.T. Kim, H. Kim, J.M. Cho, G. Yun, J. Lee, Pharmaceutical particle technologies: An approach to improve drug solubility, dissolution and bioavailability, Asian J. Pharm. Sci. 9 (2014) 304–316. https://doi.org/10.1016/j.ajps.2014.05.005.

[70] B. Van Eerdenbrugh, G. Van den Mooter, P. Augustijns, Top-down production of drug nanocrystals: Nanosuspension stabilization, miniaturization and transformation into solid products, Int. J. Pharm. 364 (2008) 64–75. https://doi.org/10.1016/j.ijpharm.2008.07.023.

[71] E.M. Merisko-Liversidge, G.G. Liversidge, Drug Nanoparticles: Formulating Poorly Water-Soluble Compounds, Toxicol. Pathol. 36 (2008) 43–48. https://doi.org/10.1177/0192623307310946.

[72] K. Kawakami, Modification of physicochemical characteristics of active pharmaceutical ingredients and application of supersaturatable dosage forms for improving bioavailability of poorly absorbed drugs, Adv. Oral Drug Deliv. Improv. Bioavailability Poorly Absorbed Drugs by Tissue Cell. Optim. 64 (2012) 480–495. https://doi.org/10.1016/j.addr.2011.10.009.

[73] M. Malamatari, K.M.G. Taylor, S. Malamataris, D. Douroumis, K. Kachrimanis, Pharmaceutical nanocrystals: production by wet milling and applications, Drug Discov. Today. 23 (2018) 534–547. https://doi.org/10.1016/J.DRUDIS.2018.01.016.

[74] J. Salazar, R.H. Müller, J.P. Möschwitzer, Combinative Particle Size Reduction Technologies for the Production of Drug Nanocrystals, J. Pharm. 2014 (2014) 1–14. https://doi.org/10.1155/2014/265754.

[75] J. Zhang, L. Wu, H.-K. Chan, W. Watanabe, Formation, characterization, and fate of inhaled drug nanoparticles, Adv. Drug Deliv. Rev. 63 (2011) 441–455. https://doi.org/10.1016/j.addr.2010.11.002.

[76] H. Chen, C. Khemtong, X. Yang, X. Chang, J. Gao, Nanonization strategies for poorly water-soluble drugs, Drug Discov. Today. 16 (2011) 354–360. http://www.sciencedirect.com/science/article/pii/S1359644610000723.

[77] D. Bobo, K.J. Robinson, J. Islam, K.J. Thurecht, S.R. Corrie, Nanoparticle-Based Medicines: A Review of FDA-Approved Materials and Clinical Trials to Date, Pharm. Res. 33 (2016) 2373–2387. https://doi.org/10.1007/s11095-016-1958-5.

[78] L. Peltonen, Peltonen, Leena, Design Space and QbD Approach for Production of Drug Nanocrystals by Wet Media Milling Techniques, Pharmaceutics. 10 (2018) 104. https://doi.org/10.3390/pharmaceutics10030104.

[79] A. Kwade, Determination of the most important grinding mechanism in stirred media mills by calculating stress intensity and stress number, Powder Technol. 105 (1999) 382–388. http://www.sciencedirect.com/science/article/pii/S003259109900162X.

[80] M. Li, M. Azad, R. Davé, E. Bilgili, Nanomilling of Drugs for Bioavailability Enhancement: A Holistic Formulation-Process Perspective, Pharmaceutics. 8 (2016) 17. https://doi.org/10.3390/pharmaceutics8020017.

[81] Y. Tanaka, M. Inkyo, R. Yumoto, J. Nagai, M. Takano, S. Nagata, Nanoparticulation of probucol, a poorly water-soluble drug, using a novel wet-milling process to improve in vitro dissolution and in vivo oral absorption, Drug Dev. Ind. Pharm. 38 (2012) 1015–1023. https://doi.org/10.3109/03639045.2011.637051.

[82] M. Malamatari, S. Somavarapu, K. Kachrimanis, G. Buckton, K.M.G. Taylor, Preparation of respirable nanoparticle agglomerates of the low melting and ductile drug ibuprofen: Impact of formulation parameters, Powder Technol. 308 (2017) 123–134. https://doi.org/10.1016/J.POWTEC.2016.12.007.

[83] B. Van Eerdenbrugh, J.A.N. Vermant, J.A. Martens, L. Froyen, J. Van Humbeeck, P. Augustijns, G. Van den Mooter, A screening study of surface stabilization during the production of drug nanocrystals, J. Pharm. Sci. 98 (2009) 2091–2103. https://doi.org/10.1002/jps.

[84] A. Afolabi, O. Akinlabi, E. Bilgili, Impact of process parameters on the breakage kinetics of poorly water-soluble drugs during wet stirred media milling: A microhydrodynamic view, Eur. J. Pharm. Sci. 51 (2014) 75–86. https://doi.org/10.1016/J.EJPS.2013.09.002.

[85] A. Bitterlich, C. Laabs, E. Busmann, A. Grandeury, M. Juhnke, H. Bunjes, A. Kwade, Challenges in Nanogrinding of Active Pharmaceutical Ingredients, Chem. Eng. Technol. 37 (2014) 840–846. https://doi.org/10.1002/ceat.201300697.

[86] a. M. Cerdeira, B. Gander, M. Mazzotti, Role of Milling Parameters and Particle Stabilization on Nanogrinding of Drug Substances of Similar Mechanical Properties, Chem. Eng. Technol. 34 (2011) 1427–1438. https://doi.org/10.1002/ceat.201100155.

[87] M. Juhnke, J. Berghausen, C. Timpe, Accelerated Formulation Development for Nanomilled Active Pharmaceutical Ingredients Using a Screening Approach, Chem. Eng. Technol. 33 (2010) 1412–1418. http://dx.doi.org/10.1002/ceat.201000062.

[88] M.J. Telko, A.J. Hickey, Dry Powder Inhaler Formulation, Respir. Care. 50 (2005) 1209–1227.

[89] A.D. Brunaugh, H.D.C. Smyth, Formulation techniques for high dose dry powders, Int. J. Pharm. 547 (2018) 489–498. https://doi.org/10.1016/j.ijpharm.2018.05.036.

[90] T.M. Crowder, M.J. Donovan, Science and Technology of Dry Powder Inhalers, in: Control. Pulm. Drug Deliv., Springer New York, New York, NY, 2011: pp. 203–222. https://doi.org/10.1007/978-1-4419-9745-6_9.

[91] M.W. Jetzer, M. Schneider, B.D. Morrical, G. Imanidis, Investigations on the Mechanism of Magnesium Stearate to Modify Aerosol Performance in Dry Powder Inhaled Formulations, J. Pharm. Sci. 107 (2018) 984–998. https://doi.org/10.1016/j.xphs.2017.12.006.

[92] A.H. de Boer, P. Hagedoorn, M. Hoppentocht, F. Buttini, F. Grasmeijer, H.W. Frijlink, Dry powder inhalation: past, present and future, Expert Opin. Drug Deliv. (2016) 1–14. https://doi.org/10.1080/17425247.2016.1224846.

[93] J.G. Weers, J. Bell, H.-K. Chan, D. Cipolla, C. Dunbar, A.J. Hickey, I.J. Smith, Pulmonary formulations: what remains to be done?, J. Aerosol Med. Pulm. Drug Deliv. 23 Suppl 2 (2010) S5–S23. https://doi.org/10.1089/jamp.2010.0838.

[94] J. Visser, Van der Waals and other cohesive forces affecting powder fluidization, Powder Technol. 58 (1989) 1–10. https://doi.org/10.1016/0032-5910(89)80001-4.

[95] J.G. Weers, D.P. Miller, Formulation Design of Dry Powders for Inhalation., J. Pharm. Sci. 104 (2015) 3259–88. https://doi.org/10.1002/jps.24574.

[96] D. Huang, Modeling of Particle Formation during Spray Drying, in: Eur. Dry. Conf. - EuroDrying'2011, 2011: pp. 26–28.

[97] A.L. Feng, M.A. Boraey, M.A. Gwin, P.R. Finlay, P.J. Kuehl, R. Vehring, Mechanistic models facilitate efficient development of leucine containing microparticles for pulmonary drug delivery., Int. J. Pharm. 409 (2011) 156–63. https://doi.org/10.1016/j.ijpharm.2011.02.049.

[98] N. Tsapis, Trojan particles: Large porous carriers of nanoparticles for drug delivery, Proc. Natl. Acad. Sci. 99 (2002) 12001–12005. http://dx.doi.org/10.1073/pnas.182233999.

[99] K. Hadinoto, P. Phanapavudhikul, Z. Kewu, R.B.H. Tan, Novel Formulation of Large Hollow Nanoparticles Aggregates as Potential Carriers in Inhaled Delivery of Nanoparticulate Drugs, Ind. Eng. Chem. Res. 45 (2006) 3697–3706. http://dx.doi.org/10.1021/ie0513191.

[100] K. Hadinoto, K. Zhu, R.B.H. Tan, Drug release study of large hollow nanoparticulate aggregates carrier

particles for pulmonary delivery, Int. J. Pharm. 341 (2007) 195–206. http://www.sciencedirect.com/science/article/pii/S0378517307002839.

[101] C. Weiler, M. Egen, M. Trunk, P. Langguth, Force control and powder dispersibility of spray dried particles for inhalation., J. Pharm. Sci. 99 (2010) 303–16. https://doi.org/10.1002/jps.21849.

[102] M.A. Boraey, S. Hoe, H. Sharif, D.P. Miller, D. Lechuga-Ballesteros, R. Vehring, Improvement of the dispersibility of spray-dried budesonide powders using leucine in an ethanol–water cosolvent system, Powder Technol. 236 (2013) 171–178. https://doi.org/10.1016/j.powtec.2012.02.047.

[103] D. Lechuga-Ballesteros, C. Charan, C.L.M. Stults, C.L. Stevenson, D.P. Miller, R. Vehring, V. Tep, M.-C. Kuo, Trileucine improves aerosol performance and stability of spray-dried powders for inhalation., J. Pharm. Sci. 97 (2008) 287–302. https://doi.org/10.1002/jps.21078.

[104] J. Elversson, A. Millqvist-Fureby, Particle size and density in spray drying-effects of carbohydrate properties., J. Pharm. Sci. 94 (2005) 2049–60. https://doi.org/10.1002/jps.20418.

[105] G. Pilcer, T. Sebti, K. Amighi, Formulation and Characterization of Lipid-Coated Tobramycin Particles for Dry Powder Inhalation, Pharm. Res. 23 (2006) 931–940. https://doi.org/10.1007/s11095-006-9789-4.

[106] E.M. Littringer, M.F. Noisternig, A. Mescher, H. Schroettner, P. Walzel, U.J. Griesser, N.A. Urbanetz, The morphology and various densities of spray dried mannitol, Powder Technol. 246 (2013) 193–200. http://dx.doi.org/10.1016/j.powtec.2013.05.004.

[107] N.Y. Chew, H.K. Chan, Use of solid corrugated particles to enhance powder aerosol performance., Pharm. Res. 18 (2001) 1570–7. http://www.ncbi.nlm.nih.gov/pubmed/11758765.

[108] S.P. Duddu, S.A. Sisk, Y.H. Walter, T.E. Tarara, K.R. Trimble, A.R. Clark, M.A. Eldon, R.C. Elton, M. Pickford, P.H. Hirst, S.P. Newman, J.G. Weers, Improved Lung Delivery from a Passive Dry Powder Inhaler Using an Engineered PulmoSphere® Powder, Pharm. Res. 19 (2002) 689–695. http://dx.doi.org/10.1023/A:1015322616613.

[109] ICH Official web site, (n.d.). https://www.ich.org/page/ich-guidelines (accessed August 8, 2020).

[110] A.M. Healy, M.I. Amaro, K.J. Paluch, L. Tajber, Dry powders for oral inhalation free of lactose carrier particles., Adv. Drug Deliv. Rev. 75 (2014) 32–52. https://doi.org/10.1016/j.addr.2014.04.005.

[111] M. Malamatari, S. Somavarapu, M. Bloxham, G. Buckton, Nanoparticle agglomerates of indomethacin: The role of poloxamers and matrix former on their dissolution and aerosolisation efficiency, Int. J. Pharm. 495 (2015) 516–526. https://doi.org/10.1016/j.ijpharm.2015.09.013.

[112] A.B. Watts, R.O.W. Iii, R.O. Williams, Nanoparticles for Pulmonary Delivery, in: H.D.C. Smyth, A.J. Hickey (Eds.), Control. Pulm. Drug Deliv., Springer New York, New York, NY, 2011: pp. 335–366. https://doi.org/10.1007/978-1-4419-9745-6.

[113] J.O.-H. Sham, Y. Zhang, W.H. Finlay, W.H. Roa, R. Löbenberg, Formulation and characterization of spray-dried powders containing nanoparticles for aerosol delivery to the lung, Int. J. Pharm. 269 (2004) 457–467. http://dx.doi.org/10.1016/j.ijpharm.2003.09.041.

[114] S. Azarmi, X. Tao, H. Chen, Z. Wang, W.H. Finlay, R. Löbenberg, W.H. Roa, Formulation and cytotoxicity of doxorubicin nanoparticles carried by dry powder aerosol particles, Int. J. Pharm. 319 (2006) 155–161. http://www.sciencedirect.com/science/article/pii/S0378517306002808 (accessed November 21, 2013).

[115] M.M. Arnold, E.M. Gorman, L.J. Schieber, E.J. Munson, C. Berkland, NanoCipro encapsulation in monodisperse large porous PLGA microparticles, Fourth Int. Nanomedicine Drug Deliv. Symp. 121 (2007) 100–109. http://www.sciencedirect.com/science/article/pii/S0168365907002842.

[116] H. Takeuchi, H. Yamamoto, Y. Kawashima, Mucoadhesive nanoparticulate systems for peptide drug delivery, Adv. Drug Deliv. Rev. 47 (2001) 39–54. http://www.sciencedirect.com/science/article/pii/S0169409X00001204.

[117] A. Grenha, B. Seijo, C. Remuñán-López, Microencapsulated chitosan nanoparticles for lung protein delivery, Eur. J. Pharm. Sci. 25 (2005) 427–437. http://www.sciencedirect.com/science/article/pii/S0928098705001302.

[118] A. Grenha, C.I. Grainger, L.A. Dailey, B. Seijo, G.P. Martin, C. Remuñán-López, B. Forbes, Chitosan nanoparticles are compatible with respiratory epithelial cells in vitro, Eur. J. Pharm. Sci. 31 (2007) 73–84. http://www.sciencedirect.com/science/article/pii/S0928098707000450.

[119] R.O. Cook, R.K. Pannu, I.W. Kellaway, Novel sustained release microspheres for pulmonary drug delivery, J. Control. Release. 104 (2005) 79–90. https://doi.org/10.1016/j.jconrel.2005.01.003.

[120] T. Hu, H. Chiou, H.-K. Chan, J.-F. Chen, J. Yun, Preparation of inhalable salbutamol sulphate using reactive high gravity controlled precipitation., J. Pharm. Sci. 97 (2008) 944–9.

https://doi.org/10.1002/jps.21026.

[121] C. Plumley, E.M. Gorman, N. El-Gendy, C.R. Bybee, E.J. Munson, C. Berkland, Nifedipine nanoparticle agglomeration as a dry powder aerosol formulation strategy., Int. J. Pharm. 369 (2009) 136–43. https://doi.org/10.1016/j.ijpharm.2008.10.016.

[122] C. Duret, N. Wauthoz, T. Sebti, F. Vanderbist, K. Amighi, Duret, Wauthoz, Sebti, Vanderbist, Amighi, New inhalation-optimized itraconazole nanoparticle-based dry powders for the treatment of invasive pulmonary aspergillosis, Int. J. Nanomedicine. 7 (2012) 5475. https://doi.org/10.2147/IJN.S34091.

[123] N. El-Gendy, C. Berkland, Combination chemotherapeutic dry powder aerosols via controlled nanoparticle agglomeration., Pharm. Res. 26 (2009) 1752–63. https://doi.org/10.1007/s11095-009-9886-2.

[124] R. Boerefijn, Z. Ning, M. Ghadiri, Disintegration of weak lactose agglomerates for inhalation applications, Int. J. Pharm. 172 (1998) 199–209. https://doi.org/10.1016/S0378-5173(98)00207-5.

[125] G. Calvert, M. Ghadiri, M. Dyson, P. Kippax, F. McNeil-Watson, The flowability and aerodynamic dispersion of cohesive powders, Powder Technol. 240 (2013) 88–94. https://doi.org/10.1016/J.POWTEC.2012.07.003.

[126] N.Y.K. Chew, H.-K. Chan, The role of particle properties in pharmaceutical powder inhalation formulations., J. Aerosol Med. 15 (2002) 325–30. https://doi.org/10.1089/089426802760292672.

[127] A. Castellanos, The relationship between attractive interparticle forces and bulk behaviour in dry and uncharged fine powders, Adv. Phys. 54 (2005) 263–376. https://doi.org/10.1080/17461390500402657.

[128] Z. Xu, A.J. Hickey, The Physics of Aerosol Droplet and Particle Generation from Inhalers, in: H.D.C. Smyth, A.J. Hickey (Eds.), Control. Pulm. Drug Deliv., 2011: pp. 75–100. https://doi.org/10.1007/978-1-4419-9745-6.

[129] G. Pilcer, N. Wauthoz, K. Amighi, Lactose characteristics and the generation of the aerosol., Adv. Drug Deliv. Rev. 64 (2012) 233–56. https://doi.org/10.1016/j.addr.2011.05.003.

[130] J. Visser, Van der Waals and other cohesive forces affecting powder fluidization, Powder Technol. 58 (1989) 1–10. https://doi.org/10.1016/0032-5910(89)80001-4.

[131] Z. Xu, H.M. Mansour, A.J. Hickey, Particle Interactions in Dry Powder Inhaler Unit Processes: A Review, J. Adhes. Sci. Technol. 25 (2011) 451–482. https://doi.org/10.1163/016942410X525669.

[132] N.Y.K. Chew, P. Tang, H.-K. Chan, J.A. Raper, How Much Particle Surface Corrugation Is Sufficient to Improve Aerosol Performance of Powders?, Pharm. Res. 22 (2005) 148–152. https://doi.org/10.1007/s11095-004-9020-4.

[133] H.M. Kinnunen, Active sites, agglomerates or increased cohesion? Investigations into the mechanism of how lactose fines improve dry powder inhaler performance, University of Bath, 2012.

[134] O. Molerus, Interpretation of Geldart's type A, B, C and D powders by taking into account interparticle cohesion forces, Powder Technol. 33 (1982) 81–87. https://doi.org/10.1016/0032-5910(82)85041-9.

[135] Preparations for inhalation, in: Eur. Pharmacopoeia, 10.0, EDQM Council of Europe, 2019: pp. 927–932.

[136] A. Barakat, J. Kraemer, C. de Souza Carvalho, C.M. Lehr, In Vitro–In Vivo Correlation: Shades on Some Non-Conventional Dosage Forms, Dissolution Technol. 22 (2015) 19–22. https://doi.org/10.1016/j.ijpharm.2011.01.010.

[137] P.R. Byron, M. Hindle, C.F. Lange, P.W. Longest, D. McRobbie, M.J. Oldham, B. Olsson, C.G. Thiel, H. Wachtel, W.H. Finlay, In vivo-in vitro correlations: predicting pulmonary drug deposition from pharmaceutical aerosols., J. Aerosol Med. Pulm. Drug Deliv. 23 Suppl 2 (2010) S59–S69. https://doi.org/10.1089/jamp.2010.0846.

[138] V.A. Gray, A.J. Hickey, P. Balmer, N.M. Davies, C. Dunbar, T.S. Foster, B.L. Olsson, M. Sakagami, V.P. Shah, M.J. Smurthwaite, J.M. Veranth, K. Zaidi, The Inhalation Ad Hoc Advisory Panel for the USP Performance Tests of Inhalation Dosage Forms, 2008. https://www.researchgate.net/publication/237379078 (accessed August 30, 2020).

[139] E. Fröhlich, Biological Obstacles for Identifying In Vitro-In Vivo Correlations of Orally Inhaled Formulations, Pharmaceutics. 11 (2019) 316. https://doi.org/10.3390/pharmaceutics11070316.

[140] G. Tian, M. Hindle, S. Lee, P.W. Longest, Validating CFD Predictions of Pharmaceutical Aerosol Deposition with in Vivo Data, Pharm. Res. 32 (2015) 3170–3187. https://doi.org/10.1007/s11095-015-1695-1.

[141] European Medicines Agency, 2.9.18. Preparations for inhalation: Aerodynamic assessment of fine particles, in: Eur. Pharmacop., n.d.: pp. 927–932.

[142] Inhaling Testing Brochure, (2012). http://www.copleyscientific.com.

[143] FDA Center for Drug Evaluation and Research, <601> Inhalation and Nasal Drug Products: Aerosols, Sprays, and Powders—Performance Quality Tests, Rockville, MD, USA, 2012.

[144] S.P. Velaga, J. Djuris, S. Cvijic, S. Rozou, P. Russo, G. Colombo, A. Rossi, Dry powder inhalers: An overview of the in vitro dissolution methodologies and their correlation with the biopharmaceutical aspects of the drug products, Eur. J. Pharm. Sci. 113 (2018) 18–28. https://doi.org/10.1016/j.ejps.2017.09.002.

[145] S. May, B. Jensen, C. Weiler, M. Wolkenhauer, M. Schneider, C.-M. Lehr, Dissolution Testing of Powders for Inhalation: Influence of Particle Deposition and Modeling of Dissolution Profiles, Pharm. Res. 31 (2014) 3211–3224. https://doi.org/10.1007/s11095-014-1413-4.

[146] S. May, B. Jensen, M. Wolkenhauer, M. Schneider, C.M. Lehr, Dissolution techniques for in vitro testing of dry powders for inhalation., Pharm. Res. 29 (2012) 2157–66. https://doi.org/10.1007/s11095-012-0744-2.

[147] Y.-J. Son, M. Horng, M. Copley, J.T. McConville, Optimization of an In Vitro Dissolution Test Method for Inhalation Formulations, Dissolution Technol. 17 (2010) 6–13.

[148] N.M. Davies, M.R. Feddah, A novel method for assessing dissolution of aerosol inhaler products, Int. J. Pharm. 255 (2003) 175–187. http://dx.doi.org/10.1016/S0378-5173(03)00091-7.

[149] D. Arora, K.A. Shah, M.S. Halquist, M. Sakagami, In vitro aqueous fluid-capacity-limited dissolution testing of respirable aerosol drug particles generated from inhaler products., Pharm. Res. 27 (2010) 786–95. https://doi.org/10.1007/s11095-010-0070-5.

[150] S. May, S. Kind, B. Jensen, M. Wolkenhauer, M. Schneider, C.-M. Lehr, Miniature In Vitro Dissolution Testing of Powders for Inhalation, Dissolution Technol. 22 (2015) 40–51. https://doi.org/10.14227/DT220315P40.

[151] M. Rohrschneider, S. Bhagwat, R. Krampe, V. Michler, J. Breitkreutz, G. Hochhaus, Evaluation of the Transwell System for Characterization of Dissolution Behavior of Inhalation Drugs: Effects of Membrane and Surfactant, Mol. Pharm. 12 (2015) 2618–2624. https://doi.org/10.1021/acs.molpharmaceut.5b00221.

[152] R.O. Salama, D. Traini, H.-K. Chan, P.M. Young, Preparation and characterisation of controlled release co-spray dried drug–polymer microparticles for inhalation 2: Evaluation of in vitro release profiling methodologies for controlled release respiratory aerosols, Eur. J. Pharm. Biopharm. 70 (2008) 145–152. https://doi.org/10.1016/j.ejpb.2008.04.009.

[153] Y.-J. Son, J.T. McConville, Development of a standardized dissolution test method for inhaled pharmaceutical formulations, Int. J. Pharm. 382 (2009) 15–22. http://dx.doi.org/10.1016/j.ijpharm.2009.07.034.

[154] P. Gerde, M. Malmlöf, L. Havsborn, C.-O. Sjöberg, P. Ewing, S. Eirefelt, K. Ekelund, DissolvIt: An In Vitro Method for Simulating the Dissolution and Absorption of Inhaled Dry Powder Drugs in the Lungs, Assay Drug Dev. Technol. 15 (2017) 77–88. https://doi.org/10.1089/adt.2017.779.

[155] D. Huh, B.D. Matthews, A. Mammoto, M. Montoya-Zavala, H.Y. Hsin, D.E. Ingber, Reconstituting Organ-Level Lung Functions on a Chip, Science (80-.). 328 (2010) 1662–1668. https://doi.org/10.1126/science.1188302.

[156] B.I. Florea, M.L. Cassara, H.E. Junginger, G. Borchard, Drug transport and metabolism characteristics of the human airway epithelial cell line Calu-3, Proceeding Seventh Eur. Symp. Control. Drug Deliv. 87 (2003) 131–138. http://www.sciencedirect.com/science/article/pii/S0168365902003565.

[157] A. Steimer, E. Haltner, C.-M. Lehr, Cell Culture Models of the Respiratory Tract Relevant to Pulmonary Drug Delivery, J. Aerosol Med. 18 (2005) 137–182. https://doi.org/10.1089/jam.2005.18.137.

[158] B.M. Rothen-Rutishauser, S.G. Kiama, P. Gehr, A three-dimensional cellular model of the human respiratory tract to study the interaction with particles, Am. J. Respir. Cell Mol. Biol. 32 (2005) 281–289. http://www.atsjournals.org/doi/abs/10.1165/rcmb.2004-0187OC?url_ver=Z39.88-2003&rfr_id=ori:rid:crossref.org&rfr_dat=cr_pub=pubmed#.VRLR5_mG98E (accessed March 25, 2015).

[159] C.I. Grainger, L.L. Greenwell, G.P. Martin, B. Forbes, The permeability of large molecular weight solutes following particle delivery to air-interfaced cells that model the respiratory mucosa, Eur. J. Pharm. Biopharm. 71 (2009) 318–324. http://www.sciencedirect.com/science/article/pii/S0939641108003640.

[160] M. Haghi, D. Traini, M. Bebawy, P.M. Young, Deposition, Diffusion and Transport Mechanism of Dry Powder Microparticulate Salbutamol, at the Respiratory Epithelia, Mol. Pharm. 9 (2012) 1717–1726. https://doi.org/10.1021/mp200620m.

[161] M. Bur, B. Rothen-Rutishauser, H. Huwer, C.-M. Lehr, A novel cell compatible impingement system to study in vitro drug absorption from dry powder aerosol formulations, Eur. J. Pharm. Biopharm. 72 (2009) 350–357. http://dx.doi.org/10.1016/j.ejpb.2008.07.019.

[162] J. Fiegel, C. Ehrhardt, U.F. Schaefer, C.-M. Lehr, J. Hanes, Large Porous Particle Impingement on Lung Epithelial Cell Monolayers—Toward Improved Particle Characterization in the Lung, Pharm. Res. 20 (2003) 788–796. https://doi.org/10.1023/A:1023441804464.

[163] D. Cooney, M. Kazantseva, A.J. Hickey, Development of a size-dependent aerosol deposition model utilising human airway epithelial cells for evaluating aerosol drug delivery., Altern. Lab. Anim. 32 (2004) 581–590. http://europepmc.org/abstract/MED/15757496.

[164] M. Haghi, D. Traini, P. Young, In Vitro Cell Integrated Impactor Deposition Methodology for the Study of Aerodynamically Relevant Size Fractions from Commercial Pressurised Metered Dose Inhalers, Pharm. Res. 31 (2014) 1779–1787. https://doi.org/10.1007/s11095-013-1282-2.

[165] L. van Rensburg, J. van Zyl, J. Smith, Deposition and transport of linezolid mediated by a synthetic surfactant Synsurf® within a pressurized metered dose inhaler: a Calu-3 model, Drug Des. Devel. Ther. Volume 12 (2018) 1107–1118. https://doi.org/10.2147/DDDT.S147035.

[166] S. Hein, M. Bur, U.F. Schaefer, C.-M. Lehr, A new Pharmaceutical Aerosol Deposition Device on Cell Cultures (PADDOCC) to evaluate pulmonary drug absorption for metered dose dry powder formulations, Eur. J. Pharm. Biopharm. 77 (2011) 132–138. http://www.sciencedirect.com/science/article/pii/S0939641110002638.

[167] A.G. Lenz, E. Karg, B. Lentner, V. Dittrich, C. Brandenberger, B. Rothen-Rutishauser, H. Schulz, G.A. Ferron, O. Schmid, A dose-controlled system for air-liquid interface cell exposure and application to zinc oxide nanoparticles., Part. Fibre Toxicol. 6 (2009) 32. https://doi.org/10.1186/1743-8977-6-32.

[168] M. Aufderheide, U. Mohr, CULTEX — an alternative technique for cultivation and exposure of cells of the respiratory tract to airborne pollutants at the air/liquid interface, Exp. Toxicol. Pathol. 52 (2000) 265–270. https://doi.org/10.1016/S0940-2993(00)80044-5.

[169] C. Meindl, S. Stranzinger, N. Dzidic, S. Salar-Behzadi, S. Mohr, A. Zimmer, E. Fröhlich, Permeation of therapeutic drugs in different formulations across the airway epithelium in vitro, PLoS One. 10 (2015) 1–19. https://doi.org/10.1371/journal.pone.0135690.

[170] J.G. Weers, Enhanced design of inhaled therapeutics: what does the future hold?, Ther. Deliv. 7 (2016) 145–8. https://doi.org/10.4155/tde-2016-0004.

[171] R. Vehring, W.R. Foss, D. Lechuga-Ballesteros, Particle formation in spray drying, J. Aerosol Sci. 38 (2007) 728–746. http://dx.doi.org/10.1016/j.jaerosci.2007.04.005.

[172] D. Pham, N. Grégoire, W. Couet, C. Gueutin, E. Fattal, N. Tsapis, Pulmonary delivery of pyrazinamide-loaded large porous particles, Eur. J. Pharm. Biopharm. 94 (2015) 241–250. https://doi.org/10.1016/j.ejpb.2015.05.021.

[173] L. Peltonen, J. Hirvonen, Drug nanocrystals – Versatile option for formulation of poorly soluble materials, Int. J. Pharm. 537 (2018) 73–83. https://doi.org/10.1016/J.IJPHARM.2017.12.005.

[174] A. Afolabi, O. Akinlabi, E. Bilgili, Impact of process parameters on the breakage kinetics of poorly water-soluble drugs during wet stirred media milling: A microhydrodynamic view, Eur. J. Pharm. Sci. 51 (2014) 75–86. https://doi.org/10.1016/J.EJPS.2013.09.002.

[175] M. Malamatari, S. Somavarapu, K. Kachrimanis, M. Bloxham, K.M.G. Taylor, G. Buckton, Preparation of theophylline inhalable microcomposite particles by wet milling and spray drying: The influence of mannitol as a co-milling agent, Int. J. Pharm. 514 (2016) 200–211. https://doi.org/10.1016/J.IJPHARM.2016.06.032.

[176] FDA Center for Drug Evaluation and Research, Guidance for Industry: Dissolution Testing of Immediate Release Solid Oral Dosage Forms, 1997. https://www.fda.gov/downloads/Drugs/GuidanceComplianceRegulatoryInformation/Guidances/UCM070237.pdf (accessed September 30, 2018).

[177] S. May, B. Jensen, C. Weiler, M. Wolkenhauer, M. Schneider, C.-M. Lehr, Dissolution Testing of Powders for Inhalation: Influence of Particle Deposition and Modeling of Dissolution Profiles, Pharm. Res. 31 (2014) 3211–3224. https://doi.org/10.1007/s11095-014-1413-4.

[178] K. Schittkowski, Numerical Data Fitting in Dynamical Systems: A Practical Introduction with Applications and Software, 1st ed., Springer US, 2002. https://doi.org/10.1007/978-1-4419-5762-7.

[179] M. Schirmbeck, Dried Nanosuspensions of Poorly Water Soluble Drugs for Bioavailability Enhancement, TU Braunschweig, 2012.

[180] W.I. Higuchi, E.N. Hiestand, Dissolution rates of finely divided drug powders I: Effect of a Distribution of Particle Sizes in a Diffusion-Controlled Process, J. Pharm. Sci. 52 (1963) 67–71. https://doi.org/10.1002/jps.2600520114.

[181] J. Wang, D.R. Flanagan, General solution for diffusion-controlled dissolution of spherical particles. 1. Theory, J. Pharm. Sci. 88 (1999) 731–738. https://doi.org/10.1021/js980236p.

[182] Y. Wang, B. Abrahamsson, L. Lindfors, J.G. Brasseur, Comparison and Analysis of Theoretical Models for Diffusion- Controlled Dissolution, Mol. Pharm. 9 (2012) 1052–1066. https://doi.org/10.1021/mp2002818.

[183] C. Galli, Experimental determination of the diffusion boundary layer width of micron and submicron particles, Int. J. Pharm. 313 (2006) 114–122. https://doi.org/10.1016/J.IJPHARM.2006.01.030.

[184] J.J. Sheng, P.J. Sirois, J.B. Dressman, G.L. Amidon, Particle diffusional layer thickness in a USP dissolution apparatus II: A combined function of particle size and paddle speed, J. Pharm. Sci. (2008). https://doi.org/10.1002/jps.21345.

[185] L.M. Bocanegra, G.J. Morris, J.T. Jurewicz, J.W. Mauger, Fluid and Particle Laser Doppler Velocity Measurements and Mass Transfer Predictions for the Usp Paddle Method Dissolution Apparatus, Drug Dev. Ind. Pharm. 16 (1990) 1441–1464. https://doi.org/10.3109/03639049009074376.

[186] D. Farin, D. Avnir, Use of Fractal Geometry To Determine Effects of Surface Morphology on Drug Dissolution, J. Pharm. Sci. 81 (1992) 54–57. https://doi.org/10.1002/JPS.2600810111.

[187] D. Farin, D. Avnir, Reactive fractal surfaces, J. Phys. Chem. 91 (1987) 5517–5521. https://doi.org/10.1021/j100306a001.

[188] P. Macheras, A. Dokoumetzidis, On the Heterogeneity of Drug Dissolution and Release, Pharm. Res. 17 (2000) 108–112.

[189] R.G. Rice, D.D. Do, Dissolution of a solid sphere in an unbounded, stagnant liquid, Chem. Eng. Sci. 61 (2006) 775–778. https://doi.org/10.1016/J.CES.2005.08.003.

[190] J. Fiegel, C. Ehrhardt, U.F. Schaefer, C. Lehr, J. Hanes, Large Porous Particle Impingement on Lung Epithelial Cell Monolayers Toward Improved Particle Characterization in the Lung, Pharm. Res. 20 (2003) 788–796. http://dx.doi.org/10.1023/A:1023441804464.

[191] M. Haghi, D. Traini, P. Young, In Vitro Cell Integrated Impactor Deposition Methodology for the Study of Aerodynamically Relevant Size Fractions from Commercial Pressurised Metered Dose Inhalers, Pharm. Res. 31 (2014) 1779–1787. https://doi.org/10.1007/s11095-013-1282-2.

[192] H.X. Ong, D. Traini, P.M. Young, Pharmaceutical applications of the Calu-3 lung epithelia cell line, Expert Opin. Drug Deliv. 10 (2013) 1287–1302. http://dx.doi.org/10.1517/17425247.2013.805743.

[193] H. Ren, N.P. Birch, V. Suresh, An optimised human cell culture model for alveolar epithelial transport, PLoS One. 11 (2016). https://doi.org/10.1371/journal.pone.0165225.

[194] B.M. Rothen-Rutishauser, S.G. Kiama, P. Gehr, A three-dimensional cellular model of the human respiratory tract to study the interaction with particles, Am. J. Respir. Cell Mol. Biol. 32 (2005) 281–289.

[195] K.J. Elbert, U.F. Schäfer, H.-J. Schäfers, K.-J. Kim, V.H.L. Lee, C.-M. Lehr, Monolayers of human alveolar epithelial cells in primary culture for pulmonary absorption and transport studies, Pharm. Res. 16 (1999) 601–608. http://link.springer.com/article/10.1023/A:1018887501927.

[196] M. Bur, H. Huwer, C.-M. Lehr, N. Hagen, M. Guldbrandt, K.-J. Kim, C. Ehrhardt, Assessment of transport rates of proteins and peptides across primary human alveolar epithelial cell monolayers, Eur. J. Pharm. Sci. 28 (2006) 196–203. https://doi.org/10.1016/J.EJPS.2006.02.002.

[197] B. Forbes, C. Ehrhardt, Human respiratory epithelial cell culture for drug delivery applications., Eur. J. Pharm. Biopharm. 60 (2005) 193–205. https://doi.org/10.1016/j.ejpb.2005.02.010.

[198] K. Šimková, B. Joost, G. Imanidis, Production of fast-dissolving low-density powders for improved lung deposition by spray drying of a nanosuspension, Eur. J. Pharm. Biopharm. 146 (2020) 19–31. https://doi.org/10.1016/j.ejpb.2019.11.003.

[199] P.J. Barnes, S. Bonini, W. Seeger, M.G. Belvisi, B. Ward, A. Holmes, Barriers to new drug development in respiratory disease, Eur. Respir. J. 45 (2015) 1197–1207. https://doi.org/10.1183/09031936.00007915.

[200] L. Horváth, Y. Umehara, C. Jud, F. Blank, A. Petri-Fink, B. Rothen-Rutishauser, Engineering an in vitro air-blood barrier by 3D bioprinting., Sci. Rep. 5 (2015) 7974. https://doi.org/10.1038/srep07974.

[201] A. Miller-Larsson, H. Mattsson, E. Hjertberg, M. Dahlbäck, A. Tunek, R. Brattsand, Reversible Fatty Acid Conjugation of Budesonide Novel Mechanism for Prolonged Retention of Topically Applied Steroid in Airway Tissue, Drug Metab. Dispos. 26 (1998) 623–630. http://dmd.aspetjournals.org/content/26/7/623.short.

[202] G. Borchard, M.L. Cassará, P.E.H. Roemelé, B.I. Florea, H.E. Junginger, Transport and local metabolism of budesonide and fluticasone propionate in a human bronchial epithelial cell line (Calu-3), J. Pharm. Sci. 91 (2002) 1561–7. https://doi.org/10.1002/jps.10151.

[203] E. Parra, J. Pérez-Gil, Composition, structure and mechanical properties define performance of pulmonary surfactant membranes and films, Chem. Phys. Lipids. 185 (2015) 153–175. https://doi.org/10.1016/J.CHEMPHYSLIP.2014.09.002.

[204] J. Bastacky, C. Lee, J. Goerke, H. Koushafar, D. Yager, L. Kenaga, T. Speed, Y. Chen, J. Clements, Alveolar lining layer is thin and continuous: low-temperature scanning electron microscopy of rat lung, J. Appl. Physiol. 79 (1995) 1615–1628. http://jap.physiology.org/content/79/5/1615.short.

[205] S. Pham, T. Wiedmann, Dissolution of aerosol particles of budesonide in Survanta (TM), a model lung surfactant, J. Pharm. Sci. 90 (2001) 98–104. http://apps.isiknowledge.com/full_record.do?product=WOS&search_mode=GeneralSearch&qid=392&SID=2BdmGm2OgID6MM3N@d6&page=1&doc=1.

[206] S. Zellnitz, L. Zellnitz, M.T. Müller, C. Meindl, H. Schröttner, E. Fröhlich, Impact of drug particle shape on permeability and cellular uptake in the lung, Eur. J. Pharm. Sci. 139 (2019). https://doi.org/10.1016/j.ejps.2019.105065.

[207] Z. Jiang, J. Reilly, B. Everatt, A method for rapidly predicting drug tissue distribution using surfactant vesicle electrokinetic chromatography, Electrophoresis. 29 (2008) 3674–3684. https://doi.org/10.1002/elps.200800236.

[208] E.J. O'Connell, Review of the unique properties of budesonide, Clin. Ther. 25, Supple (2003) C42–C60. https://doi.org/10.1016/S0149-2918(03)80305-3.

[209] Y.H. Yun, B.K. Lee, K. Park, Controlled Drug Delivery: Historical perspective for the next generation, J. Control. Release. 219 (2015) 2–7. https://doi.org/10.1016/j.jconrel.2015.10.005.

7 Lists

7.1 List of abbreviations

ADME	Absorption, Distribution, Metabolism, Excretion
ALI	Air-Liquid Interface
ALICE	Air-Liquid Interface Cell Exposure
API	Active Pharmaceutical Ingredient
APSD	Aerodynamic Particle Size Distribution
COPD	Chronic Obstructive Pulmonary Disease
CULTEX	LTC-C Computer-Controlled Long-Term Cultivation
DPI	Dry Powder Inhaler
DPPC	Dipalmitoylphopshatidylcholine
FPF	Fine Particle Fraction
FPM	Fine Particle Mass
hAEpC	human Alveolar Epithelial Cells
ICH	International Council for Harmonisation of Technical Requirements for Pharmaceuticals for Human Use
IVIVC	*in vitro-in vivo* correlation
LPP	Large Porous Particle
NGI	Next Generation Impactor
NP	Drug nanoparticle
PADDOCC	Pharmaceutical Aerosol Deposition Device on Cell Culture
pDMI	Pressurised Metered Dose Inhalers
TEER	Transepithelial Electrical Resistance
TPGS	D-α-Tocopherol Polyethylene Glycol 1000 Succinate
USP	United States Pharmacopeia
WMM	Wet Media Milling

7.2 List of symbols

γ	interfacial tension at the particle surface
η	dynamic viscosity
κ	evaporation rate
λ	mean free path of a gas
ρ_P	particle density
ρ_0	unit density
χ	shape factor
ω	stirrer angular velocity
C	dissolved drug concentration
C_C	Cunningham correction factor
C_∞	solubilities of a particle of infinite size
C_r	solubilities of a particle of radius r
Cs	drug saturation solubility
d	particle diameter
d_A	aerodynamic diameter
d_E	equivalent volume diameter
D_f, D	diffusion coefficient
D_i	diffusion coefficient of the solutes in the droplet
D_j	jet diameter
$E_{m,P}$	specific energy input
F_D	drag force
F_G	gravitational force
g	gravitational acceleration
h	thickness of diffusion boundary layer
k_B	Boltzmann's constant
m	dissolved drug amount
M	molecular weight of the solute
$M_{(t)}$	torque measured during milling
M_0	no-load torque
m_p	product mass
Pe	Péclet number
r	radius
Re	Reynolds number
S	surface area
Stk	Stokes number
t	time
T	absolute temperature
U	nozzle exit velocity
V	particle velocity
V_{TS}	terminal settling velocity

8 Appendix

8.1 Production of fast-dissolving low-density powders for improved lung deposition by spray drying of a nanosuspension

Below are shown dissolution tests of the investigated formulations. Stars represent the dissolved drug concentration in the bulk solution (Cb), whereas lines represent fitted dissolution profile using the EASY-FIT®.

8.1.1 Aerodynamically classified formulations

NS/Leu+AC

First repetition:

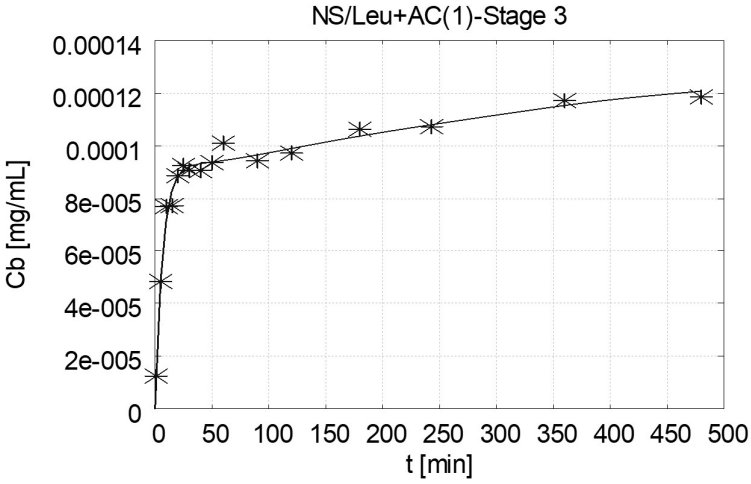

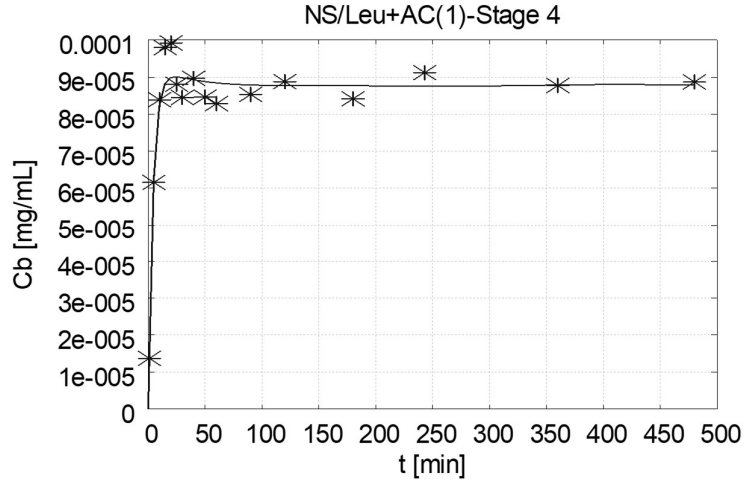

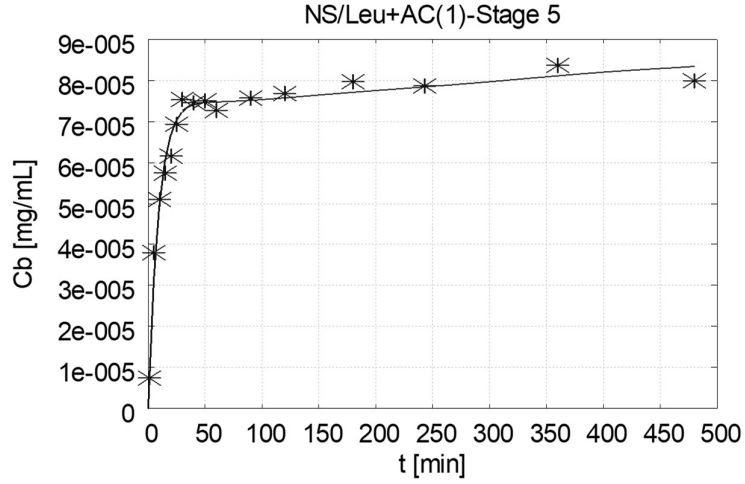

Second repetition:

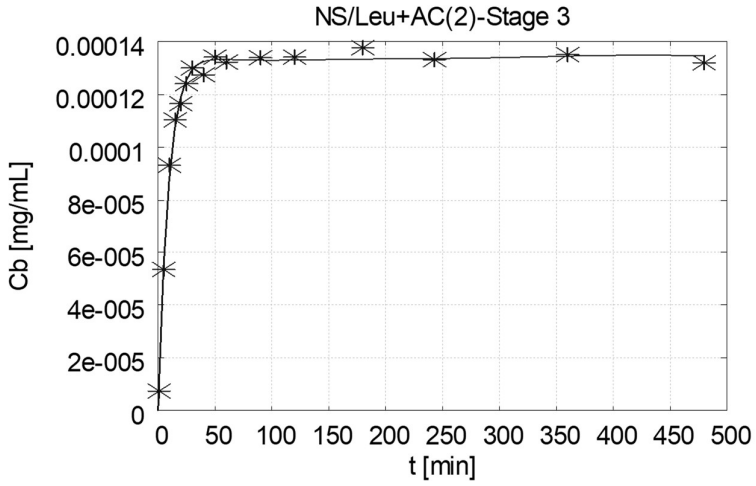

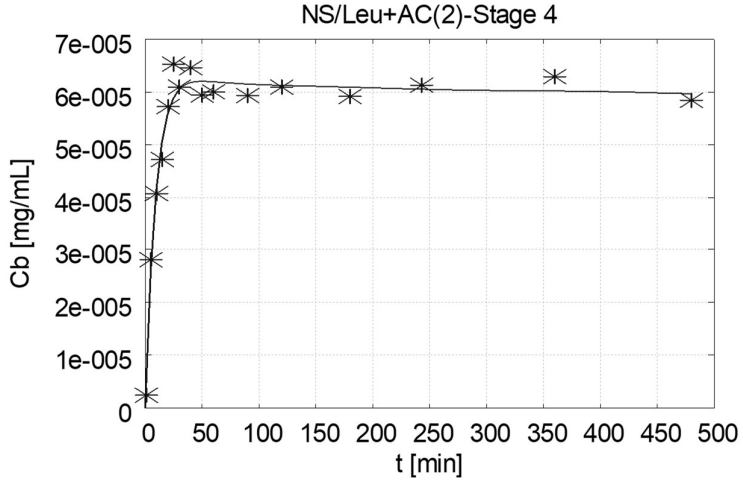

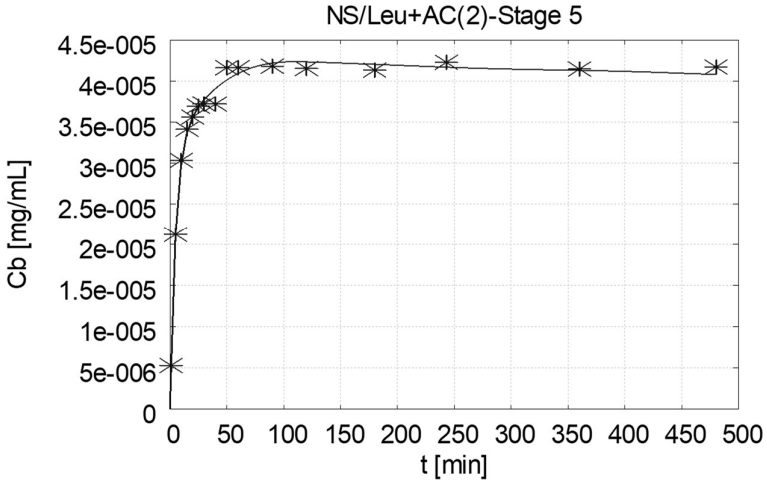

Third repetition:

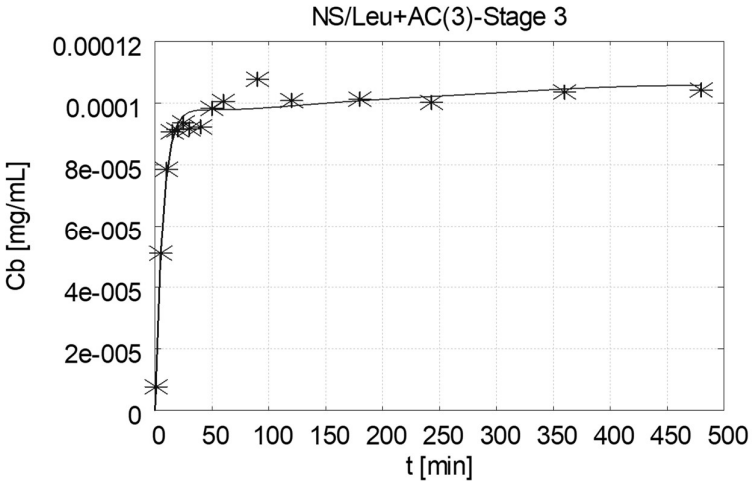

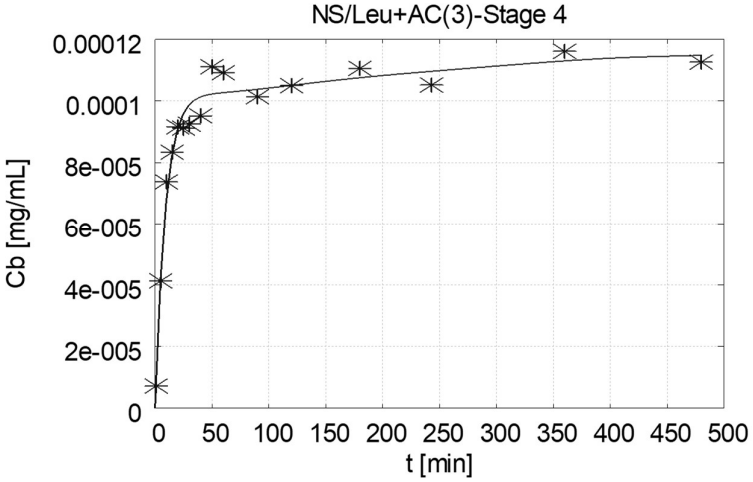

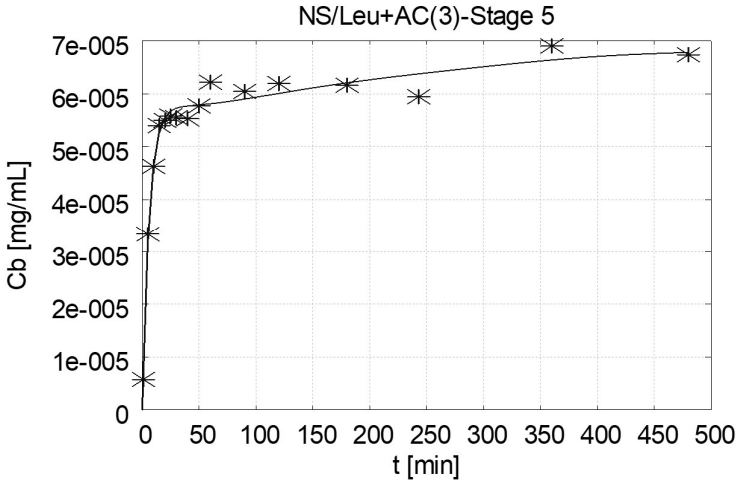

S/Leu+AC

First repetition:

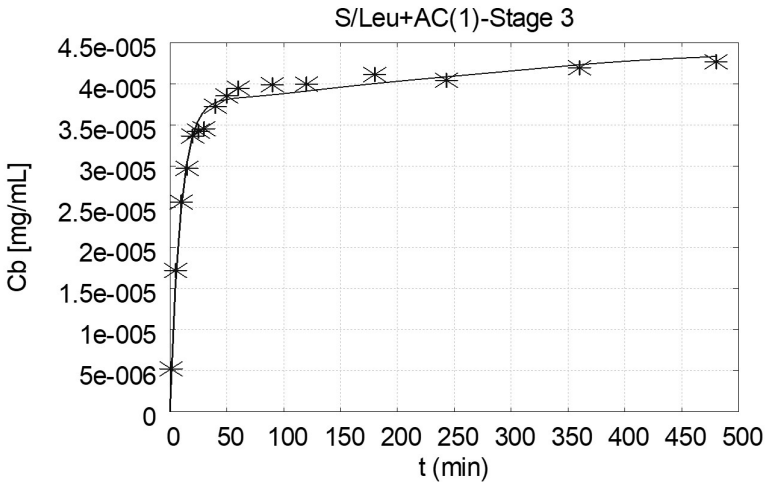

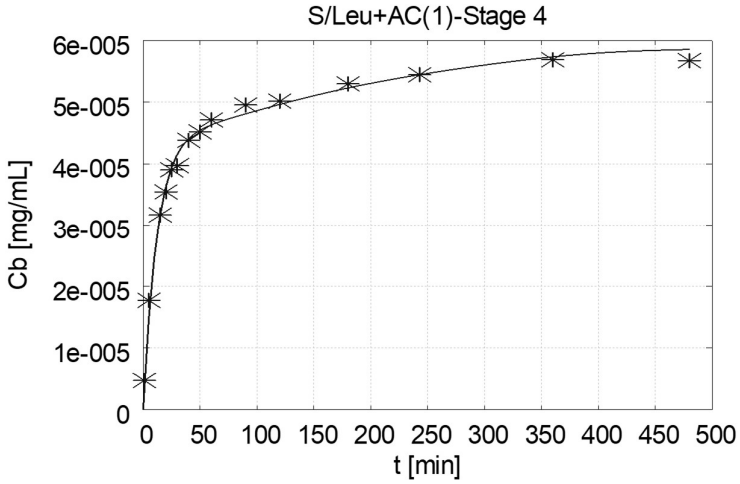

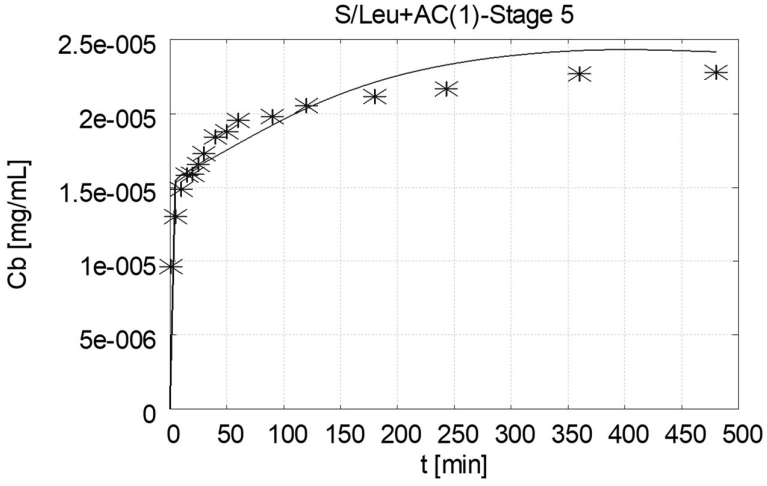

Second repetition:

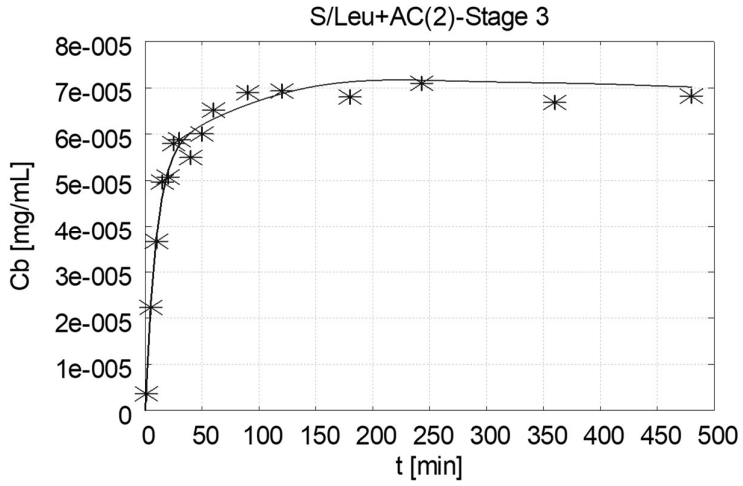

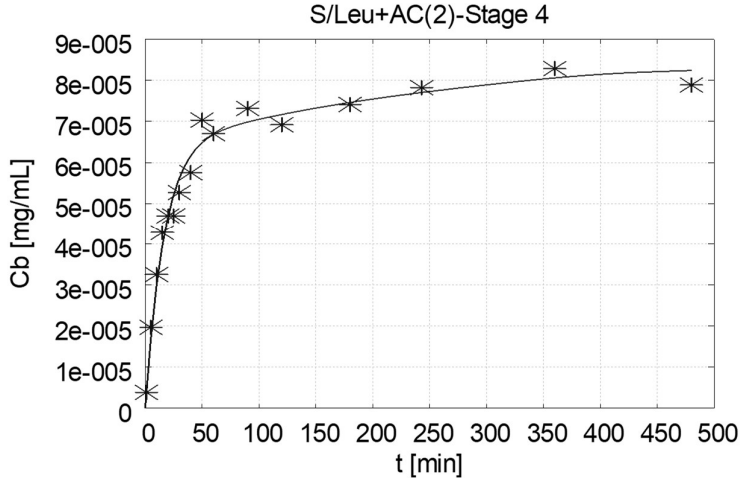

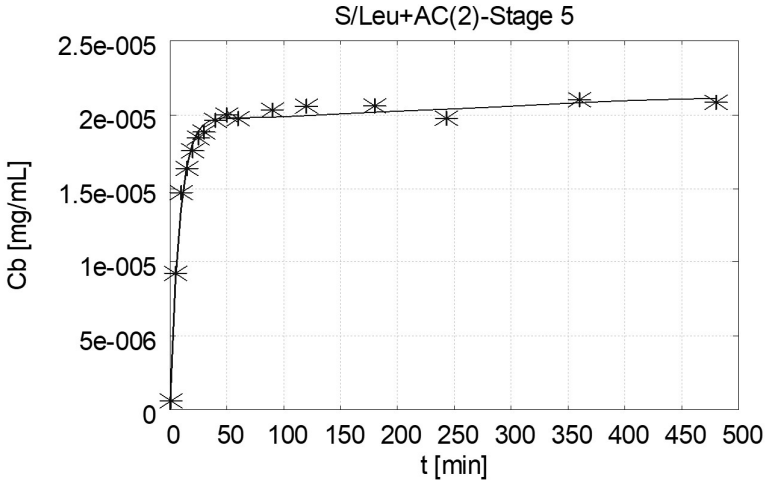

NS/Leu

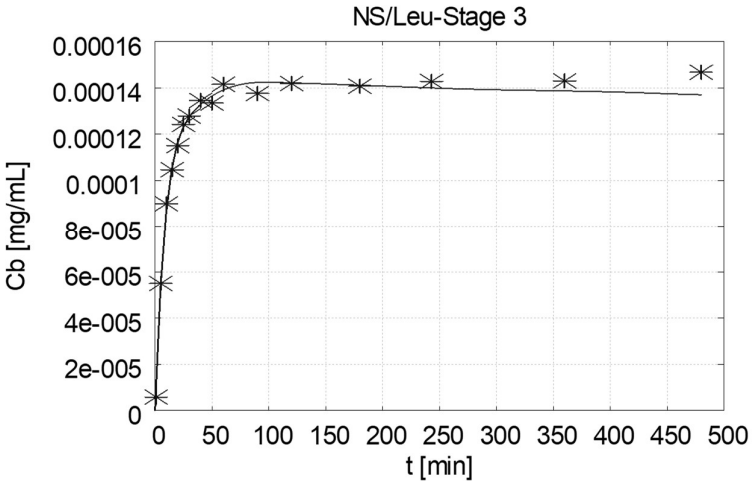
NS/Leu-Stage 3
Cb [mg/mL]
0.00016
0.00014
0.00012
0.0001
8e-005
6e-005
4e-005
2e-005
0
0 50 100 150 200 250 300 350 400 450 500
t [min]

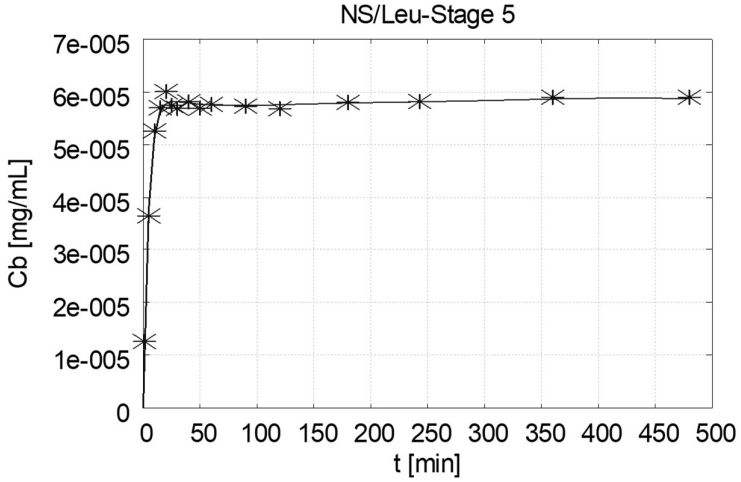
NS/Leu-Stage 5
Cb [mg/mL]
7e-005
6e-005
5e-005
4e-005
3e-005
2e-005
1e-005
0
0 50 100 150 200 250 300 350 400 450 500
t [min]

NS/Alb

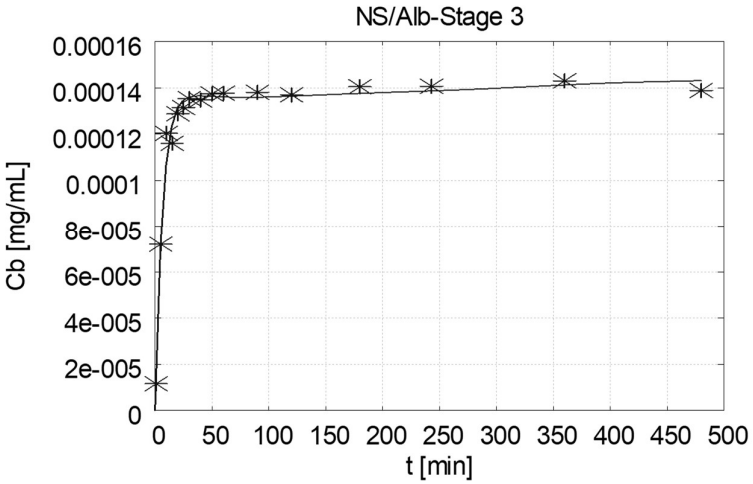
NS/Alb-Stage 3
Cb [mg/mL]
0.00016
0.00014
0.00012
0.0001
8e-005
6e-005
4e-005
2e-005
0
0 50 100 150 200 250 300 350 400 450 500
t [min]

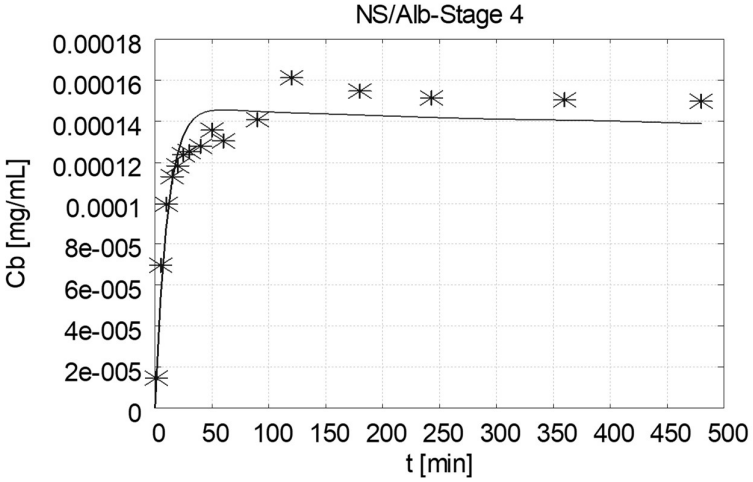
NS/Alb-Stage 4
Cb [mg/mL]
0.00018
0.00016
0.00014
0.00012
0.0001
8e-005
6e-005
4e-005
2e-005
0
0 50 100 150 200 250 300 350 400 450 500
t [min]

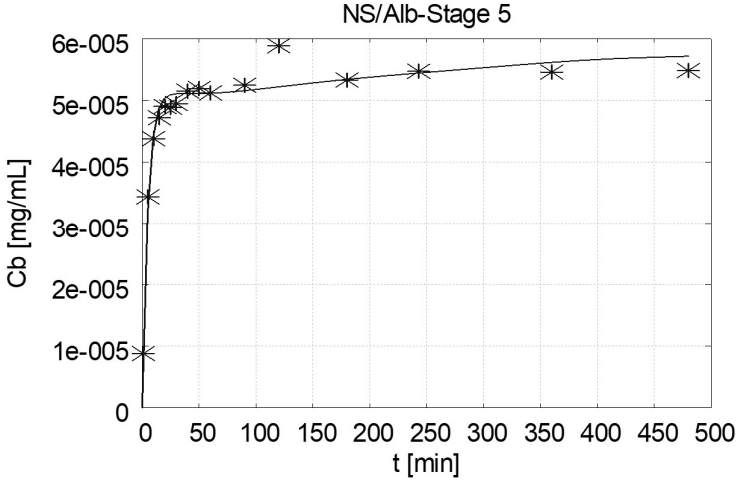
NS/Alb-Stage 5
Cb [mg/mL]
6e-005
5e-005
4e-005
3e-005
2e-005
1e-005
0
0 50 100 150 200 250 300 350 400 450 500
t [min]

Physical mixture

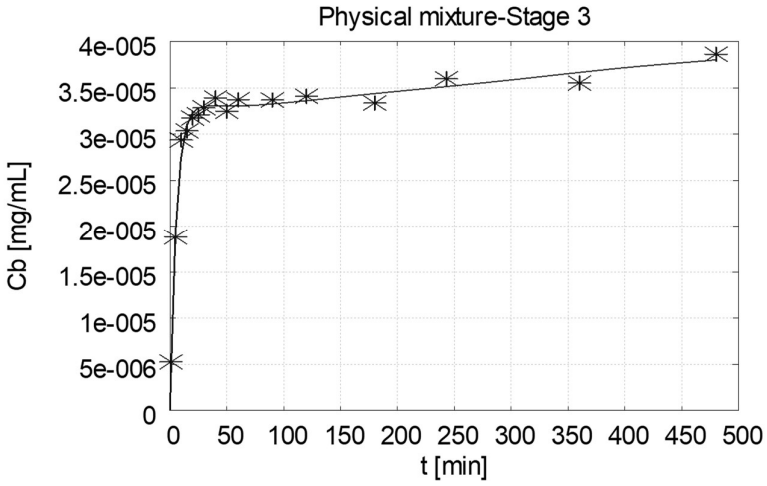

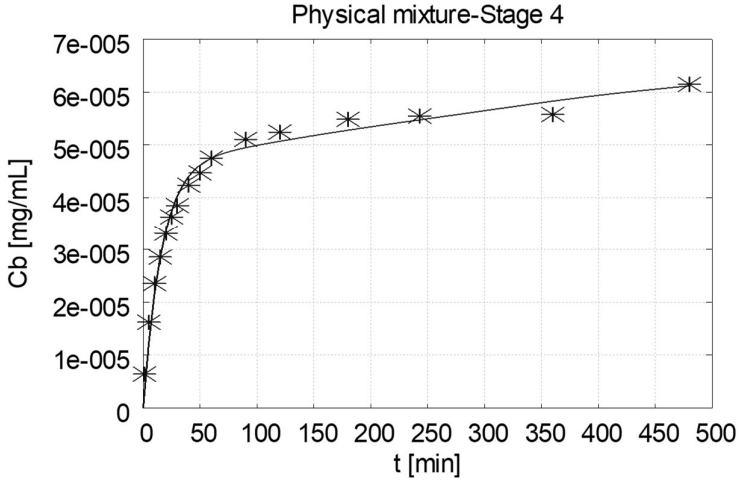

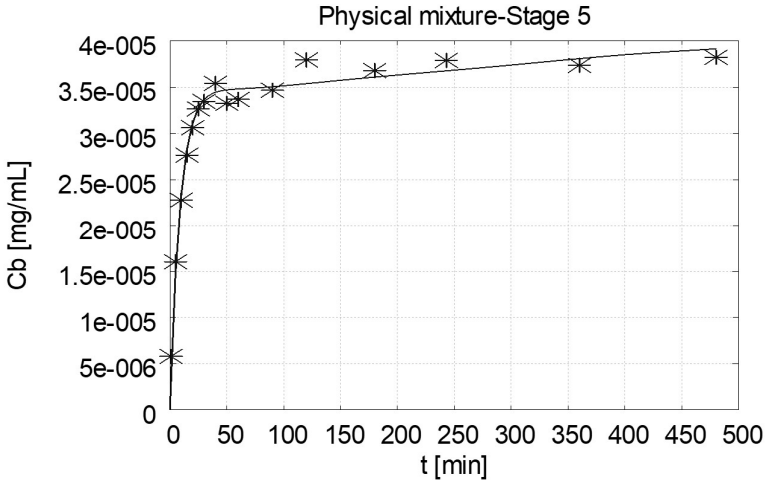

Commercial product

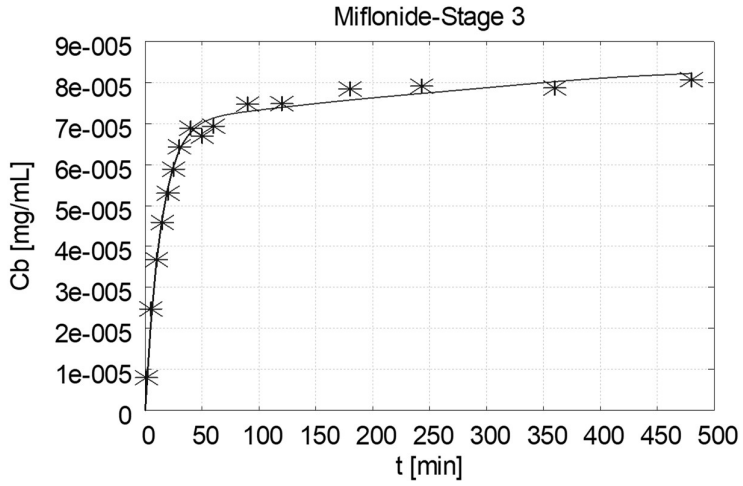

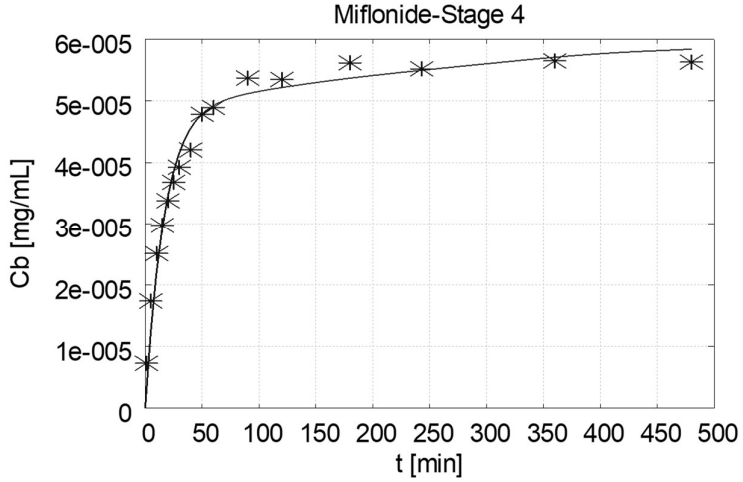

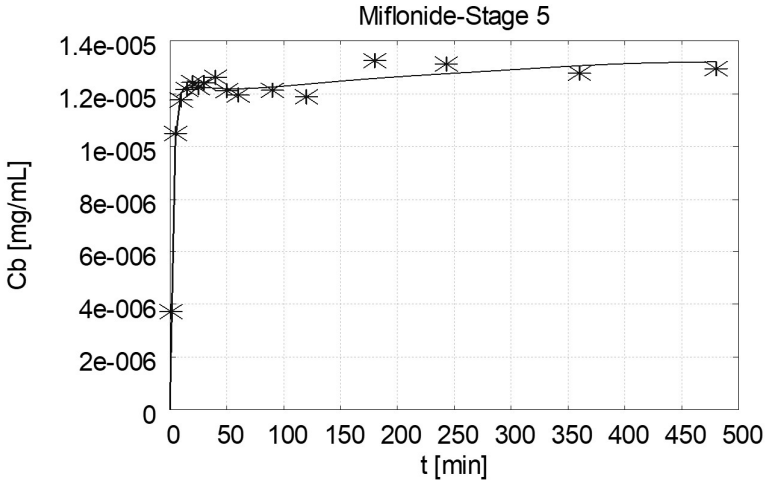

8.1.2 Complete formulations

NS/Leu+AC

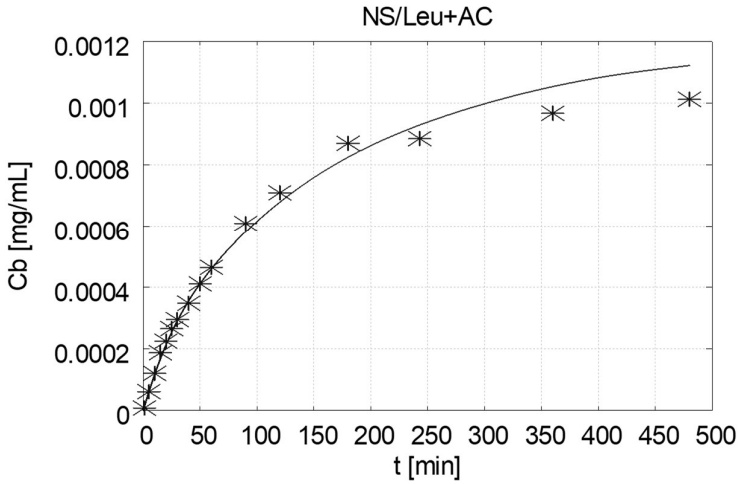

S/Leu+AC

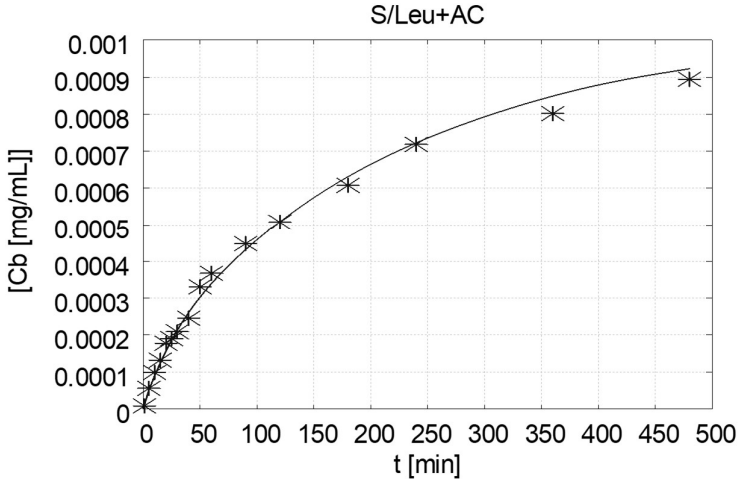

NS/Leu

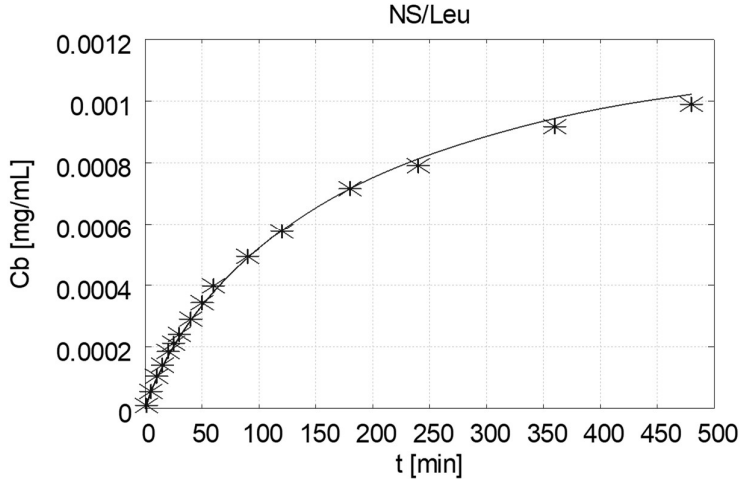

NS/Alb

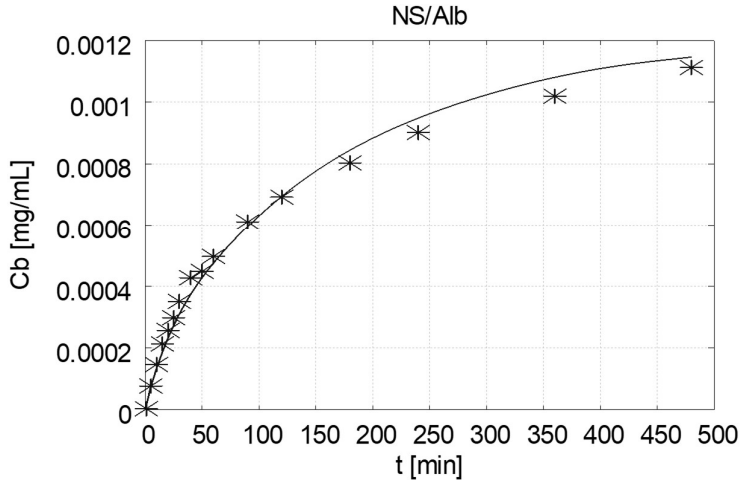

Physical mixture

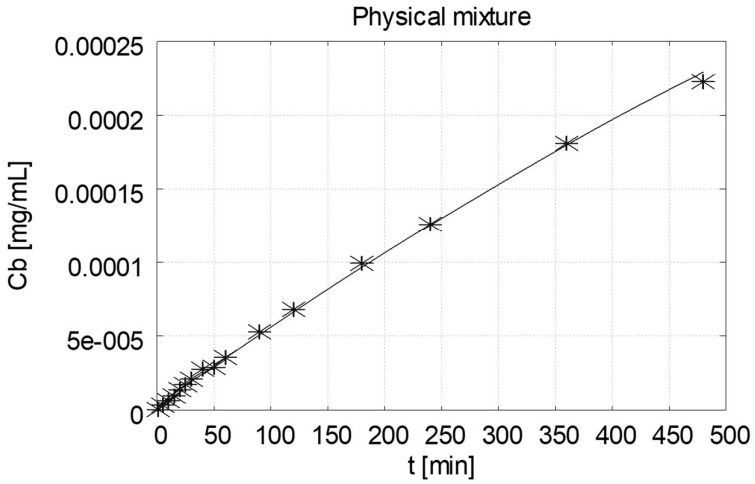

8.1.3 X-ray powder diffraction

Below are shown XRPD diffractograms of budesonide raw material, budesonide nanosuspension (WMM NS), and spray-dried nanosuspension without any matrix former (NS/-).